LBNL-41182
UC-411

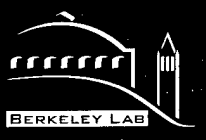

ERNEST ORLANDO LAWRENCE
BERKELEY NATIONAL LABORATORY

Optimal Separable Bases and Molecular Collisions

Lionel W. Poirier

Chemical Sciences Division

December 1997

Ph.D. Thesis

LBNL-41182

Optimal Separable Bases and Molecular Collisions

Lionel William Poirier
Ph.D. Thesis

Department of Physics and Department of Chemistry
University of California, Berkeley

and

Chemical Sciences Division
Ernest Orlando Lawrence Berkeley National Laboratory
University of California
Berkeley, CA 94720

December 1997

This work was supported by the Director, Office of Energy Research, Office of Basic Energy Sciences, Chemical Sciences Division, of the U.S. Department of Energy under Contract No. DE-AC03-76SF00098.

Optimal Separable Bases and Molecular Collisions

by

Lionel William Poirier

Sc. B. (Brown University) 1988

A dissertation submitted in partial satisfaction of the
requirements for the degree of
Doctor of Philosophy
in
Physics
in the
GRADUATE DIVISION
of the
UNIVERSITY of CALIFORNIA at BERKELEY

Committee in charge:

Professor William H. Miller, Cochair
Professor Robert G. Littlejohn, Cochair
Professor Eugene D. Commins
Professor Martin Head-Gordon

1997

Optimal Separable Bases and Molecular Collisions

by

Lionel William Poirier

Abstract

Optimal Separable Bases and Molecular Collisions

by

Lionel William Poirier

Doctor of Philosophy in Physics
University of California at Berkeley

Professor William H. Miller, Cochair
Professor Robert G. Littlejohn, Cochair

A new methodology is proposed for the efficient determination of Green's functions and eigenstates for quantum systems of two or more dimensions. For a given Hamiltonian, the best possible separable approximation is obtained from the set of all Hilbert space operators. It is shown that this determination itself, as well as the solution of the resultant approximation, are problems of reduced dimensionality for most systems of physical interest. Moreover, the approximate eigenstates constitute the optimal separable basis, in the sense of self-consistent field theory. These distorted waves give rise to a Born series with optimized convergence properties. Analytical results are presented for an application of the method to the two-dimensional shifted harmonic oscillator system.

Our primary interest however, is quantum reactive scattering in molecular systems. For numerical calculations, the use of distorted waves corresponds to numerical preconditioning. The new methodology therefore gives rise to an optimized preconditioning scheme for the efficient calculation of reactive and inelastic scattering amplitudes, especially at intermediate energies. This scheme is particularly suited to discrete variable representations (DVR's) and iterative sparse matrix methods commonly employed in such calculations.

State-to-state and cumulative reactive scattering results obtained via the optimized preconditioner are presented for the two-dimensional collinear $H + H_2 \rightarrow H_2 + H$ system. Computational time and memory requirements for this system are drastically reduced in comparison with other methods, and results are obtained for previously prohibitive energy regimes.

The method is also applied to three-body systems in two different ways. First, numerical results are obtained for zero total angular momentum using optimized preconditioning. The $J \neq 0$ results are then estimated using helicity-conserving and J-shifting approximations, after minimizing the coriolis coupling via another application of the optimal basis method. An "effective potential" interpretation of the helicity-conserving approximation is employed, which leads to an improved J-shifting scheme that automatically incorporates centrifugal distortion and other effects. Fixed-energy cumulative reaction probabilities and thermal rate constants are presented for the $O + HCl \rightarrow OH + Cl$ reactive scattering system.

This work is dedicated to my parents,
two other Dr. Poiriers.

Contents

List of Figures

List of Tables

Acknowledgements

The array of physicists, physical chemists, and mathematicians here at UC Berkeley is simply awe-inspiring. For those of us who are inclined towards the mathematical sciences, it is hard to imagine a more valuable resource than the UC faculty. Indeed, the faculty themselves should probably make greater use of this resource! In any event, I have benefited greatly from having been able to run ideas through many different minds, and to see them reflected back again from a myriad of unique and unanticipated vantage points. This has been one very fulfilling aspect of my interdepartmental status.

My research advisor, Professor William H. Miller, deserves much credit for his willingness to adopt a "foreign" student from the physics department. Throughout my graduate career he has provided support, guidance, and computer resources, whereas some of my compatriots in physics were faced with the prospect of either starving, or teaching 8A for the twelfth semester in a row. Bill is also without a doubt one of the aforementioned great minds. In the last few years, I have learned a lot from him, and also come to appreciate his very unique style of doing science.

In the physics department, I have Professor Robert G. Littlejohn to thank for acting as my advisor of record—i.e. for convincing the department to grant me a degree, even though my advisor was in chemistry. In an era when scientific research seems increasingly fragmented, Robert has consistently maintained a very interdisciplinary approach; and he is not afraid to accord the fundamentals their proper status. I have Professor Littlejohn and also Professor Eugene Commins to thank for some of the best lectures I have ever attended, and for being receptive to unorthodox questions and comments (which might have remained unasked were it not for the tenacity of Dr. Max Tegmark). Professor Alan Kaufman is singled out however, for actually agreeing to sponsor one such idea in the form of an unusual, ultimately unfruitful, but nevertheless very rewarding independent study project.

I should also acknowledge the many researchers who have been a part of the Miller group over the last three-and-a-half years—by any reckoning, an interesting and talented cast of characters. Graduate students Lionel F. X. "Lee" Gaucher and

Srihari Keshavamurthy, often confused with each other, shared my first office, adjacent to which were Dan Gezelter, Ward Thompson, and Bruce Spath. More recent additions include Sean Sun, Dave Skinner, and Kathy Sorge. I have also had the opportunity to interact with a variety of post docs, visiting students, and the like (by now a rather long list): Prof. Nick Handy, Dr. Uri Peskin, Dr. Hans Karlsson, Åke Edlund, Johannes Natterer, Dr. Günter Schmid, Dr. Joshua Wilkie, Dr. Tim Germann, Dr. Stefan Krempl, Dr. Clemens Woywod, Victor Guillar, Dr. Haobin Wang, Dr. Victor Batista, Prof. Dudley Herschbach, and Dr. Daniel Lidar. Holding it all together throughout was Cheryn Gliebe, who together with Anne Takizawa in the physics department, also managed somehow to hack through the interminable red tape associated with an interdepartmental degree.

I would be remiss not to acknowledge a few individuals who were instrumental in developing my interest in physics prior to attending graduate school. At the University of Maryland, Professor Douglas Currie provided me with a research project, and Doctor George Hinds could always be counted on for stimulating, provocative, and often humorous discussion. At Brown University, Professor Frank Levin, and especially my undergraduate thesis advisor Professor James Baird, were incredibly supportive; they also let me get away with an unconventional thesis project. I owe an even greater debt of gratitude, however, to my wonderful high school physics teacher, Mr. Ralph Bunday, aka "Papa Smurf."

I have only my family to blame prior to high school—especially my uncles, who have all been science teachers. My immediate family deserves a lot of credit for encouraging the academic pursuit rather than dismissing my efforts as an incomprehensible waste of time: especially my siblings Henry and Marie (and brother-in-law Joe) who are not scientists. The same should be said of Joel Lutzker and of the Longos, who have also provided gastronomic support on many occasions during the past few years. Finally, I would like to give special thanks to my parents and to Anne Longo, who have proven their persistence through all kinds of circumstances.

This work was supported by the Director, Office of Energy Research, Office of Basic Energy Sciences, Chemical Sciences Division of the U.S. Department of Energy under Contract No. DE-AC0376SF00098.

Chapter 1

Introduction

In the physical world, molecules are constantly colliding, interacting, and flying apart from one another. The fact that there is an interaction, i.e. that molecules are not simply invisible to each other, implies that they are transformed somehow as a result of these collisions. There are many different ways in which such a change can manifest itself, depending on the nature of the colliding particles and their interactions. Indeed, this variety is ultimately responsible for the wide diversity exhibited by bulk matter.

Nevertheless, it may not be necessary to understand the details of the interactions in order to explain the bulk properties. All that may be required is a specification of the overall change of state induced by the collision. This is the idea underlying all of scattering theory, in its many forms. It is a particularly useful notion for systems in the gas phase. Here, the time of collisions is small compared to the time between collisions, and similarly, the interaction length scale is often small compared to the average interparticle distance. Consequently, each individual collision is a well-defined event, and it is meaningful to ask what changes to the system are induced by a single collision. Moreover, only a small number of constituents are involved in a single collisional process—usually just two.

Our goal therefore, is to apply scattering theory to extract information about the chemical and physical properties of molecular systems in the gas phase. This could include the conventional scattering quantities such as transition amplitudes

and differential and total cross sections, as well as information of more interest to the chemist, such as the thermal rate constant for a chemical reaction. These inquiries are important in their own right, as there is much chemistry of practical interest that takes place in the gas phase. However, a thorough understanding of these systems can also serve as a stepping stone to more challenging realms such as the liquid phase, for which the interactions are evidently more interrelated.

In any event, an accurate treatment of scattering for molecular systems clearly requires quantum mechanical dynamics, which unfortunately poses a challenge both analytically and numerically. Given the limitations of present-day computer resources, researchers have adopted several different philosophies to deal with this challenge. One approach is to tackle the quantum problem head-on, in which case accurate results can be obtained, but only for small systems. Another approach is to use approximation methods, such as those based on quasiclassical, semiclassical or centroid dynamics.[1] These can be applied to larger systems, and moreover, often provide a pedagogical description that may be lacking in the direct quantum methods. However, the results are only approximate and—more importantly—one does not always have a reliable estimate for the error bound.

The approach that we shall adopt is in a certain sense a compromise between these two philosophies. Ultimately, we calculate the exact quantum results; however, insodoing we make use of a quantum mechanical approximation known as the "optimal separable" approximation, which has both pedagogical and quantitative significance. Quite literally, this involves finding from the set of all separable operators on the Hilbert space, the particular operator which most closely approximates the true Hamiltonian of interest. Albeit a bona fide quantum operator, the approximate Hamiltonian is easy to evaluate by virtue of its separability. Moreover, an error estimate is readily obtainable. One can also use the approximate results as the starting point in a perturbation expansion. Because the optimal separable choice is used, convergence to the correct results is achieved more quickly than would otherwise be the case.

For scattering applications, the perturbation series in question is the generalized Born expansion of the energy Green's function. All scattering quantities of

interest to both physicists and chemists can be derived directly or indirectly from this function. These quantities form a natural hierarchy, for which there is a corresponding hierarchy of the various kinds of transitions that can occur when molecules collide. It is instructive to work through this chain of command in detail; however, we shall first present a basic description of reactive chemical systems for the benefit of those readers who are not physical chemists.

The simplest type of exchange reaction in chemistry can be represented schematically via

$$A + B \rightarrow C + D \tag{1.1}$$

where A and B represent reactants and C and D are products. During the course of the collision, part of one reactant molecule gets transferred to the other, resulting in two products of possibly new chemical species. The most fundamental exchange reaction for example is $H + H_2 \rightarrow H_2 + H$, which is the exchange chemistry analogue of the hydrogen or helium atom in atomic physics. To simplify matters, it is often convenient (if artificial) to assume that the three hydrogen atoms lie on a straight line.

The reaction rate for the bimolecular reaction of Equation 1.1 is given by[2]

$$R = [A][B]k(T), \tag{1.2}$$

where [ ] denotes molar concentration, and $k(T)$ is the thermal rate constant. The quantity $k(T)$ is clearly statistical—formally involving all 10^{23} constituent particles. However, under the ideal (rarefied) gas conditions which are assumed here, each reactant collision process can be treated independently. One can therefore think of a single pair of reactant molecules as constituting a legitimate subsystem, in thermal equilibrium with the rest of the gas. Under these conditions, the thermal quantities for the system as a whole (such as $k(T)$) are obtained by simply Boltzmann-averaging the appropriate microcanonical (fixed-energy) scattering quantities for a single set of reactants.

The true Hamiltonian describing Equation 1.1 involves all nucleons and electrons for a single set of reactants. However, for small molecular systems at typical

energies, the Born-Oppenheimer approximation is usually valid, and electronic transitions are often improbable. In such cases, we need only consider nuclear dynamics on the ground electronic potential energy surface. For each particular system considered, a new ground state surface must be obtained over the relevant region of nuclear configuration space. There are many "quantum chemistry" techniques available for determining these surfaces, ranging from semiempirical to rigorous *ab initio* methods. For our purposes, the ground surface is presumed to be known *a priori*.

Using the ground electronic surface to define an effective nuclear Hamiltonian, we can characterize quantitatively what happens when reactants collide. The various transitions that can occur as a result of collisions can be arranged (in increasing order of energy and complexity) as follows:

- Elastic Scattering—$H + H_2 \rightarrow H_2 + H \qquad (\mathbf{k} \rightarrow \mathbf{k}')$
- Inelastic Scattering—$H + H_2(v) \rightarrow H + H_2(v')$
- Reactive (Exchange) Scattering—$H + H_2(v) \rightarrow H_2(v') + H$
- Dissociation—$H + H_2 \rightarrow H + H + H$

Under elastic scattering, internal properties of the reactants are unaffected by the collision. In inelastic scattering, the internal states (in the collinear $H + H_2$ example, the vibrational quantum number of the H_2 molecule) can undergo transitions, as a result of which the translational kinetic energy is also changed. In exchange scattering, the molecules themselves are altered, although the number of reactants and products is the same. Finally, if the energies are sufficiently high, dissociation of reactants into a larger number of products can also occur.

All of these processes can be dealt with using quantum scattering theory, albeit of increasing sophistication as one proceeds down the list. Obviously, the number of possible transitions grows very rapidly; and the situation can become very complicated even for fairly small molecules. Fortunately, one is not necessarily always interested in calculating fully detailed information for such systems. In reactive scattering for example, there is a hierarchy of increasingly averaged quantities that can be derived from the multichannel S-matrix transition amplitudes $S_{vv'}$ as follows:

- State-to-state reaction probability—$P_{vv'} = |S_{vv'}|^2$
- Cumulative reaction probability—$N(E) = \sum_{vv'} P_{vv'}$
- Thermal rate constant—$k(T) = \langle N(E) \rangle_{\text{Boltzmann}}$

Moreover, methods have been developed for calculating each of these quantities directly, i.e. without referring to the less averaged quantities which are lower in the hierarchy.

We conclude this introduction with a brief overview of the remaining chapters. The general theory underlying the optimal separable approach is presented in Chapter 2, which also includes a treatment of the Born expansion of the energy Green's function relevant to scattering theory. In Chapter 3, we shall make use of certain shortcuts for obtaining the averaged quantities of the preceding paragraph directly. Moreover, the ideas of Chapter 2 are developed into an efficient numerical algorithm. As a test application, the collinear $H + H_2 \rightarrow H_2 + H$ system is considered. Finally, all of the ideas developed in the other chapters are applied to the challenging $O + HCl \rightarrow OH + Cl$ reaction in Chapter 4, wherein we also make use of improvements in the approximate separation of rotational and vibrational motions.

Chapter 2

Optimal Separable Basis Theory

2.1 Introduction

Since the time of Newton, if not earlier, physicists have tried to solve complicated problems by breaking them down into simpler components. The trick lies in "carving up" the initial problem in just the right way so that the components are independent of one another and can be solved separately. In classical mechanics, for instance, one seeks the first integrals or action-angle variables because these partition the Hamiltonian in the most natural way. Of course, finding the best way to slice a particular problem may be very difficult, if not impossible. Even in such cases however, one may still be able to find a *separable substitute* that accurately approximates the true system.

In this chapter, we consider separable approximations of quantum mechanical systems. For a given multi-dimensional Hamiltonian $\hat{H}$, a separable approximation $\hat{H}_0$ is an operator whose eigenstates are products of coordinate functions. The simplest class of such functions are the direct-product basis sets, which have been utilized, for example, in vibrational problems.[3,4] These basis sets correspond to what we shall in Section 2.2 call "strongly separable" $\hat{H}_0$'s. However, the general case also includes *weakly* separable $\hat{H}_0$'s which may provide more accurate approximations of $\hat{H}$. One such $\hat{H}_0$ gives rise to the "dressed" eigenfunctions of the truncation/recoupling method.[5]

It would clearly be desirable if we could somehow examine all possible separable $\hat{H}_0$'s, and select from that pool the best approximation to the true Hamiltonian. Such a procedure would first require a rigorous definition of the metric, or "distance" between two operators. The resultant search for the closest separable $\hat{H}_0$ could then be effected by applying the variational calculus to the distance functional on the set of all Hilbert-space *operators*. At first glance, this appears far more formidable than the original problem! Nevertheless, we shall demonstrate that with a suitable operator metric—specifically, the Frobenius norm of the residual $(\hat{H} - \hat{H}_0)$—the variational problem *itself* corresponds to a conventional quantum mechanics problem of reduced dimensionality.

The optimal $\hat{H}_0$ obtained in this manner can be usefully exploited in a variety of ways. The eigenstates of $\hat{H}_0$ turn out to be the best mutually orthogonal separable approximations to the true eigenstates, in the sense of self-consistent field theory. This "optimal separable basis" is therefore a natural starting point for a time-independent perturbation expansion of $\hat{H}$. In scattering applications, the stationary scattering states of $\hat{H}_0$ are "distorted waves,"[6] in a certain generalized sense (Section 2.4.2). These give rise to an optimized distorted wave Born expansion of the energy Green's function. This expansion may converge quickly even if the standard Born series is slowly convergent or *divergent*, as is the case for many scattering systems of interest.

The optimal separable basis methodology is also well-suited to numerical applications. In the calculation of quantum bound state energies for example, such as those relevant to spectroscopy, the standard perturbation expansion is often replaced by an iterative* Krylov-space algorithm for obtaining eigenvalues, such as that originally proposed by Lanczos.[7,8] The efficiency of such algorithms is significantly improved by selecting a suitable starting vector, which we suggest could be obtained from the $\hat{H}_0$ eigenstates (Section 2.4.1). In microcanonical scattering applications, where one often requires energy Green's function calculations, the matrix representation of $\hat{H}_0$ leads to an optimized preconditioner[9] (Chapter 3), which can be implemented separately from—or in conjunction with—the various other numerical

*though not "iterative" in the sense of Cullum and Willoughby.[7]

Green's function techniques currently in use.

The remainder of this chapter is organized as follows. Section 2.2 provides the mathematical preliminaries, including precise definitions of the operator metric and separability. Section 2.3 comprises the bulk of the theory underlying the optimal separable basis approach. Section 2.4 applies the method to series expansions, and examines the issue of convergence. Section 2.5 discusses a simplification that arises when the method is applied to Hamiltonians of a standard form. Section 2.6 presents analytical results for a benchmark two-dimensional system. This "shifted harmonic oscillator" problem has not, to the author's knowledge, been previously considered.

2.2 Mathematical Preliminaries

2.2.1 Separability

We begin with a completely general n-dimensional quantum mechanical Hamiltonian

$$\hat{H} \equiv H(\hat{q}_1, \hat{p}_1, \ldots, \hat{q}_n, \hat{p}_n). \tag{2.1}$$

The position operators $\hat{q}_1, \ldots, \hat{q}_n$ and associated $\hat{p}_1, \ldots, \hat{p}_n$ satisfy the following commutation relations:

$$\begin{aligned} [\hat{q}_i, \hat{q}_j] &= [\hat{p}_i, \hat{p}_j] = 0 \\ [\hat{q}_i, \hat{p}_j] &= \delta_{ij} F_i(\hat{q}_i, \hat{p}_i) \end{aligned} \tag{2.2}$$

Under the simplest scenario, $\hat{q}_i$ and $\hat{p}_i$ are canonically conjugate operators for which $F_i = i\hbar$—i.e., standard rectilinear position and momenta. However, it is often convenient to use generalized $\hat{q}$'s, such as angular coordinates, which are not canonical in the strictest sense.[10] In small molecular systems for example, angular representations of the Hamiltonian are very often employed, as a means of reducing the number of degrees of freedom.[11,12] In such cases, the corresponding momentum operators (if they can be defined) do *not* equal $-i\hbar\partial_q$, and the standard commutation relations simply do not apply[13] (Chapter 4). We do not wish to exclude such coordinates from consid-

eration, given the important role they play in molecular applications; consequently in all that follows we require only that $F_i \neq 0$.

We now divide the degrees of freedom into two categories. To be more specific, we designate some set of $k < n$ degrees of freedom as *inner coordinates*, and the remaining $(n-k)$ as *outer coordinates*. We represent this separation in the operator functional form of the Hamiltonian with the following notation:

$$\hat{H} = H(\hat{q}_1, \hat{p}_1, \ldots, \hat{q}_k, \hat{p}_k; \hat{q}_{k+1}, \hat{p}_{k+1}, \ldots, \hat{q}_n, \hat{p}_n) \tag{2.3}$$

where $\hat{q}_1, \hat{p}_1, \ldots, \hat{q}_k, \hat{p}_k$ are the inner coordinates. The precise determination of which degrees of freedom are considered inner coordinates is completely arbitrary. In practice the issue can and should be decided by analytic or computational convenience; several practical schemes are presented in Section 2.5.2.

A "separable basis" is now defined as a basis which is separable in the position representation by inner and outer coordinates. In other words, each basis function can be expressed as the product of some inner coordinate function multiplied by some outer coordinate function. We must distinguish between two distinct types of separability: "strong" and "weak." The former corresponds to inner and outer factors which are completely independent; i.e.,

$$\Phi_{\ell m} = \phi_\ell(q_1, \ldots, q_k)\, \varphi_m(q_{k+1}, \ldots, q_n). \tag{2.4}$$

This symmetric situation corresponds to the eigenfunctions of a strongly separable $\hat{H}_0$ of the form

$$\hat{H}_0 = H_{\text{in}}(\hat{q}_1, \hat{p}_1, \ldots, \hat{q}_k, \hat{p}_k) + H_{\text{out}}(\hat{q}_{k+1}, \hat{p}_{k+1}, \ldots, \hat{q}_n, \hat{p}_n), \tag{2.5}$$

which follows directly from the commutation relations as specified in Equations 2.2. If the classical system corresponding to $\hat{H}_0$ is (partially) integrable, then the indices in Equation 2.4 above are to be considered composite indices. In this case, ℓ and m represent *collections* of (up to) k and $(n-k)$ quantum numbers, respectively. However, we need not restrict ourselves to integrable approximations; the general case includes nonintegrable $\hat{H}_0$'s for which ℓ and m must each represent a single index only.

In any event, insofar as approximating $\hat{H}$ is concerned, the class of strongly separable $\hat{H}_0$'s is somewhat limited. The range of possible eigenvalue spectra, for example, is restricted to additive spectra only. In other words,

$$E^0_{\ell m} = E^{\text{in}}_{\ell} + E^{\text{out}}_{m} \tag{2.6}$$

which may not describe the true spectrum very well, even qualitatively.

Fortunately, there is a much broader class of separable bases—i.e., those satisfying the weak separability condition and characterized by eigenfunctions of the form

$$\Phi_{\ell m} = \phi^{(m)}_{\ell}(q_1, \ldots, q_k)\, \varphi_m(q_{k+1}, \ldots, q_n), \tag{2.7}$$

where the inner coordinate functions are now labelled by m as well as ℓ. The meanings of these two labels are very different however; the $\phi^{(m)}_{\ell}$ should be viewed as a family of different basis sets ϕ_ℓ parametrized by m. Thus, the states corresponding to the various values of ℓ are mutually orthogonal for fixed m, but not the other way around. As before, the indices ℓ and m may be either singular or composite.

In any event, Equations 2.2 now imply a corresponding weakly separable $\hat{H}_0$ conforming to

$$\hat{H}_0 = H_{\text{in}}(\hat{q}_1, \hat{p}_1, \ldots, \hat{q}_k, \hat{p}_k, H^1_{\text{out}}(\hat{q}_{k+1}, \hat{p}_{k+1}, \ldots, \hat{q}_n, \hat{p}_n), H^2_{\text{out}} \ldots) \tag{2.8}$$

where the H^i_{out} comprise an independent set of mutually commuting operators whose simultaneous eigenstates are the $\varphi_m(q_{k+1}, \ldots, q_n)$. Note that in addition to being manifestly asymmetric, Equation 2.8 is seen to incorporate a much broader range of operators than Equation 2.5. Moreover, the corresponding energy eigenspectra are completely unrestricted, and need not in general conform to the additive restriction of Equation 2.6. The weakly separable situation is therefore much improved with respect to mimicking the energy spectrum of the true Hamiltonian.

In finding the best separable approximation $\hat{H}_0$ to the full Hamiltonian $\hat{H}$, we must specify which definition of separability is to be used. There are undoubtedly certain situations for which it is appropriate to consider symmetric separability only. This might be the case for example, for a system possessing a natural symmetry to

begin with. Nevertheless, Equation 2.5 is a special case of Equation 2.8; and we shall clearly do much better, in general, by extending the search to include the entire weakly separable domain.

2.2.2 The Nature of Weak Separability

It is worth digressing a bit on the nature of the two forms of separability we have just defined. The strong form is what we usually associate with independent, or "uncoupled" systems. These systems can be "solved"—i.e. all relevant physical quantities determined—by solving a single reduced-dimensional subsystem for each category of coordinates, e.g. H_{in} and H_{out} in Equation 2.5. Due to symmetry, it is immaterial which of the two reduced problems is tackled first. In contrast, a lack of symmetry arises in the weakly separable case because the inner functions depend on the quantum numbers of the outer functions, but not vice-versa. Although this situation is a familiar one encountered often in quantum mechanics—e.g., the Y_l^m spherical harmonic functions—the generic form of the corresponding $\hat{H}_0$ as expressed in Equation 2.8 is not usually considered.

In any event, the inherent asymmetry of the weakly separable situation is very evident in $\hat{H}_0$; it is clear that such operators are in general neither independent nor uncoupled. Nevertheless, the coupling in such systems can be regarded as trivial, in that the entire system can still be solved completely by solving a collection of reduced-dimensional subsystems—although the *number* of subsystems that must be solved is larger than in the strongly separable case. Specifically, by solving the H_{out}^i eigenproblems first, these operators can be replaced by their corresponding eigenvalues (labelled by m) in the expression for $\hat{H}_0$. Equation 2.8 then becomes an m-parametrized collection of independent subsystems of the inner coordinates only.

Note that the asymmetry induces a natural ordering for the coordinate categories, in that the outer coordinate problem must be tackled *before* the inner coordinate problem can be dealt with. This feature is characteristic of adiabatic approximations; indeed, it is probably appropriate to view Equation 2.8 as a kind of generalized adiabatic operator, where the fast and slow degrees of freedom correspond to inner

and outer coordinates, respectively. The standard adiabatic approximation ensues in the special case for which the H^i_{out} are the position operators for the slow degrees of freedom.

We conclude with a rough analogy—of solely pedagogical value—between separable operators and systems of simultaneous linear equations. Solutions to the latter satisfy the standard linear algebra equation

$$\hat{A}\vec{x} = \vec{b} \tag{2.9}$$

where $\vec{x}$ is the unknown. In the general case, the number of operational steps required to solve Equation 2.9 scales as N^3, where N is the number of equations and unknowns. However, if $\hat{A}$ is diagonal, the solution requires only N operations. Moreover, each component of $\vec{x}$ can be solved independently, in any order. Diagonal matrices are thus like strongly separable operators. On the other hand, weakly separable operators are like *triagonal* matrices, for which $\vec{x}$ can be efficiently solved on a component-by-component basis, but *only* if the components are evaluated in a particular order (starting from the top of the triangle and ending at the base). The effort is greater than the diagonal case, but far less than the general case, for which a component-by-component analysis is not even possible.

2.2.3 Defining the Operator Metric

Our ultimate goal is to apply the variational calculus in order find the weakly separable $\hat{H}_0$ that most closely approximates $\hat{H}$. An operator metric must be defined; i.e. some mapping that associates a non-negative real number with a pair of operators. In analogy with the complex vector space notion of a dot product, we define the inner product of two *operators* $\hat{A}$ and $\hat{B}$ as follows:

$$\hat{A} * \hat{B} \equiv \text{tr}(\hat{\text{A}}^\dagger\hat{\text{B}}) \tag{2.10}$$

In keeping with the vector analogy, the norm of $\hat{A}$ is then given by $|\hat{A}|^2 = \text{tr}(\hat{\text{A}}^\dagger\hat{\text{A}})$, and the distance between $\hat{A}$ and $\hat{B}$ by $|\hat{B} - \hat{A}|$.

In any explicit matrix representation, the above definition of the norm becomes

$$|\hat{A}|^2 \equiv \sum_{i,j} |A_{ij}|^2 \tag{2.11}$$

where the A_{ij} are the individual matrix elements. In this form, Equation 2.11 is known as the Frobenius, or "F-norm".[14] The Frobenius norm is but one of several competing matrix norm definitions, of which the so-called "Euclidean Norm"[15,16] is usually preferred in conjunction with Hilbert space operators. One reason is that the Euclidean norm of such operators is often finite, whereas the Frobenius norm is usually infinite.

Nevertheless, for our purposes, the Frobenius norm turns out to be the most appropriate definition (Section 2.3.2). Despite the aforementioned infinities (which do not pose a significant problem—Section 2.3.3), it has many advantages. Like the standard vector norm, the Frobenius norm is representation-independent; yet it is readily calculated in any given representation as the sum of the individual matrix element square moduli. Clearly, Equation 2.11 is the most intuitive extension of the conventional complex vector norm, $|\vec{v}|^2 = \sum_i |v_i|^2$. The most compelling justification however, which at this stage is also the least obvious, is that different *subblocks* of $\hat{A}$ contribute independently to the total norm (Section 2.3.1).

2.3 Obtaining the Optimal Separable Basis

The problem of obtaining the optimal $\hat{H}_0$ is now well-formulated; namely, we seek to minimize $|\hat{H} - \hat{H}_0|$ with respect to variations of $\hat{H}_0$ subject to the weak separability constraint. This is best approached in two stages. First, for a particular choice of outer basis φ_m, we determine the best $\hat{H}_0$ and corresponding inner bases $\phi_\ell^{(m)}$. This gives rise to a new interpretation of the relationship between $\hat{H}$ and $\hat{H}_0$, as is discussed in Section 2.3.1. The second stage, discussed in Section 2.3.2, is to optimize with respect to a variation of the outer basis set.

2.3.1 Optimization with Respect to a Fixed Outer Basis

For this subsection, a definite, fixed choice of the outer basis set φ_m is assumed throughout; although the particular choice itself is arbitrary. Consider the explicit representations of $\hat{H}$ and $\hat{H}_0$ in the partially diagonal basis

$$|q_1, \ldots, q_k, m\rangle = |q_1, \ldots, q_k\rangle|\varphi_m\rangle \tag{2.12}$$

Now consider all weakly separable variations of $\hat{H}_0$ whose eigenfunctions incorporate the particular outer basis set φ_m selected above. While the form of $\hat{H}$ in the new basis is generally quite arbitrary, the form of $\hat{H}_0$ is constrained to be block-diagonal in m (i.e. a $\delta_{mm'}$ factor is present). Apart from this constraint however (as well as that of hermiticity), the form of $\hat{H}_0$ is otherwise completely arbitrary. From Equation 2.11 however, it is clear that *the minimal* $|\hat{H} - \hat{H}_0|$ *ensues when* $\hat{H}_0$ *is defined as the block-diagonal portion of* $\hat{H}$.

This fact is true because the block-diagonal and the off-block-diagonal portions of $\hat{H}$ contribute to the total F-norm independently. Specifically, the contribution of the latter to the norm of the residual must be the same for all choices of $\hat{H}_0$, whereas the former can clearly be reduced to nothing by simply declaring $\hat{H}_0$ to be the actual diagonal blocks of $\hat{H}$. Adopting this choice for $\hat{H}_0$, the residual matrix $\hat{\Delta} \equiv \hat{H} - \hat{H}_0$ is comprised of just the off-block-diagonal matrix elements of $\hat{H}$.

We shall find it very convenient to interpret $\hat{H}$ as a collection of coupled k-dimensional subsystems. To be more specific, each block of $\hat{H}_0$ represents a particular subsystem of the inner coordinates only (labelled $\tilde{H}_{mm}$); and the whole $\hat{H}_0$ represents an $(n-k)$-dimensional collection of such subsystems parametrized by the outer index m.

According to this interpretation, the off-block-diagonal elements $\hat{\Delta}$ must clearly represent the coupling constants between subsystem pairs. Since the full $\hat{H}$ is in general a rank-$2n$ tensor, and $\hat{H}_0$—by virtue of being block-diagonal—is a tensor of rank $(n+k)$, the coupling constants are of larger rank than the subsystems themselves, generally speaking.[†] For most Hamiltonians of physical or chemical interest however,

[†]In this context "rank" refers to the dimensionality of a generalized tensor, rather than to the number of non-zero eigenvalues of a matrix.

$\hat{H}$ is *sparse* in that the majority of the position representation matrix elements are zero; and the inner coordinates can be chosen so that $\hat{\Delta}$ is actually of rank $(2n-k)$ or less (Section 2.5.1).

Having determined the optimal $\hat{H}_0$ for a particular outer basis set φ_m, it remains only to minimize $|\hat{\Delta}|$ with respect to a variation of this outer basis. According to the coupled subsystems picture, this is equivalent to *minimizing the total subsystem coupling* in the usual least-squares sense. This intuitively satisfying interpretation holds only by virtue of the Frobenius norm metric; indeed, the coupled subsystem perspective *itself* would be inappropriate if one were to use a different definition of the norm.

2.3.2 Optimizing the Outer Basis

In quantum mechanics, a general change of basis is effected via a unitary transformation. For our purposes, since we are interested in varying the outer basis only, we must restrict ourselves to unitary transformations involving *only* the outer coordinates $\hat{q}_{k+1}, \hat{p}_{k+1}, \ldots, \hat{q}_n, \hat{p}_n$. In other words we consider only those unitary transformations[‡]

$$\hat{H}' = \hat{U}^\dagger \hat{H} \hat{U} \quad \text{for which} \quad \hat{U} = U(\hat{q}_{k+1}, \hat{p}_{k+1}, \ldots, \hat{q}_n, \hat{p}_n). \tag{2.13}$$

This restriction has two advantages, the first being that $\hat{U}$ has no effect on the $\hat{q}_1, \hat{p}_1, \ldots, \hat{q}_k, \hat{p}_k$ due to Equations 2.2, so that the $\hat{H}$ dependence on these coordinates is unaffected by the transformation. Classically, $\hat{U}$ (if unitary) is analogous to a canonical transformation of the following form:

$$\left.\begin{aligned} Q_i &= q_i \\ P_i &= p_i \end{aligned}\right\} \text{for } i \leq k. \tag{2.14}$$

$$\left.\begin{aligned} Q_i &= Q_i(q_{k+1}, p_{k+1}, \ldots, q_n, p_n) \\ P_i &= P_i(q_{k+1}, p_{k+1}, \ldots, q_n, p_n) \end{aligned}\right\} \text{for } i > k.$$

The (passively) transformed $\hat{H}$ can therefore be written as

$$\hat{H} = H'(\hat{q}_1, \hat{p}_1, \ldots, \hat{q}_k, \hat{p}_k; \hat{Q}_{k+1}, \hat{P}_{k+1}, \ldots, \hat{Q}_n, \hat{P}_n), \tag{2.15}$$

[‡]Strictly speaking, $\hat{U}$ may be isometric.

for which the new position representation would correspond to what we have been calling the "partially diagonal basis."

The second advantage is that determining the optimal outer basis is a problem of reduced dimensionality. Mathematically, we have a constrained eigenvector problem where the *inner* coordinates now play the role of parameters. The k-dimensional constraint on $\hat{U}$ generally disallows complete block-diagonalization of $\hat{H}$; nevertheless, minimizing $|\hat{\Delta}|$ has the effect of removing all *unessential* non-separability from the system. Indeed, if $\hat{H}$ happens to be weakly separable to begin with, then it can be block-diagonalized by some $\hat{U}$ of the Equation 2.13 form, in which case *all* of the coupling is removed, as is intuitively appropriate. In the general case $|\hat{\Delta}|$ cannot be made to vanish altogether, but can be greatly reduced—via the optimal choice of outer basis—so as to reflect only the minimal coupling actually inherent in the system.

Note that since $|\hat{H}|^2$ is representation-independent and

$$|\hat{H}|^2 = |\hat{H}_0|^2 + |\hat{\Delta}|^2, \tag{2.16}$$

minimizing $|\hat{\Delta}|$ is equivalent to maximizing $|\hat{H}_0|$.[§] The latter approach is often more convenient because the total $\hat{H}_0$ contribution above is simply $\sum_m |\tilde{H}_{mm}|^2$, where the norm is now a dimensionally-reduced version of Equation 2.11 acting on the inner coordinates only.

In any event, we seek the optimal choice of the set φ_m; and as with all variational methods, optimization is signalled by candidates which satisfy an appropriate stationarity condition. In our case, $|\hat{\Delta}|$ must be stationary with respect to all infinitesimal outer unitarity transformations, of which we need only consider the elementary (pair-wise) transformations explicitly. By evaluating all pairs independently, we obtain the following:

$$\boxed{\tilde{H}_{mm'} * (\tilde{H}_{mm} - \tilde{H}_{m'm'}) = 0 \qquad \text{for all } \{m, m'\}} \tag{2.17}$$

where $\tilde{H}_{mm'} \equiv \langle \varphi_{m'} \mid \hat{H} \mid \varphi_m \rangle$. The operators $\tilde{H}_{mm'}$ etc., being blocks of the full Hamiltonian in the partially diagonal representation, act on the inner coordinates

[§]One must be careful when infinities are involved, however.

only. The '$*$' operation is simply the inner coordinate version of the Equation 2.10 matrix dot product affiliated with the Frobenius norm metric.

Equation 2.17 above is thus the desired optimization condition, and perhaps the central result of this entire dissertation. Note that this equation can be naturally interpreted as a *mutual orthogonality condition* on the blocks of $\hat{H}$. Although Equation 2.17 is simple and intuitive, it applies only in the φ_m representation. It does not, for instance, provide us with some differential equation in the *original* coordinates, as do many other applications of the variational method.

Nevertheless, Equation 2.17 still serves as a very useful guide in particular applications. The optimal outer basis can always be determined numerically, for example, using a simple block algorithm[17] that is the focus of Chapter 3. Analytically, any intuitively selected candidate for the optimal φ_m can always be checked directly against Equation 2.17. Even if the equality fails, the lack of orthogonality can be used a measure of "efficiency," or proximity to optimality. If the optimal basis is analytically intractible, then a nearly optimal subsitute should do almost as well (Section 2.5.2).

This situation is somewhat analogous to that of Weinberg's quasiparticle approach to converging the Born series.[18] Weinberg's approach allows us to define a quasiparticle however we like; and a physically intuitive choice is almost always beneficial even if the mathematically optimal solution is unattainable. In the Weinberg formalism however, there is no analogue of Equation 2.17—and thus no way to determine whether or not a given choice is close to optimal.

2.3.3 Existence, Uniqueness, and Infinities

It is important to note that Equation 2.17 is in principle applicable even to non-square-integrable Hamiltonians—i.e., to systems for which the Frobenius norm of $\hat{H}$ is infinite. In numerical applications, for which the matrix representations must be finite, these infinities do not arise of course. However, if one is interested in an exact mathematical analysis of the true Hilbert space operators, this fact is very significant because almost all Hamiltonians of physical interest are infinite!

Note that the divergence of $|\hat{H}|$ does *not* imply that $|\hat{\Delta}|$ is also infinite—indeed, $|\hat{\Delta}|$ is finite for all systems that conform to the standard scattering criteria.[6] This is easily shown using the optimal *strongly* separable basis, and the fact that said basis is necessarily weakly separable. For standard T+V Hamiltonians (Section 2.5), the optimal strongly separable $\hat{H}_0$ has the form $\hat{T} + \hat{V}_{\text{in}.} + \hat{V}_{\text{out}}$, so that the residual $(\hat{V} - \hat{V}_{\text{in}} - \hat{V}_{\text{out}})$ is a simple function of position. $|\hat{\Delta}|^2$ is therefore just the integral of the square of this function over configuration space. But this quantity is finite by virtue of the asymptotic restrictions imposed upon the potential by standard scattering theory.[6]

Nevertheless, there are undoubtedly certain physically interesting cases for which $|\hat{\Delta}|$ *is* infinite in all representations (Section 2.6), as a result of which it may not be intuitively obvious which representation is the best. Even in such cases however, the stationarity condition is still meaningful because Equation 2.17 relies only on the *orthogonality* of the $\tilde{H}_{mm'}$, and not on their normalizability.

Normalizability in and of itself is therefore not the principal concern. Of greater importance is whether or not an optimal solution actually exists for a given system. Equation 2.17 is silent on this subject—it merely reflects the conditions that would have to be satisfied, should a solution exist. There might be no stationary solutions, or several. In the latter event, one would like to be able to distinguish the true minimal solutions from the maxima and saddle points. Although we do not at present know how to resolve these questions for a completely arbitrary system, we can nevertheless prove that at least one stationary minimum exists if certain reasonable conditions are maintained.

Consider a parametrized, outer coordinate unitary transformation operator

$$\hat{U}(\phi_1, \phi_2, \ldots) \tag{2.18}$$

such that $\hat{U}$ is periodic in each of the parameters ϕ_i, and such that any arbitrary unitary operator can be obtained by plugging in an appropriate set of parameter values. This could be constructed from a (possibly infinite) product of successive elementary unitary transformations between different (m, m') pairs. Each elementary operator, being a 2×2 (unimodular) unitary matrix, is parametrized by three angles,

and is periodic in those angles. The collection of all such angles can thus be taken to be the ϕ_i above; and by incorporating an arbitrarily large number and variety of elementary operators, we can generate any desired $\hat{U}$. (It does not matter if the set of all $\hat{U}$'s is overspecified).

By incorporating the parametrized $\hat{U}$ above, the residual norm in any representation is conveniently expressed as a real-valued function of the parameters; i.e. $|\hat{\Delta}|^2 \equiv F(\phi_1, \phi_2, \ldots)$. A stationary outer basis is therefore presented to us whenever the first partial derivatives of F with respect to the ϕ_i are all zero. If F is continuous and differentiable everywhere, then at least one stationary minimum exists. This is true because the parameter space, being a product of compact spaces, is itself compact by virtue of Tychonoff's theorem.[19]¶

The above result can be extended to non-continuous F's by requiring only that continuous first partial derivatives

$$\frac{\partial F(\phi_1, \phi_2, \ldots)}{\partial \phi_i} = f_i(\phi_1, \phi_2, \ldots) \tag{2.19}$$

exist everywhere, and by invoking the finite intersection property for the family of contour sheets defined by $(f_i = 0)$.[19] This enables us to prove the existence of a stationary point even when F is non-finite.‖ However, the partial derivative condition is still more restrictive than is necessary. Section 2.6 for example, presents a system for which the partial derivatives can be infinite even though a stationary point exists. Consequently, we suspect that a more comprehensive existence proof can be obtained; and this possibility will be a subject for future investigation.

2.3.4 Self-Consistent Field Interpretation

We conclude this section with a brief comparison between the optimal separable basis approach and the Hartree-Fock or self-consistent field theories. In the latter, one considers separable approximations of the form

$$\Phi_{\ell m} = \phi_\ell^{(m)}(q_1, \ldots, q_k)\, \varphi_m^{(\ell)}(q_{k+1}, \ldots, q_n). \tag{2.20}$$

¶This even holds for a non-countably infinite product of compact spaces.

‖An example of a non-finite function with well-defined first partial derivatives everywhere is $F(\phi_1, \phi_2, \ldots) = \cos(\phi_1) + \cos(\phi_2) + \ldots$

The optimal $\Phi_{\ell m}$'s are usually defined as those for which the expectation value of the energy is stationary. Since both inner and outer functions depend on *all* the quantum numbers, the $\Phi_{\ell m}$ are not generally orthogonal and do not form a basis.

In contrast, the optimal separable basis consists of $\Phi_{\ell m}$ wave-functions which *are* mutually orthogonal. Moreover, the stationarity criterion is *identical* to that of the self-consistent field. The comparison is most easily made by representing $\hat{H}$ in the optimal separable basis itself. $\hat{H}_0$ now comprises the diagonal matrix elements of $\hat{H}$, which are nothing more than the energy expectation values of the $\Phi_{\ell m}$. Because $|\hat{H}|^2 = |\hat{H}_0|^2 + |\hat{\Delta}|^2$ is representation-independent, we have a stationarity condition on the *sum* of the energy expectation value square moduli, rather than on the individual expectation values themselves. Our approach can therefore be considered a self-consistent field approximation of the complete energy *basis*, rather than of the individual energy eigenfunctions.

In numerical applications, which are of necessity finite, it is not the entire Hilbert space basis that is optimized, but only some finite subset. This fact can actually be used to advantage—for example, to optimize a separable basis for a specific energy range. In comparison, Hartree-Fock theory offers two standard possibilities, each with certain drawbacks. If Equation 2.20 is applied to each state in the given energy range, the non-orthogonality of the resulting wavefunctions implies, for example, a non-trivial multi-configuration expansion. Alternatively, one can use the Hartree-Fock ground state potential to obtain *all* of the states in a specified range, not just the ground state. The resultant wavefunctions are now orthogonal, but are no longer optimized for the excited states.

It is also interesting to ask, in light of Section 2.3.3, whether the existence of Hartree-Fock solutions are in general guaranteed. Curiously, despite the long-standing use of self-consistent methods, this question has only been addressed in comparatively recent history. Indeed, the general question still remains unanswered; although for atomic and molecular systems, Lieb proved the interesting result that a minimizing solution is not guaranteed when the system has more electrons than protons.[20]

2.4 Series Expansions

A separable basis approximation of the eigenstates of a multi-dimensional Hamiltonian is certainly desirable in its own right—particularly one that is "best" in the self-consistent field sense. It is also of interest, however, to obtain more accurate results via series expansions that use the optimal $\hat{H}_0$ as a starting point. When actually performing such expansions, whether analytically or numerically, the issue of series convergence always arises. Intuitively, we expect convergence to improve as the residual $\hat{\Delta}$ is diminished. Thus the optimal $\hat{H}_0$ suggested above should result, heuristically speaking, in the fastest convergence. Rigorously speaking however, it is not always clear what constitutes "optimal convergence" for an *operator* series, as the situation is less straightforward than in the usual real or complex number case.

2.4.1 Time-independent Perturbation Theory

We shall first consider a time-independent perturbation expansion for the eigenvalues and eigenfunctions of $\hat{H}$. We designate the optimal separable $\hat{H}_0$ of Section 2.3 as the zeroth-order approximation to the full Hamiltonian. Thus, the optimal separable basis itself comprises the zeroth-order eigenfunction approximations. The zeroth-order energies $E^{(0)}_{\ell,m}$, due to the definition of $\hat{H}_0$ (Section 2.3.1), are conveniently expressed as the diagonal matrix elements of $\hat{H}$ when the latter is represented in the optimal separable basis. Note that once the φ_m are known, one can get $\hat{H}_0$ directly in the partially diagonal basis without obtaining the $\phi^{(m)}_\ell$. In a perturbation treatment however, we must solve for the $\phi^{(m)}_\ell$ explicitly by diagonalizing $\hat{H}_0$. In the partially diagonal representation, this is a comparatively simple task, in light of $\hat{H}_0$'s block-diagonal structure. The diagonalization problem—now separable—reduces to a k-dimensional eigenproblem parametrized by the outer index m.

It can be shown that our choice for $\hat{H}_0$ is always sufficiently close to $\hat{H}$ that the first order perturbation theory corrections to the eigenenergies are all *zero*. These are given by standard time-independent perturbation theory as follows:

$$E^{(1)}_{\ell,m} = \langle\varphi_m|\langle\phi^{(m)}_\ell|\hat{\Delta}|\phi^{(m)}_\ell\rangle|\varphi_m\rangle \tag{2.21}$$

In the partially diagonal basis, the block-diagonal nature of $\hat{H}_0$ implies outer coordinate wavefunctions that are delta functions. On the other hand, the matrix elements of $\tilde{\Delta}_{mm'} = (1 - \delta_{mm'})\tilde{H}_{mm'}$ are by definition zero for m equal to m'. Thus, the first order energy corrections in Equation 2.21 above must be zero.

The first-order corrections to the eigenfunctions are as follows:

$$|\Phi_{n\ell}\rangle^{(1)} = |\Phi_{n\ell}\rangle + \sum_{n\ell \neq n'\ell'} C_{n\ell,n'\ell'}|\Phi_{n'\ell'}\rangle \tag{2.22}$$

$$\text{where} \qquad C_{n\ell,n'\ell'} = \frac{\langle \Phi_{n'\ell'}|\hat{\Delta}|\Phi_{n\ell}\rangle}{E^{(0)}_{n\ell} - E^{(0)}_{n'\ell'}} \tag{2.23}$$

Equation 2.23 informs us that the optimal basis is the one which minimizes, in the usual least-squares sense, the collection of first-order eigenfunction corrections weighted by the energy differences. This interpretation cannot be extended beyond the first order. When higher orders are considered however, it is not at all clear that "optimal convergence" is even well-defined; since the minimization condition varies with the order of expansion (Chapter 3 appendix, page 85). Nevertheless, corrections of any given order involve as many factors of the $\hat{\Delta}$ matrix elements; and it is clear that convergence will improve, generally speaking, as $|\hat{\Delta}|$ is diminished.

2.4.2 Born Series Expansion

In microcanonical scattering applications (Chapter 3), the main object of interest is the energy Green's operator

$$\hat{G}(E) = \lim_{\epsilon \to 0}(E + i\epsilon - \hat{H})^{-1}. \tag{2.24}$$

Although $\hat{G}(E)$ is actually a (non-Hermitian) operator, the position representation is often referred to as the "Green's function."[21–23] The diagonal representation, also known as the "Lehmann representation"[24–26] is closely related to the spectral density function.

In evaluating Equation 2.24, we shall find it useful to divide the Hamiltonian $\hat{H}$ into two pieces so that

$$\hat{H} = \hat{H}_0 + \hat{\Delta} \tag{2.25}$$

where for the moment, $\hat{H}_0$ is arbitrary. It is assumed only that $\hat{H}_0$ is invertible (non-singular), so that the corresponding $\hat{G}_0(E) = \lim_{\epsilon\to 0}(E + i\epsilon - \hat{H}_0)^{-1}$ is well-defined. In the standard approach, $\hat{H}_0$ is the asymptotic form of the Hamiltonian, whose characteristic functions are the asymptotic scattering states most frequently associated with the S-matrix.[6,27–29]

However, it is often more convenient to use so-called "distorted waves," corresponding to a more general $\hat{H}_0$. In the usual distorted wave methodology, the residual $\hat{\Delta}$ has the form of a potential (i.e. it depends on the $\hat{q}_i$ only); and $\hat{G}_0$ is called the "distorted wave Green's function."[6,30] However, we find it appropriate to make use of the same terminology even when $\hat{\Delta}$ and $\hat{H}_0$ may take the completely general form of Equation 2.25.

In any event, the full Green's function $\hat{G}$ can be expressed in terms of the distorted wave Green's function $\hat{G}_0$ via the following "distorted wave Born expansion:"

$$\hat{G} = \hat{G}_0 + \hat{G}_0\hat{\Delta}\hat{G}_0 + \hat{G}_0\hat{\Delta}\hat{G}_0\hat{\Delta}\hat{G}_0 + \ldots \tag{2.26}$$

In principle, one attempts to partition as much of $\hat{H}$ into $\hat{H}_0$ as possible, so that the resultant expansion converges quickly. Thus, whereas in elastic scattering $\hat{H}_0$ is typically just the kinetic energy, the usual distorted $\hat{H}_0$ includes some of the potential as well. On the other hand, $\hat{G}_0$ must be known explicitly; so that nothing is gained unless inverting $(E+i\epsilon-\hat{H}_0)$ is significantly more tractable than the original problem, i.e. inverting $(E + i\epsilon - \hat{H})$ itself.

The optimal separable basis methodology provides us with a different kind of candidate for $\hat{H}_0$. Note that this choice satisfies both of our criteria for a good distorted wave Green's function. Specifically, block-diagonality can be exploited so as to render the inversion a parametrized k-dimensional problem rather than an n-dimensional one; yet at the same time, the minimization of $|\hat{\Delta}|$ is expected to improve the convergence of Equation 2.26. The optimal separable basis functions themselves therefore constitute an optimized set of distorted waves.

Note that the optimal separable $\hat{H}_0$ is not constrained to yield a potential-like residual; consequently Equation 2.26 will converge faster than for any conventional choice of distorted wave. However, there is one other unconventional dis-

torted wave method—to our knowledge the only other one—which does not require a potential-like residual. This method is the S-matrix version of the Kohn variational principle.[28–35] It would be interesting to compare the present methodology versus an application of the S-matrix Kohn method for a particular molecular system, although this dissertation does not include such a direct comparison.

In any event, insofar as a rigorous analysis of convergence is concerned, we can make some progress by acknowledging that Equation 2.26 is essentially a geometric series of the dimensionless kernel matrix $\hat{A} \equiv \hat{G}_0\hat{\Delta}$ (Section 3.4). In fact, if $\hat{\Delta}$ satisfies certain conventional scattering criteria, then the convergence of the Born series is determined solely by the eigenvalues of $\hat{A}$.[18,36] In particular, Equation 2.26 converges if and only if

$$|\lambda_i| < 1 \qquad \text{for all } i, \tag{2.27}$$

where the λ_i are the eigenvalues of $\hat{A}$.

One can derive, in terms of the λ_i, an expression for the rate of convergence out to any finite-indexed term in the Equation 2.26 expansion—the details are worked out in the appendix of Chapter 3 (page 85). Unfortunately, the resulting minimization condition depends on the level of expansion, so that a general definition of "optimal" convergence for all orders of expansion is not in general possible. Nevertheless, it is clear from Equation 2.26 that convergence will—as a rule—improve as $|\hat{\Delta}|$ is decreased, since both $\hat{\Delta}$ and $\hat{G}_0$ diminish with $|\hat{\Delta}|$.

2.5 Application to T+V Hamiltonians

2.5.1 Orthogonality Condition

Although the method presented in Section 2.3 is certainly applicable to arbitrary quantum systems, we ask in this section whether the analysis can be at all simplified if the Hamiltonian is of the form $\hat{T} + \hat{V}$ where $\hat{T}$ and $\hat{V}$ are kinetic and potential energies, respectively. Invariably, $\hat{V}$ is a function of the position coordinates only; i.e. $V = V(\hat{q}_1, \ldots, \hat{q}_n)$. If the $\hat{q}_i$ and $\hat{p}_i$ are standard rectilinear coordinates,

then the kinetic energy usually takes the strongly separable form

$$\hat{T} = T(\hat{p}_1, \ldots, \hat{p}_n) = \sum_{i=1}^{n} T_i(\hat{p}_i). \tag{2.28}$$

If generalized coordinates are being used however, the kinetic energy will depend on the position coordinates (Chapter 4). The most general kinetic energy is an arbitrary position-dependent quadratic form in the $\hat{p}_i$. In molecular applications however, one often encounters orthogonal kinetic energies; i.e. there are no cross terms in the $\hat{p}_i$, so that $\hat{T}$ is a position-dependent version of Equation 2.28.

As it happens, the optimal separable approach is greatly simplified if the kinetic energy can be expressed in the following form:

$$\hat{T} = T_{\text{in}}(\hat{q}_1, \hat{p}_1, \ldots, \hat{q}_k, \hat{p}_k) + T_{\text{out}}(\hat{q}_1, \ldots, \hat{q}_k; \hat{q}_{k+1}, \hat{p}_{k+1}, \ldots, \hat{q}_n, \hat{p}_n), \tag{2.29}$$

The kinetic energy thus separates into an inner term and an outer term, each of which may depend on position. There is an asymmetry however, in that T_{out} may depend on the inner coordinates, but not vice-versa. Generally speaking, the class of Equation 2.29 kinetic energies is less restrictive than the class of orthogonal kinetic energies, although the two concepts are closely related. In fact, almost all orthogonal kinetic energies that are encountered in practice will conform to Equation 2.29 for at least one partitioning of the coordinates. However, it is mathematically possible to construct an orthogonal kinetic energy that does not conform to Equation 2.29; this will be the case if and only if every term in Equation 2.28 depends on *all* of the position coordinates.

Hamiltonians of the Equation 2.29 form—i.e. $\hat{H} = \hat{V} + \hat{T}_{\text{in}} + \hat{T}_{\text{out}}$—exhibit a large amount of sparsity, in that each term is a tensor of reduced dimensionality. Specifically, $\hat{V}$ is a rank-n tensor, while $\hat{T}_{\text{in}}$ and $\hat{T}_{\text{out}}$ are tensors of rank $2k$ and $(2n-k)$ respectively. What is important for our purposes is that the sparse form of Equation 2.29 is *retained under a unitary transformation of the outer coordinates.* The $\hat{T}_{\text{in}}$ component is, of course, completely unaltered because it is a function of the inner coordinates only. The $\hat{H}_{\text{out}} \equiv \hat{T}_{\text{out}} + \hat{V}$ operator—treated as a single unit—is a sparse tensor of rank $(2n-k)$ that is block diagonal in the $(q_1, \ldots, q_k)$, both before and after the unitary transformation is applied.

These facts are very beneficial from the standpoint of trying to find the optimal outer basis. In particular, the preservation of sparsity ensures that the vast majority of the coupling constants will be zero. Moreover, $\hat{T}_{\text{in}}$ can be completely ignored, as a result of which the orthogonality condition (Equation 2.17) reduces to a simple integral:

$$\int H_{\text{out}}^{mm'*}(q)(H_{\text{out}}^{mm}(q) - H_{\text{out}}^{m'm'}(q))\, dq = 0 \qquad \text{for all } \{m, m'\} \tag{2.30}$$

where $q \equiv (q_1, \ldots, q_k)$.

Note that where the outer basis is concerned, $\hat{H}_{\text{out}}$ has replaced $\hat{H}$ as the relevant operator. It is natural to view the former as a collection of $(n-k)$-dimensional *outer* subsystems parametrized by the *inner* coordinates. By optimizing the outer basis, we are in effect trying to *simultaneously diagonalize the entire collection collection of* $(n-k)$*-dimensional subsystems* $\hat{H}_{\text{out}}$. In the general case, one cannot *actually* diagonalize all of the subsystems using a single basis; but the optimal choice is the best compromise in the least-squares sense.

2.5.2 Partitioning of Coordinates

For an n-dimensional problem, there are 2^n distinct partitionings of coordinates into inner and outer categories, each of which can potentially lead to a different optimal $\hat{H}_0$. In deciding which particular partitioning should be adopted, the results of the previous subsection can serve as a useful guide.

One should, if possible, choose a (nontrivial) partitioning which satisfies Equation 2.29; for in addition to simplifying the analysis, the majority of the coupling constants will be *zero* by virtue of the sparse form of $\hat{H}_{\text{out}}$. The availability of such choices is related to the separability of the kinetic energy. If $\hat{T}$ is completely separable, as in the standard rectilinear case, then any partitioning will do. Only when the kinetic energy is completely *non*-separable can no such partitioning be found, in which case a change of coordinates might be employed to induce a separation.

As is evident from Equation 2.29, the kinetic energy need not be *strongly* separable, as $\hat{T}_{\text{out}}$ may depend on all of the position coordinates. If $\hat{T}$ does happen to

be strongly separable however, then exchanging the inner for the outer coordinates also satisfies Equation 2.29. To determine which is the better choice, the simultaneous diagonalization interpretation of Section 2.5.1 can be fruitfully called upon. If $(\hat{T}_{\text{out}} + \hat{V})$ were to vary only *slightly* with the inner coordinate parameters, then the various subsystems would be almost identical, and would therefore be almost entirely diagonalized by the best-fit outer basis. One is thus led to select—as inner coordinates—those $\hat{q}_i$ upon which the original Hamiltonian has the *least* dependence.

As a special case, consider the completely separable position-independent kinetic energy of Equation 2.28, for which the coordinates have been mass-weighted so that the T_i's are all of identical form. The subsystems of $(\hat{T}_{\text{out}} + \hat{V})$ are now identical except for the potential energy $\hat{V}$ which depends on the positions only; thus, selecting inner coordinates involves nothing more than a straightforward analysis of the function $V(q_1, \ldots, q_n)$. A simple intuitive candidate for the optimal basis is suggested—namely, that basis which diagonalizes $\hat{T}_{\text{out}} + \langle \hat{V} \rangle_q$ where $\langle \hat{V} \rangle_q$ is the collection-averaged potential energy function. While this choice is not generally the optimal one—indeed, the true optimum may not even be of the form $T_{\text{out}}(\hat{p}_{k+1}, \ldots, \hat{p}_n) + V(\hat{q}_{k+1}, \ldots, \hat{q}_n)$—it should nevertheless reduce the coupling significantly, and is in any case readily obtainable even when a determinination of the true optimum is intractible.

2.5.3 Inelastic Scattering

In inelastic scattering applications, the above $\hat{T}_{\text{out}} + \langle \hat{V} \rangle_q$ candidate is closely related to the coupled channel approximation, for which one uses the asymptotic, rather than the average potential. In fact if we were to generate our outer basis from $\hat{T}_{\text{out}} + V_{\text{as}}(\hat{q}_{k+1}, \ldots \hat{q}_n)$, and restrict ourselves to the energetically accessible bound states only (the open channels), then exactly the coupled channel approximation would result. In such inelastic applications, a natural separation between internal (intrafragment) and translational (interfragment) coordinates arises. The potential usually varies less with the latter, which is why the internal coordinates are chosen (perhaps counterintuitively) to be the *outer* coordinates. The asymptotic potential is then defined as the limit of V as q approaches infinity.

A primary advantage of the coupled channel approach is that $\hat{G}(E)$ can be accurately determined using a small and finite outer basis, provided the energy E is sufficiently lower than some cutoff value used to truncate the basis set. Although finite, the various channels are still coupled together. An uncoupled approximation can be obtained by ignoring the off-block-diagonal matrix elements of $\hat{H}$. This is, in fact, a standard way to *define* distorted waves in the multi-channel case.

It is clear that the uncoupled channel approximation above constitutes, in our language, a choice of $\hat{H}_0$. We can therefore think of the *optimal* $\hat{H}_0$ as the choice which redefines the channels in the best possible way, vis-a-vis minimizing the interchannel coupling. This should generally improve the convergence of the resultant multichannel distorted wave Born expansion, although very little is rigorously known about this subject.[6]

2.6 Results—Shifted Harmonic Oscillator

As an analytical benchmark system, we consider the two-dimensional shifted harmonic oscillator Hamiltonian, i.e.

$$\hat{H} = \frac{\hat{p_x}^2}{2m} + \frac{\hat{p_y}^2}{2m} + \frac{m\omega^2}{2}(\hat{y} - f(\hat{x}))^2 \tag{2.31}$$

where $f(x)$ is the shifting function. Physically, this Hamiltonian might describe a particle in a surface channel etched along the curve $y = f(x)$, or perhaps a simple harmonic oscillator whose equilibrium position was somehow constrained to lie on the curve (Figure 2.1). For the first part of our analysis we can allow the shifting function to be arbitrary; although later a specific form will be provided. For now, it should simply be mentioned that in the limit $f(x) \to 0$, $\hat{H}$ approaches the separable system consisting of a free particle in x and a harmonic oscillator in y.

If $f'(x)$ approaches zero in the infinite limits, then separable asymptotic states exist in those limits, and we can think of this as a scattering system with channels defined along y. As a scattering system it is somewhat unusual however; for although there is a clearly defined reaction path along $y = f(x)$, there is no transition state or equilibrium geometry *per se*, as the potential is constant along the reaction

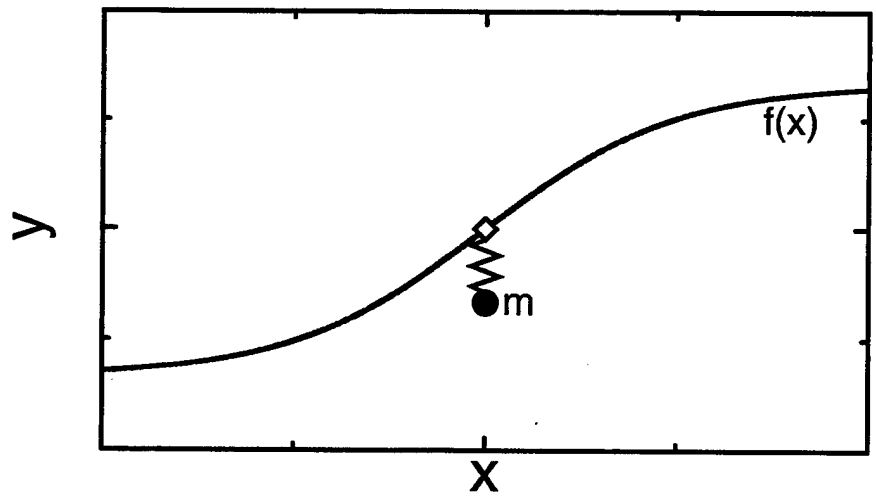

Figure 2.1: Physical schematic of the shifted harmonic oscillator.

path. Adopting the reaction path perspective, any scattering that may arise is thus solely attributable to the curvature of the path itself rather than the potential along the path. Although the dynamical effects of curvature may be just as significant as those of the potential itself in many real systems, the contribution of the former is generally less well understood. The shifted harmonic oscillator system can therefore serve as a useful benchmark application because it isolates the effects of curvature.

Since the kinetic energy is completely separable and position-independent, Equation 2.29 is satisfied by any partitioning into inner and outer coordinates. The only nontrivial value for k is unity; so we are left with deciding whether x or y is the inner coordinate. We expect $V(x, y)$ to vary less with x than with y, which is particularly valid as $f(x)$ becomes small. In light of Section 2.5.2, The natural choice for the inner coordinate is thus x.

The first task is to optimize the outer basis via a unitary transformation in $\hat{y}$ and $\hat{p}_y$. As we have seen (Section 2.5.1), this is equivalent to finding the basis which best diagonalizes the following x-parametrized collection of one-dimensional

Hamiltonians:

$$\hat{H}_{\text{out}}(x) = \frac{\hat{p_y}^2}{2m} + \frac{m\omega^2}{2}(\hat{y} - f(x))^2 \tag{2.32}$$

In light of Section 2.5.3, we choose the eigenfunctions of $\hat{p_y}^2/2m + \frac{1}{2}m\omega^2(\hat{y} - \langle f \rangle)^2$ as our initial guess, where $\langle f \rangle$ is the mean value of $f(x)$. For convenience, we force $\langle f \rangle = 0$ by constraining $f(x)$ to be an odd function. This results in $V(y) = ky^2/2$ which, as it happens, is also equal to $\langle V(y) \rangle$ apart from an immaterial constant.

Our candidate outer basis functions then, are the well-known harmonic oscillator eigenstates. We have not yet proven that this is an optimal choice; but we will soon do so—even for $f(x)$ not small—by demonstrating that Equation 2.30 is satisfied. When expressed in the partially diagonal basis, $\hat{H}_{\text{out}}$ takes on a *block-tridiagonal* form, where the off-block-diagonal terms arise from the $yf(x)$ cross terms in the potential. Specifically, we have

$$H^{ll'}_{\text{out}}(x) = \frac{(2l+1)\hbar\omega + m\omega^2 f^2(x)}{2} \qquad \text{for } l - l' = 0 \tag{2.33}$$

$$H^{ll'}_{\text{out}}(x) = -\sqrt{\frac{\max(l,l')\hbar\omega^3 m}{2}} f(x) \qquad \text{for } |l - l'| = 1 \tag{2.34}$$

$$H^{ll'}_{\text{out}}(x) = 0 \qquad \text{otherwise} \tag{2.35}$$

where l and l' index the y-oscillator states. Clearly, Equation 2.30 is zero for $|l-l'| \neq 1$. When $|l-l'| = 1$, the result is proportional to $\int f(x)\,dx$, which is also zero by virtue of $f(x)$ being odd. The candidate outer basis is therefore optimal! The coupling—which in the general two-dimensional case would be a tensor of rank four—is seen above to be a rank-2 function of l and x only. Note also that $H^{l,l\pm1}_{\text{out}}$ is proportional to $f(x)$—i.e., the inherent coupling vanishes as the shifting approaches zero, as expected.

Having obtained the best outer basis functions, we now examine the inner coordinate problem; i.e. the diagonalization of the diagonal blocks $\hat{T}_{\text{in}} + \hat{H}^{ll}_{\text{out}}$ that comprise $\hat{H}_0$. Note that even though the original potential involved cross terms, the new potential $\hat{H}^{ll}_{\text{out}}(x)$ is completely additive in x and l. Consequently, all blocks of $\hat{H}_0$ are diagonalized by the *same* inner basis. Thus, although the inner eigenstates are formally parametrized by l; for this particular system the l-dependence happens to disappear—i.e. the optimal *weakly* separable basis happens to be strongly separable.

Apart from an l-dependent constant, all $\hat{H}_0$ blocks are equivalent to the following one-dimensional Hamiltonian in x:

$$\hat{H}_{\text{in}} = \frac{\hat{p_x}^2}{2m} + \frac{m\omega^2}{2} f^2(\hat{x}) \tag{2.36}$$

Since $f(x)$ is odd, we have an even potential well that is concave and centered at the origin. Such a well may admit bound state solutions.

To proceed any further however, we must specify a particular form of the shifting function $f(x)$. The choice $f(x) = T_0 \tanh(\alpha x)$ is a useful one in that it represents a smooth, sigmoid progression from a $(-T_0)$-centered oscillator to a T_0-centered one. The amount of coupling can be adjusted by varying the parameter T_0, whereas the rate of change is determined by α. Moreover, the resultant inner Hamiltonian

$$\hat{H}_{\text{in}} = \frac{\hat{p_x}^2}{2m} + \frac{m\omega^2 T_0^2}{2} \tanh^2(\alpha \hat{x}) \tag{2.37}$$

can be diagonalized analytically.

In the appendix of this chapter (page 39), the (normalized) bound state eigenfunctions of Equation 2.37 are shown to be

$$\phi_n^{(\nu)}(\eta) = \frac{\sqrt{(\nu - n)\Gamma(2\nu - n + 1)}}{n!\frac{1}{2}2^\nu \Gamma(\nu + 1)} (1 - \eta^2)^{\frac{-(\nu-n)}{2}} \left(\frac{d}{d\eta}\right)^n (1 - \eta^2)^\nu \tag{2.38}$$

where $\eta = \tanh(\alpha x)$, $\sqrt{\nu(\nu+1)} = m\omega T_0/\alpha\hbar$, and $n = \{0, 1, \ldots, \text{int}(\nu)\}$. Curiously, a bound state always exists even in the limit $T_0\alpha \to 0$ (page 43).

This fact reveals an interesting feature of $\hat{H}$. If there is no shifting, there are no bound states; however, *any* amount of shifting, no matter how small, *necessarily induces at least one bound state* in $\hat{H}_0$. In the small coupling limit, $\hat{H}_0$ becomes a valid replacement for $\hat{H}$. However, since the latter has no actual bound states, the bound states of $\hat{H}_0$ must correspond to *long-lived resonances* of $\hat{H}$. This qualitative result can be used as a benchmark for comparisons with other separable or adiabatic approximation methods, such as those based on the "reaction path".[37–39]

The most rigorous adiabatic version of the reaction path Hamiltonian is probably that of Miller.[40] In this formalism, the reaction coordinate s is defined by the reaction path together with nearby paths that are locally parallel to it. In two

dimensions, the reaction coordinate contours are straight lines normal to the reaction path, which also serve to define the perpendicular coordinate Q. The approximate Hamiltonian of Miller is adiabatic in that the Q portion of the Hamiltonian (incorporating quadratic terms only) is parametrized by s.

Upon solving the quadratic problem at each point along the reaction path, one is left with an effective one-dimensional Hamiltonian in s

$$H_n^{\mathrm{RP}} = \frac{p_s^2}{2m}\left(1 - \frac{(2n+1)\kappa^2(s)}{\omega(s)}\right)^{-3/2} + V_{\mathrm{eff}}(s), \tag{2.39}$$

where n and $\omega(s)$ are respectively the vibrational quantum number and frequency associated with the Q oscillator at each point s, and $\kappa(s)$ is the curvature of the reaction path $y = f(x)$.

For the shifted harmonic oscillator system, the effective potential in the small shifting ($T_0\alpha \to 0$) limit becomes

$$V_{\mathrm{eff}} = (n + \frac{1}{2})\hbar\omega(s) = \frac{\hbar}{2}\omega\sec(\theta) \tag{2.40}$$

where $\tan(\theta)$ is the magnitude of the slope of $f(x)$. Note that the effective potential that results is actually a *barrier*, rather than a well. This is in stark qualitative contrast to the effective potential of Equation 2.37, and a somewhat surprising result. In particular, the reaction path approximation does not predict any resonances, even in the small coupling limit. Even if one were to change to the coordinate $\xi(x)$, defined so as to render the kinetic energy of Equation 2.39 equivalent to that of Equation 2.37, the resultant potential would still be a barrier due to the monotonicity of V_{eff} with respect to $|x|$.

We now consider a perturbation theory expansion of the bound states of $\hat{H}$. The optimal $\hat{H}_0$ leads to the following zeroth-order eigenfunctions and eigenvalues:

$$\Phi_{nl}(\eta, y) = \phi_n(\eta)\varphi_l(y) \tag{2.41}$$

$$E_{nl} = \frac{m\omega^2 T_0^2}{2}\left[1 - \frac{(\nu - n)^2}{\nu(\nu+1)}\right] + (l + 1/2)\hbar\omega \tag{2.42}$$

where the $\varphi_l(y)$ are the harmonic oscillator eigenstates. Since the first-order energy corrections are all zero, the additive Equation 2.42 result is correct to first order.

Moreover, the first-order eigenfunction corrections $C_{nl,n'l'}$ are all zero except when $|l-l'|=1$ and $|n-n'|$ is odd. We choose $l=l'+1, \quad n>n'$ and define $C_{l,n'n} \equiv C_{nl,n'l'}$ which are given by

$$C_{l,n'n} = \frac{\sqrt{l\hbar\omega m/2}\, T_0\, J_\nu^{(n',n)}}{\hbar + m\omega T_0^2 \left[(n^2-n'^2)/\nu - 2(n-n')\right]/(\nu+1).} \tag{2.43}$$

The first-order corrections specified in Equation 2.43 are obtained from the one-dimensional integrals

$$J_\nu^{(n',n)} \equiv \int_{-1}^{1} \phi_{n'}^{(\nu)}(\eta)\, \phi_n^{(\nu)}(\eta)\, \frac{\eta}{(1-\eta^2)}\, d\eta \tag{2.44}$$

whose closed-form expressions for the bound states are derived in the appendix. Generally speaking, the magnitudes of these integrals are much less than unity (Figure 2.2). The curves all reach an extremum at some $\nu_{\max}$ on the order of n, and then approach zero monotonically as ν is increased. The largest magnitudes are of order unity only when $n \approx n' \approx \nu$, and in general diminish as $|n-n'|$ or ν is increased. Thus, for a particular ν, the most significant contributions to Equation 2.22 will be from the $n, n' \approx \nu$ terms.

The limits $T_0\alpha \to 0$ and $T_0\alpha \to \infty$ are of interest. The former limit is that in which the shifting function and coupling—and thus, the first-order corrections—are expected to approach zero. Indeed, we find that

$$C_{l,n'n} \approx \nu\sqrt{lT_0\alpha/2}\, J_\nu^{(n',n)} \qquad \text{for} \quad \nu^2(T_0\alpha) \ll 1. \tag{2.45}$$

Thus, it is possible to have a large number of bound states ν, even as the $C_{l,n'n}$ approach zero. If we also impose a large ν limit, we find that the highly excited and continuum corrections to the low-lying eigenstates become negligible even in a relative sense. The corresponding resonances of $\hat{H}$ are therefore expected to be very long-lived indeed.

The second case of $T_0\alpha \to \infty$ represents the other extreme, in which $f(x)$ approaches a step function. In this limit we have

$$C_{l,n'n} \approx \sqrt{\frac{l}{2T_0\alpha}} \left[\frac{\nu+1}{n^2-n'^2-2(n-n')\nu}\right] J_\nu^{(n',n)} \qquad \text{for} \quad \nu(T_0\alpha) \gg 1. \tag{2.46}$$

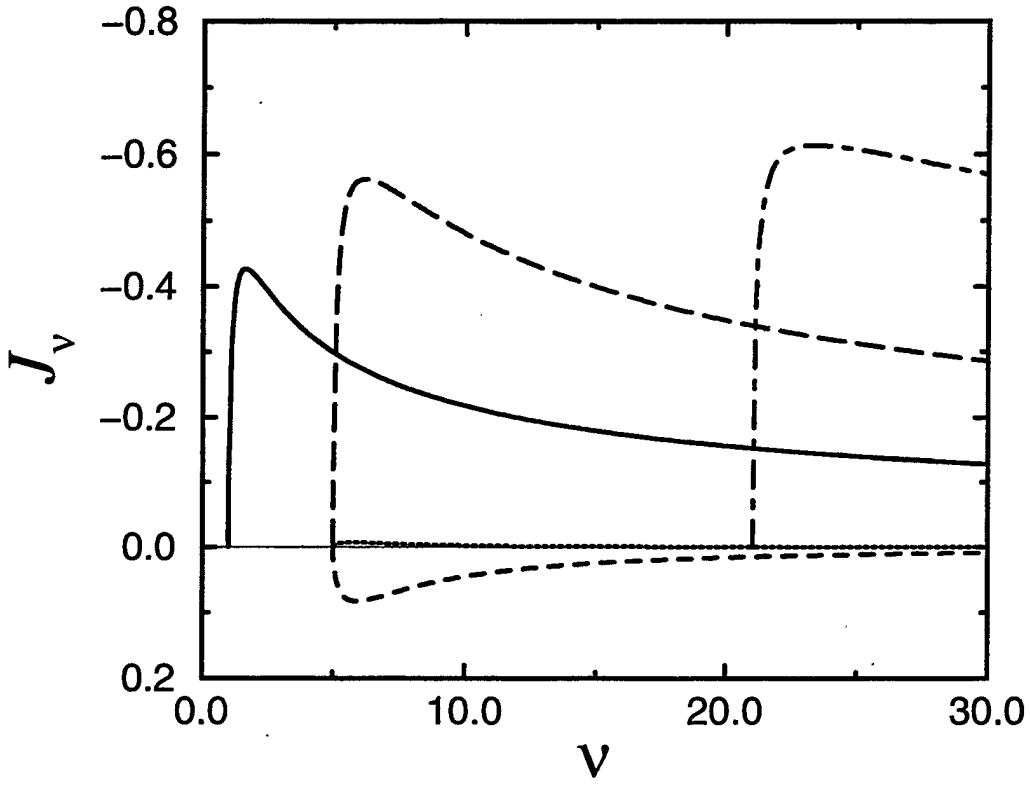

Figure 2.2: $J_\nu^{(n',n)}$ as a function of the action parameter ν, for several values of (n', n): ——— (0,1); - - - - - (0,5); — — — (2,5); ——— (4,5); - — - — - (20,21). The curves all reach an extremum at some $\nu_{\max}$ on the order of n, and then approach zero monotonically as ν is increased.

Curiously, the first-order corrections approach zero in this limit also. This is true despite the fact that the $\hat{\Delta}$ coupling terms are comparatively large, because in this limit the energy separations between the bound states are even larger.

Our final task is to evaluate the kernel matrix $\hat{A}$ pertaining to the generalized Born expansion of Equation 2.26. Because $\hat{H}$ is block-tridiagonal, and also because the $\hat{H}_0$ blocks can all be simultaneously diagonalized, it turns out to be convenient to use the Φ_{nl} basis. In this representation,

$$H_0^{l,n'n} = (E - E_{nl} + i\epsilon)\delta_{n'n} \tag{2.47}$$

is diagonal—even with the addition of the $E + i\epsilon$ terms appropriate for a Green's function analysis (Chapter 3). The coupling constants, as determined previously, are all zero except for $|l - l'| = 1$; i.e.

$$\Delta_{l,n'n} = -\sqrt{\frac{l\hbar\omega^3 m}{2}}\, T_0\, J_\nu^{(n',n)}. \tag{2.48}$$

Thus, in the corresponding representation of $\hat{A}$, only the $|l - l'| = 1$ blocks are non-zero, as follows:

$$A_{l,n'n} = \frac{\sqrt{l\hbar\omega^3 m/2}\, T_0\, J_\nu^{(n',n)}}{m\omega^2 T_0^2 \left[1 - (\nu - n)^2/\nu(\nu+1)\right]/2 + (l + 1/2)\hbar\omega - E - i\epsilon}. \tag{2.49}$$

In the limits $T_0\alpha \to 0$ and $T_0\alpha \to \infty$, Equation 2.49 reduces to the following:

$$A_{l,n'n} \approx \frac{\nu\sqrt{lT_0\alpha/2}\, J_\nu^{(n',n)}}{(l + \frac{1}{2}) - (E + i\epsilon)/\hbar\omega} \qquad \text{for} \quad \nu^2(T_0\alpha) \ll 1 \tag{2.50}$$

$$A_{l,n'n} \approx \frac{\sqrt{lT_0\alpha/2}\, J_\nu^{(n',n)}}{T_0\alpha\left[(n + \frac{1}{2}) - (n+1)^2/2(\nu+1)\right] - (E + i\epsilon)/\nu\hbar\omega} \qquad \text{for} \quad \nu(T_0\alpha) \gg l \tag{2.51}$$

In both limits, the matrix elements of $\hat{A}$ are small provided E is sufficiently far from a resonance.

We shall not consider higher order terms in the present analysis, except insofar as to comment that a treatment of the continuum states should first be applied.

2.7 Conclusions

The primary purpose of this chapter has been to demonstrate that an optimal separable basis can be defined for an arbitrary quantum Hamiltonian in a mathematically rigorous fashion. Separable approximations are invaluable in physics and chemistry not only for their simplicity, but also for the intuitive insights they provide. One is especially interested in approximations that are not only *separable*, but also *accurate*; and what has been lacking thus far is a systematic way to obtain such operators. The mutual orthogonality criterion of Equations 2.17 and 2.30 goes a

long way towards this goal by providing *the* separable $\hat{H}_0$ which most closely approximates the true Hamiltonian, for a given factorization of configuration space. Such an operator is clearly imbued with a physical significance; as is the residual $\hat{\Delta}$, which embodies the physically-relevant inherent coupling of the system.

The optimal separable basis also provides an advantageous starting point for series expansions. The fact that this method is useful for both Green's function and eigenfunction expansions is not surprising; as both involve the same perturbation $\hat{\Delta}$. Similarly, the applicability of the method to both analytical and computational pursuits is also to be expected; as in either case it is of great benefit to be able to lower the dimensionality. It is significant that in the latter case a computer algorithm can be developed to perform the optimization automatically[17] (Chapter 3). The corresponding analytical problem may in individual cases prove to be intractible, albeit dimensionally-reduced; but even then the physical picture developed in Sections 2.3 and 2.5 can be used to obtain a worthy substitute. It is also significant that the method—though applicable to arbitrary multi-dimensional operators—is particularly suited to sparse Hamiltonians, in that sparsity is maintained throughout.

The results for the shifted harmonic oscillator system of Section 2.6 are quite encouraging. Not only were we able to obtain the analytically optimal outer basis for any shifting function $f(x)$, our physical intuition led us immediately to the correct answer. All that was required was a simple integral verification of Equation 2.30. Although this situation is to some extent fortuitous, it nevertheless indicates that the average potential candidate probably does lead to an excellent, if not optimal, outer basis in the general case.

Having obtained the optimal outer basis for the generic shifted oscillator system, the inner problem was also reduced to a particularly simple form. The strong separability of the new potential allowed us to solve the full $\hat{H}_0$ problem by simply diagonalizing a *single* one-dimensional system, rather than a *collection* of systems. In addition, the inherent residual coupling was found to be of rank two only. Thus, with comparatively little effort we were able to obtain the most accurate zeroth- and first-order approximations for this non-trivial two-dimensional system, and to prove

the existence of resonances even in the limit of infinitesimal shifting.

Although the results were encouraging for the two-dimensional system discussed in this chapter, the method is expected to be even more effective for higher dimensionalities—at least for numerical applications. One reason is that there is generally more freedom of choice with respect to coordinate partitionings as the dimensionality is increased. Another reason is that the sparsity usually increases with dimensionality; so that a greater percentage of the matrix elements of $\hat{\Delta}$ will be zero. We will investigate a non-trivial three-dimensional system in Chapter 4.

If the kinetic energy is more separable than indicated in Equation 2.29, one might wonder whether the present approach could be modified to exploit this additional sparsity. Instead of just two tiers of coordinates, one could define three or more layers. Under the most favorable scenario of Equation 2.28, each coordinate would constitute a separate layer, to be "peeled off" one at a time. The tremendous initial sparsity of such a system would be preserved throughout; moreover, the convergence at the top-most level should be very good, since the preconditioner involves all but one of the coordinates. This recursive possibility is discussed in more detail in Chapter 5.

Although a recursive approach may be beneficial in some cases, a straightforward application as presented in this chapter should be suitable for just about any reasonably small system of interest. Moreover, there are plenty of applications for which a two-tiered approach is most natural. In molecular systems for example, there is an obvious distinction between electronic and nuclear degrees of freedom. In non-rigid rotors, three global rotational degrees of freedom are naturally distinguished from the others. This partitioning results in the so-called "Coriolis" coupling, whose minimization via the optimal separable basis we shall consider in Chapter 4. Scattering Hamiltonians also exhibit a separation between internal and translational coordinates, by virtue of the asymptotic form of the potential. Numerical results for a simple molecular reactive scattering system[17] are obtained in Chapter 3, wherein we also present an efficient algorithm for obtaining the optimal outer basis.

2.8 Appendix: The $\tanh^2$ Potential Hamiltonian

The $\tanh^2$ potential is equivalent to a $-\text{sech}^2$ potential, apart from a constant of unity. The latter potential, also known as the "Eckart well" or the "symmetric Poschl-Teller hole,"[41] was introduced by Rosen and Morse[42] who first solved the quantum problem in an analysis of polyatomic molecular vibration energies. It has since been reconsidered in various other fields, including soliton research.[43]

Traditionally, the eigenproblem is solved by transforming Schrödinger's differential equation in x to an equivalent differential equation in the variable $\sinh^2(\alpha x)$. If Ψ is divided by certain powers of $\cosh(\alpha x)$ and $\sinh(\alpha x)$, then this equation becomes consistent with the generic hypergeometric differential equation. Unnormalized solutions are therefore obtainable in terms of hypergeometric functions;[44] although the parameter values do not satisfy any special properties, and even and odd functions must be handled separately. Analytic normalization constants are also highly nontrivial, as they involve integrations of hypergeometric and hyberbolic sinusoidal functions. Indeed, these constants were not obtained for some time after the unnormalized solutions were first discovered—and even then, only as very complicated expressions involving sums of products of eleven gamma functions.[45]

Our approach to the problem is much more straightforward, and involves the substitution of $\tanh(\alpha x)$ rather than $\sinh^2(\alpha x)$. With no further massaging, we are led directly to Legendre's differential equation, whose solutions for our particular problem are simple algebraic expressions. Moreover, the normalization constants can be obtained from algebraic integrals that are comparatively simple.

2.8.1 Solving the Eigenproblem

We wish to find the eigenfunctions and discrete eigenvalues of the following one-dimensional differential equation:

$$-\frac{\hbar^2}{2m}\frac{d^2}{dx^2}\phi(x) + \frac{m\omega^2 T_0^2}{2}\tanh^2(\alpha x)\,\phi(x) = E\phi(x). \tag{2.52}$$

By transforming to the coordinate $\eta = \tanh(\alpha x)$, we obtain (with $\eta' \equiv 1 - \eta^2$)

$$-\frac{\hbar^2}{2m}\alpha^2\eta'\left(\eta'\frac{d^2}{d\eta^2}\phi(\eta) - 2\eta\frac{d}{d\eta}\phi(\eta)\right) + \left(\frac{m\omega^2 T_0^2}{2}\eta^2 - E\right)\phi(\eta) = 0. \tag{2.53}$$

Dividing by $-\alpha^2\eta'\hbar^2/2m$ yields Legendre's differential equation[46]

$$(1-\eta^2)\,\ddot{\phi}(\eta) - 2\eta\,\dot{\phi}(\eta) + \left[\nu(\nu+1) - \mu^2/(1-\eta^2)\right]\phi(\eta) = 0, \tag{2.54}$$

provided $\nu(\nu+1) \equiv (m\omega T_0/\alpha\hbar)^2$ and $\mu^2 \equiv \nu(\nu+1)[1 - 2E/m\omega^2 T_0^2]$.

If μ and ν are taken to be positive (imaginary) square roots, then the solutions to Equation 2.54 are the associated Legendre functions of the first and second kind, $P_\nu^{\pm\mu}$ and $Q_\nu^{\pm\mu}$. For energies $E > \frac{1}{2}m\omega^2 T_0^2$, the parameter μ is pure imaginary as is appropriate for the continuum states. Bound states arise when E is less than $\frac{1}{2}m\omega^2 T_0^2$, in which case μ is real, and taken to be positive.

For integral ν, the P_ν^μ are the standard Legendre polynomials, which are well known to be square-integrable if $|\mu|$ is an integer less than or equal to ν. The generalization for non-integral values of ν turns out to be that the *difference* between ν and μ must be integral. This condition can be determined by evaluating the asymptotic convergence of the Legendre functions. The asymptotic expression for the $P_\nu^{+\mu}$ solutions, for example, is as follows:[47,48]

$$\begin{aligned}\lim_{z\to\pm1} P_\nu^{+\mu}(z) \;=\; & 2^\mu \pi^{1/2}(z^2-1)^{-\mu/2} \\ & \times\left(\frac{\Gamma(\frac{1}{2})\Gamma(\mu)}{\Gamma^2(\frac{1}{2}-\frac{\nu}{2}-\frac{\mu}{2})\Gamma(-\frac{\nu}{2}+\frac{\mu}{2})\Gamma(1+\frac{\nu}{2}-\frac{\mu}{2})}\right. \\ & \left.\mp\frac{2\Gamma(\frac{3}{2})\Gamma(\mu)}{\Gamma(1+\frac{\nu}{2}+\frac{\mu}{2})\Gamma(1+\frac{\nu}{2}-\frac{\mu}{2})\Gamma(1-\frac{\nu}{2}+\frac{\mu}{2})\Gamma(-\frac{\nu}{2}-\frac{\mu}{2})}\right)\end{aligned} \tag{2.55}$$

Given that the poles of the Γ function occur only at non-negative integers, it is easy to show that convergence occurs only when *both* ν and μ are integers.

This condition is clearly too restrictive, since ν is an arbitrary action parameter that can take any positive value. We must therefore consider the $P_\nu^{-\mu}$ solutions. (Note that contrary to the special case of integral ν, the $P_\nu^{-\mu}$ are *not* in general

proportional to the $P_\nu^{+\mu}$!) The corresponding asymptotic expressions are[47]

$$\lim_{z\to+1} P_\nu^{-\mu}(z) = \left(\frac{z-1}{2}\right)^{\frac{\mu}{2}} \frac{1}{\Gamma(1+\mu)} \tag{2.56}$$

$$\lim_{z\to-1} P_\nu^{-\mu}(z) = \left(\frac{-z}{z+1}\right)^{\frac{\mu}{2}} \frac{\Gamma(\mu)}{\Gamma(1+\mu+\nu)\Gamma(\mu-\nu)}, \tag{2.57}$$

from which it is easily established that the bound states occur whenever $(\nu-\mu)$ is a non-negative integer.

Defining $n \equiv (\nu-\mu)$, the bound state solutions $\phi_n(\eta)$ are thus proportional to $P_\nu^{n-\nu}(\eta)$, where n ranges from zero to the largest integer less than ν. These functions are simple polynomials in η and $\sqrt{\eta'}$ (closely related to the Gegenbauer or "ultraspherical" polynomials[45]) multiplied by $\eta'^{\nu/2}$. The corresponding energy values are

$$E_n = \frac{1}{2}m\omega^2 T_0^2 \left[1 - \frac{(\nu-n)^2}{\nu(\nu+1)}\right], \tag{2.58}$$

from which the ground state energy is seen to be $E_0 = \hbar^2\alpha^2\nu/2m$. Figure 2.3 depicts the eigenenergies as a function of the action parameter ν.

The bound state solutions satisfy a somewhat unusual orthonormality condition. Because the coordinate η is used instead of x, we have

$$\int_{-1}^{1} \phi_{n'}^{(\nu)}(\eta)\, \phi_n^{(\nu)}(\eta)\, \frac{1}{(1-\eta^2)}\, d\eta = \delta_{nn'} \tag{2.59}$$

where a factor of $\sqrt{\alpha}$ is understood to be removed from the definition of $\phi(\eta)$ to keep things dimensionless. (This factor must be resupplied when working with $\phi(x)$.) In terms of the $P_\nu^{n-\nu}$, the above integral can be analytically evaluated to determine the proper normalization constants.[49] This yields

$$\phi_{n'}^{(\nu)}(\eta) = \sqrt{\frac{(\nu-n)\Gamma(2\nu-n+1)}{n!}} P_\nu^{n-\nu}(\eta). \tag{2.60}$$

Alternatively, we can use the Leibnitz and Rodrigues formulas[50] to derive the excited states by differentiating the following expression for the ground state:[46]

$$\phi_0(x) \propto P_\nu^{-\nu}(\tanh(\alpha x)) \propto \sin^\nu(\theta), \tag{2.61}$$

$$\text{where} \quad \sin^2(\theta) \equiv 1 - \tanh^2(\alpha x).$$

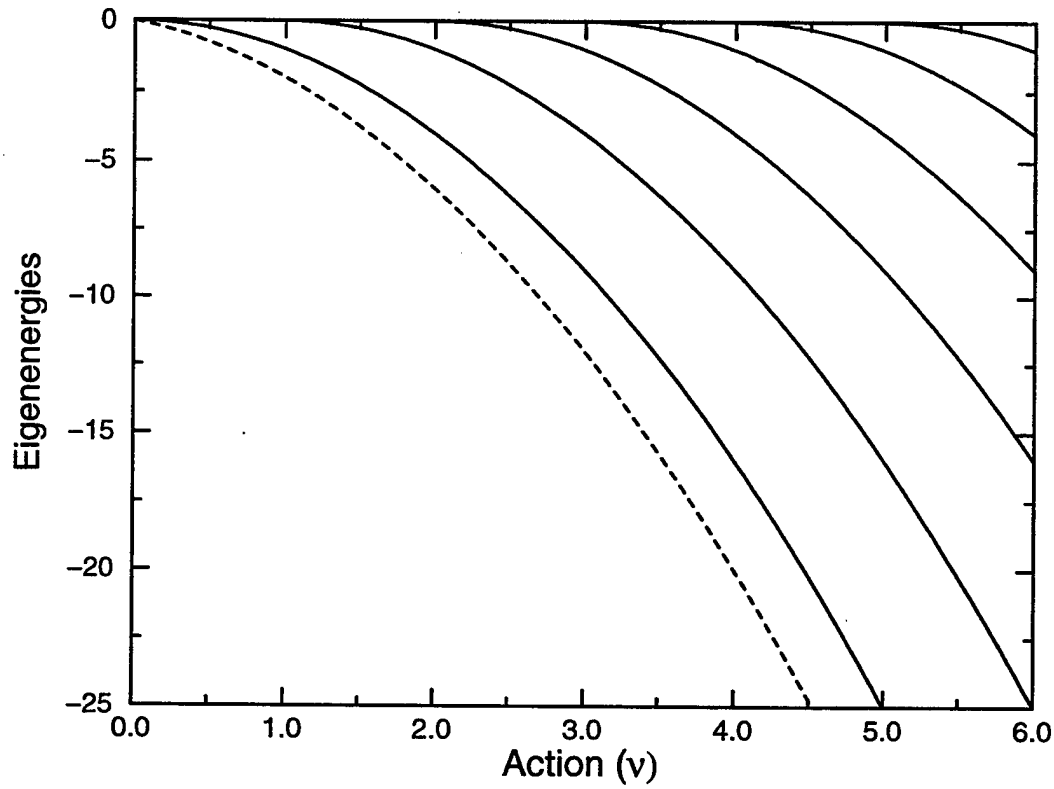

Figure 2.3: Eigenenergies of the $\tanh^2$ potential Hamiltonian (in units where $\alpha^2\hbar^2/2m = 1$) as a function of the action parameter ν, for the ground and several excited states ($n = 0$–5). Zero energy is defined at the continuum threshold. Solid lines represent eigenenergies; the dashed line represents the well-depth. Note the existence of a ground state even for $\nu \ll 1$.

This results in the normalized formula of Equation 2.38.

The limiting case behaviour of the bound state solutions is also quite interesting. Since ν must be positive, there is always a bound state—even in the limit as the well depth (T_0) or width ($1/\alpha$) approaches zero, and the corresponding action becomes arbitrarily small in relation to Planck's constant. This egregious departure from WKB theory is in marked contrast to most other solved potentials. Only one bound state remains in these limits however, since $\nu \to 0$. According to Equation 2.61, it must be proportional to $(1-\eta^2)^{(\nu/2)}$. Thus, the ground state is in essence simply a power of the original potential! As ν approaches zero, ϕ_0 approaches a uniform distribution; moreover, the corresponding energy is seen from Equation 2.58 to approach the continuum threshold. These results are consistent with the limiting functional form of the potential itself, which approaches a constant in the small-ν limit.

2.8.2 Obtaining the $J_\nu^{(n',n)}$

We wish to evaluate the J_ν integrals of Equation 2.44. Using a well-known recursion relation of the P_ν^μ to expand $\phi_{n'}$,[50] we can write

$$J_\nu^{(n',n)} = -\frac{1}{2}\sqrt{\frac{(2\nu-n')(n'+1)}{(\nu-n'-1)(\nu-n')}}\, I_\nu^{(n'+1,n)} - \frac{1}{2}\sqrt{\frac{(2\nu-n'+1)n'}{(\nu-n'+1)(\nu-n')}}\, I_\nu^{(n'-1,n)}, \tag{2.62}$$

$$I_\nu^{(n',n)} \equiv \int_{-1}^{1} \phi_{n'}^{(\nu)}(\eta)\, \phi_n^{(\nu)}(\eta)\, (1-\eta^2)^{-1/2}\, d\eta. \tag{2.63}$$

The quantity I_ν is non-zero only when $n, n' \geq 0$ and $n-n'$ is even. Using the Leibnitz formula, the (unnormalized) eigenfunctions can be expressed as a sum of algebraic functions of η:

$$\begin{aligned}\tilde{\phi}_n^{(\nu)} &\equiv (1-\eta^2)^{\frac{-(\nu-n)}{2}} \left(\frac{d}{d\eta}\right)^n (1-\eta^2)^\nu \\ &= \sum_{i=0}^{n} (-1)^i \binom{n}{i} \frac{\nu!}{(\nu-i)!}\frac{\nu!}{(\nu-n+i)!} (1-\eta)^{\frac{\nu}{2}+\left[\frac{n}{2}-i\right]} (1+\eta)^{\frac{\nu}{2}-\left[\frac{n}{2}-i\right]}\end{aligned} \tag{2.64}$$

The integral in Equation 2.63 can be analytically evaluated by expanding both ϕ_n and $\phi_{n'}$ using Equation 2.64 above. The result is the following:

$$I_\nu^{(n',n)} = \frac{1}{2}\sqrt{\left(1-\tfrac{n}{\nu}\right)\left(1-\tfrac{n'}{\nu}\right)}\, \frac{\binom{2\nu}{\nu}}{\left[\binom{2\nu}{n}\binom{2\nu}{n'}\right]^{1/2}} \sum_{\substack{0\leq i\leq n \\ 0\leq j\leq n'}} (-1)^{i+j} \frac{\binom{\nu}{i}\binom{\nu}{n-i}\binom{\nu}{j}\binom{\nu}{n'-j}}{\binom{2\nu-1}{\nu+(n+n')/2-(i+j)-\frac{1}{2}}} \tag{2.65}$$

The R.H.S. of Equation 2.65 is a somewhat unwieldy double summation involving $(n+1)(n'+1)$ terms. A simpler expression involving a sum of only $(\frac{1}{2}n'+1)$ terms can be obtained by deriving a recursion relation for the I_ν. It turns out to be more convenient to derive the relation for the $\tilde{I}_\nu$, defined via Equation 2.63 with respect to the $\tilde{\phi}_n$ rather than the ϕ_n. Using integration by parts and Equation 2.62, the following recursion relation is easily derived:

$$(n-n')\tilde{I}_\nu^{(n'+1,n)} = n'(2\nu-n'+1)(2\nu-n'-n)\tilde{I}_\nu^{(n'-1,n)} - 2(\nu-n')\tilde{I}_\nu^{(n',n+1)} \tag{2.66}$$

Thus, an arbitrary $\tilde{I}_\nu$ can always be expressed in terms of the $\tilde{I}_\nu$ for which $n' = 0$. These are analytically obtained via direct integration of Equation 2.63, resulting in[51]

$$\tilde{I}_\nu^{(0,n)} = (-1)^{\frac{n}{2}}\pi^{1/2}[(n-1)!!]^2\frac{(\nu-\frac{n}{2}-\frac{1}{2})!}{(\nu-\frac{n}{2})!} \tag{2.67}$$

for n even.

By combining the results of the last paragraph, any particular $\tilde{I}_\nu$ value can be determined. The first few are as follows:

$$\left.\begin{aligned}\tilde{I}_\nu^{(0,0)} &= \pi^{1/2}(\nu-\tfrac{1}{2})!/\nu!\end{aligned}\right\}(n+n')=0 \tag{2.68}$$

$$\left.\begin{aligned}\tilde{I}_\nu^{(0,2)} &= -\pi^{1/2}(\nu-\tfrac{3}{2})!/(\nu-1)!\\ \tilde{I}_\nu^{(1,1)} &= 2\nu\pi^{1/2}(\nu-\tfrac{3}{2})!/(\nu-1)!\end{aligned}\right\}(n+n')=2 \tag{2.69}$$

$$\left.\begin{aligned}\tilde{I}_\nu^{(0,4)} &= 9\pi^{1/2}(\nu-\tfrac{5}{2})!/(\nu-2)!\\ \tilde{I}_\nu^{(1,3)} &= -6\nu\pi^{1/2}(\nu-\tfrac{5}{2})!/(\nu-2)!\\ \tilde{I}_\nu^{(2,2)} &= 12\nu(\nu-1)\left[1-\tfrac{1}{3}\left(\tfrac{\nu-3/2}{\nu-1}\right)^2\right]\pi^{1/2}(\nu-\tfrac{5}{2})!/(\nu-2)!\end{aligned}\right\}(n+n')=4 \tag{2.70}$$

In general, the factor in brackets is a sum over $\text{int}(\frac{1}{2}n')+1$ terms. The properly normalized formula for an arbitrary I_ν is

$$I_\nu^{(n',n)} = (-1)^{\frac{n-n'}{2}}\pi^{1/2}(n-n'-1)!!\sqrt{(2\nu-n)!(2\nu-n')!}\frac{\sqrt{(\nu-n)(\nu-n')(n'!/n!)}}{\nu!2^{2\nu}}\times \tag{2.71}$$
$$\sum_{i=0}^{\text{int}(n'/2)}(-1)^i 2^{(n'-i)}\binom{\nu-(n+n')/2+i-\frac{1}{2}}{k}\frac{(n+n'-2i-1)!!}{(\nu-n'+i)!(n'-2i)!}\frac{(\nu-(n+n')/2+i-\frac{1}{2})!}{(\nu-(n+n')/2+i)!}.$$

Chapter 3

Reaction Probabilities and Optimized Preconditioning

3.1 Introduction

In this chapter, we discuss how the optimal separable basis approach of Chapter 2.3 can be usefully applied to actual numerical calculations for real molecular systems. Although the method is certainly applicable to bound state calculations (Chapter 2), this chapter addresses scattering calculations only—especially of chemical systems that undergo reactive scattering. We also limit the discussion to the microcanonical scattering quantities described in Chapter 1.

The evaluation of the energy Green's operator $\hat{G}(E)$ is paramount in the calculation of microcanonical quantum scattering quantities of all kinds, including those pertinent to inelastic and reactive scattering systems. Using the discrete variable representation (DVR) grid methodology developed by Light and others,[52–62] the Hamiltonian operator and associated scattering states are represented as finite matrices and vectors, respectively. These are defined with respect to a grid of discrete points over configuration space. Since scattering systems are by definition of infinite extent, some method most be adopted for keeping the effective configuration space finite in the asymptotic regions. A simple truncation of the grid will not do, as it will introduce spurious reflections of outgoing waves that are obviously not physical.

One solution is to introduce complex optical potentials into the Hamiltonian, which have the effect of absorbing the outgoing flux before it reaches the end of the grid. This kind of approach has a very well established history in physics and chemistry.[6,63–68] Seideman and Miller developed a version for time-independent DVR scattering applications, for which the $i\epsilon$ term in Equation 2.24 is replaced with the (pure imaginary) absorbing potential.[69–71] A matrix representation of the Green's operator $\hat{G}(E)$ can then be obtained numerically using straightforward linear algebra techniques to perform the matrix inversion of Equation 2.24.

To obtain accurate results the absorbing potential must be positive and "small," yet large enough that the flux is almost all absorbed before reaching the end of the grid. The proper values for the parameters describing ϵ and other aspects of the DVR grid—such as the spacing between adjacent grid points, and the potential cutoff used to truncate energetically inaccessible regions of the grid—are not known *a priori*. In practice, these must be obtained empirically by sequentially varying the parameters until "convergence" is attained—i.e. until a significant variation of any of the parameters does not affect the final numerical results appreciably.

Proper convergence of the DVR parameters is a significant, but not insurmountable, hurdle impeding accurate numerical determination of the microcanonical scattering quantities. A far more significant difficulty however, is the fact that the numerical burden of the DVR approach scales very unfavourably with energy and dimensionality—primarily because the matrix sizes becomes inordinately large, even to be handled by modern computers. This problem has been ameliorated somewhat through the use of certain specialized linear algebra techniques, e.g. Krylov and other sparse matrix methods.[7,8,72–74] Nevertheless, scattering calculations to date have been for the most part limited to small systems at relatively low energies.[34,75–79]

In recent years however, a technique known as "numerical preconditioning" has been explored in conjunction with DVR Green's function calculations.[9,73,80,81] The use of preconditioners in chemical reactive scattering applications has thus far exhibited significant promise.[82,83] Unfortunately, selecting a good preconditioner for a given system *a priori* has proven to be something of a "black art;" as it is numerically unclear how to predict the quantitative effect of a particular choice of preconditioner,

short of actually applying it and performing the calculation.

A major motivation of this work has been the desire to develop some quantitative means of evaluating different preconditioning schemes, so that an optimally efficient preconditioner can be systematically tailored for a given physical system. This can be achieved by taking the view that the DVR Hamiltonian is a physical object rather than simply a numerical object. We should therefore look for something physical that corresponds to the numerical process of preconditioning.

Such a correspondence can in fact be obtained;[84] in Section 3.4 it will be shown that numerical preconditioning is physically equivalent to the propagation of distorted waves, as per the distorted wave Born expansion (Equation 2.26). In particular, the preconditioner matrix represents the zeroth-order Green's operator $\hat{G}_0$, defined in terms of the approximate $\hat{H}_0$ of Equation 2.25 whose stationary scattering states are the distorted waves.[6]

By exploiting this correspondence, we can estimate the performance of a numerical preconditioner by analyzing the convergence of the corresponding distorted wave Born expansion. Physical intuition can then be brought to bear on the problem of developing an efficient preconditioner. In particular, an optimal preconditioning scheme[84] is suggested by Chapter 2: namely, that $\hat{H}_0$ be chosen to be the optimal weakly separable approximation to the true Hamiltonian.

Obtaining the optimized preconditioner numerically is a two-stage process. First, the optimal $\hat{H}_0$ is determined; then, the preconditioner $\hat{G}_0$ is obtained via a matrix inversion. The crucial point is that *both* of these are reduced-dimensional, well-defined algorithmic operations (Section 3.5). Thus, the optimized preconditioner can be systematically computed using only a fraction of the CPU time and memory required by the full problem.

Section 3.2 relates the fundamentals of the DVR formalism, together with the modifications required for using absorbing potentials. Section 3.3 describes certain unique aspects of reactive scattering, and also presents explicit DVR formulas for the quantities of interest. Section 3.4 examines the use of preconditioned sparse matrix methods in DVR scattering calculations, and also explores the connection with the distorted wave methodology of Section 2.4.2. The optimized preconditioning scheme

is considered in Section 3.5 wherein a numerical algorithm is developed in some detail.

Section 3.6 presents results for the benchmark collinear $H + H_2 \rightarrow H_2 + H$ chemical reaction. Converged cumulative and state-to-state reaction probabilities were computationally much more easily achieved when the optimized preconditioner was employed. Moreover, the preconditioner enabled exact quantum results to be calculated for energies as high as 6 eV, which is significantly higher than what has thus far been reported in the literature.

3.2 DVR-ABC Formalism

3.2.1 Discrete Variable Representations

In the DVR formalism, a finite grid of points is laid out over the region of interest in configuration space; and the density and extent of the points are presumed sufficient to adequately represent the underlying continuous coordinates for a given application. This DVR grid can then be used to obtain approximate, position-like representations of quantum mechanical operators and wavefunctions. An operator is represented in the DVR as an $N \times N$ matrix, where N is the total number of grid points. Similarly, a wavefunction is represented by a vector of length N.[56,57,85]

Although there are numerically many ways that one could obtain such an approximate representation, the DVR formalism is appealing in that it uses physical arguments as much as possible. One starts with the eigenstates of some soluble operator, usually the kinetic energy. These are then truncated in some fashion, usually via energy considerations. The resultant collection of basis functions spans a finite subspace of the true Hilbert space. By projecting an operator onto this subspace, one obtains the so-called "finite basis representation" or FBR.[57] The FBR projection can not possibly represent the corresponding operator in its entirety, but may adequately capture all features relevant to a particular application. For example, all kinetic energy eigenstates above a certain energy can be ignored if one is interested in calculating the spectrum of some Hamiltonian operator for some finite energy range only.

The FBR is not the same as the DVR, for the explicit matrix form of the former is not position-like. To obtain the DVR from the FBR, one applies a finite unitary transformation, defined as the transformation which diagonalizes the FBR projection of the position operator(s) $\hat{q}$. The new basis functions are thus position-like, i.e. approximately equal to Dirac delta functions. Moreover, the corresponding eigenvalues of the $\hat{q}$ FBR specify the discrete values of the DVR grid.

In the one-dimensional rectilinear case where $\hat{T} = \hat{p}^2/2m$ for example, the restriction to particle-in-a-box eigenstates results in a uniformly-spaced DVR grid with sinc function DVR basis functions. Specifically, if q_i is the location of the i'th grid point, then the corresponding basis function $|q_i\rangle$ is

$$\langle q|q_i\rangle = \sin\left(\pi(q-q_i)/\Delta q\right) / \left(\pi(q-q_i)\right) \tag{3.1}$$

where Δq is the spacing between successive grid points.[34] Note that in the $\Delta q \to 0$ limit, $\langle q|q_i\rangle$ approaches the Dirac delta function, as expected.

The sinc-function DVR representation of the one-dimensional rectilinear kinetic energy[34] is given by

$$T_{ii'} = \frac{\hbar^2(-1)^{i-i'}}{2m\Delta q^2} \begin{cases} \pi^2/3 & i = i' \\ 2/(i-i')^2 & i \neq i' \end{cases} . \tag{3.2}$$

In general, a discrete representation of an arbitrary operator is obtained using the DVR basis functions such as in Equation 3.1. When representing $\hat{T}+\hat{V}$ Hamiltonians however, an additional approximation is usually made: one uses actual Dirac delta functions for the potential rather than DVR functions, to ensure that the matrix representation of $\hat{V}$ is diagonal. As a result, more DVR points are usually required than would otherwise be necessary; but the advantage is that the resultant representation of the Hamiltonian is sparse, if there is more than one degree of freedom (Section 3.5.1).

3.2.2 Absorbing Boundary Conditions

The DVR formalism as described in the last subsection is perfectly suited to bound state calculations. The general procedure is to use a kinetic energy cutoff in

the FBR to limit the density of grid points, as well as a potential energy cutoff in the DVR to limit the extent of the grid. Bound state problems are really "bound" in that one can define a finite region of configuration space outside of which the probability is arbitrarily small (for any finite energy).

Consequently, a finite DVR can be obtained for the Hamiltonian which is adequate for say, calculating the bound state energies up to some point. One does not know ahead of time exactly which grid spacing and potential cutoff values are appropriate; but by decreasing the former and increasing the latter one will eventually reach the point where the calculated eigenenergies remain essentially constant, to within some predetermined tolerance. At this point the calculations are said to be "converged." In practice, one should not push these parameters far beyond the point of convergence, as the commensurate increase in grid size will result in a more difficult linear algebra problem.

Although these comments apply equally well to scattering calculations, in the latter case there is a more fundamental problem: namely, that the configuration space regions are unbounded in the asymptotic channels (corresponding to reactants and products in reactive scattering). As per Section 3.1, this situation is dealt with by introducing a negative imaginary absorbing potential $i\epsilon(q)$. This can be thought of as a generalization of the constant parameter $i\epsilon$ in the Green's function as expressed in Equation 2.24. Indeed, our naive numerical procedure for obtaining $\hat{G}(E)$ is simply to invert the complex symmetric DVR matrix for the inverse Green's function, with the absorbing potential substituted for $i\epsilon$. Moreover, the restriction to negative imaginary potentials will automatically provide the correct (retarded) boundary conditions for a $G^{+}(E)$ Green's function. However, this procedure will only yield meaningful results if the energy is suitably restricted and $\epsilon(q)$ is sufficiently "small" in some sense.

On the other hand, $i\epsilon(q)$ is solely responsible for the absorption of outgoing flux, and must therefore be sufficiently large as to absorb the vast majority of the flux before it can be reflected back at the edge of the grid. To see that this is the case, it is helpful to use a different interpretation, wherein the Hamiltonian is conceptually

replaced with an effective Hamiltonian[86–88]

$$\hat{H}_{\text{eff}} \equiv \hat{H} - i\hat{\epsilon} \tag{3.3}$$

governing the evolution of a fictitious dynamical system. Note that $\hat{H}_{\text{eff}}$ is no longer Hermitian, so that probability is not conserved; and this is of course what accounts for the absorption of flux. The degree to which flux is absorbed is thus dependent on the size of the absorbing potential.

Armed with these perspectives, we can address the issue of selecting an appropriate absorbing potential function $\epsilon(q)$. In light of Equation 3.3, the absorbing potential should clearly be zero or negligible in the interaction region, as the true and fictitious dynamics should differ only in the asymptotic channel regions. Assuming that the absorbing potentials are "turned on" as soon as one has comfortably entered the asymptotic regions, and "turned off" again as soon as the flux has been adequately absorbed (at which point the DVR grid can be truncated), how far out must one go?

Clearly, if ϵ is increased—whatever the specific functional form—the absorbing boundary will be narrower, and vice-versa. A narrower boundary is desired from the perspective of reducing the grid size. However, in light of Equation 2.24 we expect that ϵ should not be too big. In fact, one finds in practice that the abrupt changes in the potential implied by a large ϵ and narrow boundary induce a certain amount of artificial reflection.[67,69]

In practical applications therefore, one finds it necessary to converge the calculations with respect to the absorbing boundary width and heighth, as well as grid spacing and potential energy cutoff. One could also vary the functional form of $\epsilon(q)$, in order to minimize reflection and maximize absorption for a given boundary width. In the one-dimensional case, semiclassical arguments have been made in favor of $q^{1.5}$ potentials[69] and other arguments support quadratic potentials,[89] although these do not extend readily to the multi-dimensional case. Numerical experiments performed previously for power law and Woods-Saxon potentials seem to indicate that the particular choice does not matter very much.[69] In any event, we have found quartic potentials to be quite satisfactory; these are used throughout this work except where explicitly stated otherwise.

3.3 Quantum Reactive Scattering Calculations

Having established the form of the DVR for the inverse Green's operator, including absorbing boundary conditions, we are ready to calculate microcanonical state-to-state and cumulative reaction probabilities. As discussed in Chapter 1, all relevant microcanonical scattering quantities can be obtained from the energy Green's operator $\hat{G}(E)$, which itself could be obtained directly by inverting the $(E + i\hat{\epsilon} - \hat{H})$ DVR matrix. However, there are many practical reasons why such an approach is not recommended for large systems. Apart from the poor scaling of a direct matrix inversion (N^3 where N is the number of grid points), the resultant Green's function matrix is decidedly not sparse, and may thus require far more storage than its inverse.

From a computational standpoint, it is therefore more convenient to make use of more specialized techniques that are specifically designed to elicit a particular type of information. These techniques are based on corresponding analytical expressions which have been derived using scattering theory. In particular, we shall focus on just two scattering quantities—reactive state-to-state probabilities, and cumulative reaction probabilities—as these are the only quantities that we have actually calculated explicitly within the scope of this dissertation. Moreover, as these pertain specifically to reactive scattering, the following discussion may be beneficial for the general reader who may be more familiar with elastic or inelastic scattering.

3.3.1 Asymptotic States

As per Chapter 1, the elements of the scattering or S-matrix $S_{nn'}(E)$ represent the transition amplitudes between asymptotic states, where the indices n and n' label initial and final states, respectively. However, the quantity $S_{nn'}$ is only meaningful once the asymptotic states themselves have been suitably defined. In elastic or inelastic scattering, defining appropriate asymptotic states is fairly straightforward: one solves the asymptotic potential problem to obtain a mutually orthogonal set of states.

In reactive scattering, however, where the initial and final states must cor-

respond respectively to reactants and products, the situation is a little more complicated. The reason is that if the asymptotic scattering states are defined in the usual way—i.e. as separable products of internal fragment bound states times plane waves in the translational coordinates between fragments—then the set of asymptotic reactant states is *not* orthogonal to that of products.

To be more specific, let r and R symbolically represent the internal and translational coordinates, respectively corresponding to a pair of reactants A and B. In the large R limit, the potential approaches an asymptotic form $V_{\rm as}(r)$ that is independent of R. The asymptotic scattering states

$$\phi_n(r,R) \propto \sqrt{\frac{\mu}{\hbar k_n}} e^{-ik_n R} \varphi_n(r) \tag{3.4}$$

are therefore solutions to an approximate Hamiltonian $\hat{H}_0 = \hat{H} - \hat{V} + \hat{V}_{\rm as}$ which gives rise to an interaction potential $\hat{\Delta} = (\hat{V} - \hat{V}_{\rm as})$ in the notation of Equation 2.25.

The description thus far would be completely adequate for inelastic scattering (Section 2.5.3). In reactive scattering however, A and B are transformed into products C and D which are characterized by a completely different set of coordinates r' and R'. These give rise to primed quantities such as $V'_{\rm as}(r')$, $\phi_{n'}(r',R')$, and $\hat{H}_0{}'$ which are incompatible with those corresponding to reactants. In particular,

$$\langle \phi_{n'} \mid \phi_n \rangle \neq 0. \tag{3.5}$$

One solution is to divide configuration space into two regions using some "dividing surface," where one region corresponds to products and the other to reactants. The asymptotic states described above are then modified by introducing a step function centered along the dividing surface to ensure that reactant states have zero probability in the product region, and vice-versa. In other words, we make the substitution

$$\begin{aligned} \phi_n(q,Q) &\rightarrow h(q,Q)\phi_n(q,Q) \\ \phi_{n'}(q,Q) &\rightarrow (1-h(q,Q))\,\phi_{n'}(q,Q) \end{aligned} \tag{3.6}$$

where $h(q,Q)$ represents a step function centered at the dividing surface which is zero in the products region and unity in the reactant region. The coordinates (q,Q) are

arbitrary, and are introduced simply to demonstrate that products and reactants are treated on an equal footing. The resultant asymptotic states are now orthogonal, but no longer separable except in the corresponding asymptotic limits. Nevertheless, we shall find them to be well-suited to reactive scattering applications.

Using the orthogonal asymptotic states as described above, we can now proceed to obtain the S-matrix in a manner exactly analagous to that of elastic or inelastic scattering. Note that since we are considering reactive transitions—i.e. in $S_{nn'}$, n refers only to reactant states and n' only to products—the diagonal elements of the S-matrix can be ignored. This means for example, that the S-matrix is effectively proportional to the T-matrix, in that the additional δ function term that appears in the usual expression[6] can be ignored.*

3.3.2 State-to-State Reaction Probabilities

As per Chapter 1, the state-to-state reaction probabilities are given by

$$P_{nn'} = |S_{nn'}(E)|^2. \tag{3.7}$$

Using the well-known relation[6]

$$\hat{T}(E) = \hat{\Delta} + \hat{\Delta}\hat{G}(E)\hat{\Delta} \tag{3.8}$$

(where $\hat{T}(E)$ is the transition operator, not the kinetic energy), the reactive S-matrix can be expressed in terms of the energy Green's operator as follows:

$$S_{nn'}(E) = \frac{i}{\hbar}\langle\phi_{n'}(E)|\hat{\Delta} + \hat{\Delta}\hat{G}(E)\hat{\Delta}|\phi_n(E)\rangle \tag{3.9}$$

At this point we must contend with a certain ambiguity, sometimes ignored, as to whether $\hat{\Delta} = (\hat{V} - \hat{V}_{\text{as}})$ refers to reactants or products—it cannot be both! Moreover, the use of one or the other introduces an undesirable reactant or product bias.

*Technically, the orthogonalizing modification discussed above requires the distorted wave methodology, for which the δ-function term is replaced with the zeroth-order S-matrix $S^0_{nn'}$. However, the distorted Hamiltonian $\hat{H}_0$ is specifically designed to preclude transitions between reactants and products—hence $S^0_{nn'} = 0$.

This dilemma, which is peculiar to reactive scattering, can be resolved in various ways. One approach which we shall find useful is to use the reactant asymptotic potential on the reactant side of the dividing surface, and similarly for products. In particular, we make the substitution

$$\Delta(q,Q) \rightarrow h(q,Q)\Delta(q,Q) + (1-h(q,Q))\,\Delta'(q,Q) - V_{\mathrm{DS}}(q,Q), \tag{3.10}$$

which is manifestly "covariant" with respect to exchanging reactants with products. Note in particular the addition of a V_{DS} term, which represents an infinite, or very large potential barrier in the neighborhood of the dividing surface. By including such a term in $\hat{\Delta}$, the corresponding $\hat{H}_0$ automatically provides both reactant *and* product states that satisfy Equation 3.6.

The Equation 3.10 choice of $\hat{\Delta}$ is particular helpful with respect to evualating Equation 3.9 above. The first term vanishes, because $\hat{\Delta}$ is a potential, and because at every point of configuration space either $\phi_n(q,Q)$ or $\phi_{n'}(q,Q)$ is zero. We also have

$$(\hat{H}_0 - E)|\phi_n\rangle = 0 \tag{3.11}$$

by construction, where $\hat{H}_0$ now corresponds to the symmetric $\hat{\Delta}$ of Equation 3.10.

We can therefore replace the $\hat{\Delta}$ operator to the right of $\hat{G}(E)$ in Equation 3.9 above with the operator

$$(\hat{H} - E) = (i\hat{\epsilon} - \hat{G}^{-1}). \tag{3.12}$$

We can also do the same for the $\hat{\Delta}$ to the *left* of $\hat{G}(E)$ however, since the product states $|\phi_{n'}\rangle$ are *also* characteristic functions of $\hat{H}_0$.

Using the above substitutions, Equation 3.9 becomes

$$S_{nn'}(E) = \frac{i}{\hbar}\langle\phi_{n'}(E)|\hat{G}^{-1} - 2i\hat{\epsilon} - \hat{\epsilon}\hat{G}\hat{\epsilon}|\phi_n(E)\rangle \tag{3.13}$$

where the first two terms above both vanish, again due to the fact that $|\phi_n\rangle$ and $|\phi'_n\rangle$ never share a common region of configuration space. In matrix form, we are thus left with the elegant expression[70]

$$S_{nn'}(E) = -\frac{i}{\hbar}\,\vec{\phi}^{\,\mathrm{T}}_{n'} \cdot \hat{\epsilon}_{\mathrm{p}}\hat{G}(E)\hat{\epsilon}_{\mathrm{r}} \cdot \vec{\phi}_n \tag{3.14}$$

Here, ϵ_r and ϵ_p are the absorbing potential functions in the reactant and product regions, respectively. Similarly, $\vec{\phi}_n$ and $\vec{\phi}_{n'}$ are DVR vector representations of the asymptotic scattering states (including weight factors).[70] These can refer to either Equation 3.4 or Equation 3.6, since ϵ_r and ϵ_p already incorporate the appropriate $h(q,Q)$ factors.

Equation 3.14 is very convenient from a DVR perspective. In order to calculate a particular state-to-state transition probability, it is only necessary to compute the action of the Green's operator on a a single vector, rather than computing the entire Green's function. This is equivalent to solving the standard linear algebra problem of Equation 2.9—an operation which is, moreover, amenable to the sparse numerical methods to be discussed in Section 3.4.

3.3.3 Cumulative Reaction Probabilities

Our next task is to develop a similar expression for a direct calculation of the cumulative reaction probability

$$N(E) = \sum_{nn'} P_{nn'}, \tag{3.15}$$

i.e., an expression that does not involve the explicit summation above. A suitable starting point is the following expression in terms of the flux operator[75,90]

$$N(E) = \frac{1}{2}(2\pi\hbar)^2 \mathrm{tr}\left[\hat{\mathrm{F}}\delta(\mathrm{E}-\hat{\mathrm{H}})\hat{\mathrm{F}}\delta(\mathrm{E}-\hat{\mathrm{H}})\right], \tag{3.16}$$

where $\hat{F}$ is the flux operator. The Green's function enters in via the identity

$$\delta(E-\hat{H}) = -\frac{1}{\pi}\mathrm{Im}\,\hat{\mathrm{G}}(\mathrm{E}). \tag{3.17}$$

The flux operator $\hat{F}$ can be expressed in many ways. Seideman and Miller found the form

$$\hat{F} = \frac{i}{\hbar}\left[\hat{G}^{-1}(E) - i\hat{\epsilon}, h(\hat{q},\hat{Q})\right] \tag{3.18}$$

where [,] denotes commutation, to be particularly useful.[69] Indeed, when Equations 3.18 and 3.17 are substituted into Equation 3.16, simplifications of the type

encountered in Equation 3.9 are possible, giving rise to the following expression

$$N(E) = 4\,\mathrm{tr}[\hat{G}(E)^*\,\hat{\epsilon}_\mathrm{p}\,\hat{G}(E)\,\hat{\epsilon}_\mathrm{r}], \tag{3.19}$$

which is well-suited to a DVR analysis.

In explicit matrix form, Equation 3.19 becomes

$$N(E) = 4\sum_{i,i'} \epsilon_r(q_i)\epsilon_p(q_{i'})\,|G_{ii'}(E)|^2\,, \tag{3.20}$$

where i and i' index the DVR grid points that lie in the reactant and product regions, respectively. Note that although we are no longer acting $\hat{G}$ on a single vector, the calculation is nevertheless simplified in that only a small portion of the $\hat{G}$ matrix needs to be calculated. In particular, we only need the block of $\hat{G}$ corresponding to reactant absorbing boundary rows and product absorbing boundary columns.

3.4 Numerical Preconditioning and the Distorted Wave Born Expansion

3.4.1 Sparse Matrix Methods

For the DVR Hamiltonians considered in this dissertation, the matrix representations are all sparse. One obvious advantage is that less computer memory is required to store the Hamiltonian than would be required by a full matrix of the same size. Another advantage—less obvious, but equally important—is that the time required for a Hamiltonian multiply is also greatly reduced. By "Hamiltonian multiply" we refer to the multiplication of a vector by the matrix representation for $\hat{H}$ or $\hat{G}^{-1}$.

It may not be clear why this is helpful, as Equations 3.14 and 3.20 require multiplications by $\hat{G}$ rather than $\hat{G}^{-1}$. However, there is a class of numerical methods loosely based on the conjugate gradient method[91]—e.g. GMRES,[92] CGS,[93] and QMR[94]—that accomplish a $\hat{G}$ multiply through an iterative sequence of multiplications by $\hat{G}^{-1}$. The linear subspace spanned by the sequence of vectors that is generated by this process is known as the "Krylov space."[7,8]

The first step is to rewrite the $\hat{G}$ multiply as a standard linear algebra problem in the form of Equation 2.9. We have

$$\begin{aligned} \hat{G}\vec{x} &= \vec{y} \\ \hat{G}^{-1}\vec{y} &= \vec{x} \end{aligned} \tag{3.21}$$

where $\hat{G}^{-1}$ and $\vec{x}$ are known explicitly, whereas $\vec{y}$ is the unknown vector that we seek to obtain. One starts with a random initial guess $\vec{y_0}$, and calculates the error, or length of the residual vector $|G^{-1}\vec{y_0} - \vec{x}|^2$. To obtain a better approximation, a correction $\vec{\xi_0}$ is added, in the direction of steepest descent with respect to minimizing the residual. This turns out to be just the "direction" of $\hat{G}^{-1}$ multiplied by the residual vector. The process can be repeated iteratively to obtain successively better approximations $\vec{y_i}$ until convergence is achieved.

The success of the conjugate gradient algorithms depends on the $\hat{G}^{-1}$ multiply being a comparatively fast operation, which is why these methods are ideal for sparse matrices. However, they also demand that the total number of iterations required for convergence be comparatively small with regard to the matrix size N; and this is a more subtle issue. It is well-known[91] that the convergence rate is generally related to the condition number of the matrix. Thus, for ill-conditioned matrices convergence is usually slow and ineffectual. Unfortunately, for most molecular systems the conditioning of $\hat{G}^{-1}(E)$ tends to deteriorate as the energy is increased, due to a higher density of states.

3.4.2 Preconditioning and Distorted Waves

Fortunately, the convergence can be improved using a numerical technique known as preconditioning. This consists of multiplying both sides of Equation 3.21 with the same matrix—the preconditioner—prior to obtaining the iterative conjugate gradient solution. The basic strategy is to reduce the condition number of the new matrix by as much as possible, so as to improve convergence. Apart from an immaterial scaling factor, this is equivalent to minimizing the difference between the new matrix and the identity matrix. The procedure is therefore most effective when the

preconditioner matrix is closest to $\hat{G}$.

Multiplying both sides of Equation 3.21 on the left by the preconditioner results in the new linear equation

$$\left(\hat{I} - \hat{A}\right)\vec{y} = \vec{b}, \tag{3.22}$$

where $\hat{I}$ is the identity, and $\hat{A}$ is the difference which is to be minimized by the choice of preconditioner. If we now multiply both sides of Equation 3.22 by the expanded inverse of $(\hat{I} - \hat{A})$, we obtain

$$\vec{y} = \left(\hat{I} + \hat{A} + \hat{A}^2 + \hat{A}^3 + \cdots\right)\vec{b}. \tag{3.23}$$

Clearly, there is a close association between the convergence of the inverse expansion in Equation 3.23 and the convergence of the conjugate gradient methods, as both are improved by minimizing $\hat{A}$. The advantage of Equation 3.23 however, is that it corresponds directly to something physical: namely, *the distorted wave Born expansion of Equation 2.26.*

It is worth taking a detailed look at this correspondence. The preconditioner matrix itself corresponds to the distorted wave Green's operator $\hat{G}_0$, defined in terms of some approximate Hamiltonian $\hat{H}_0$ (Section 2.4.2). The matrix $\hat{A}$ corresponds to the dimensionless kernel matrix $\hat{G}_0\hat{\Delta}$, whose eigenvalues alone determine the convergence of the Born expansion. Finally, we note that Equation 3.23 above is transformed into Equation 2.26 by simply making the substitution $\vec{b} = \hat{G}_0\vec{x}$.

The correlation between the convergence of the Krylov-based conjugate gradient methods and the convergence of the distorted wave Born expansion provides us with an analytic means of evaluating different numerical preconditioning schemes *a priori*, wherein we can bring physical intuition to bear on the problem of obtaining a good preconditioner for a given system. For example, the discussion in Section 2.4.2 vis-a-vis convergence is also completely relevant to this section. Generally speaking, the strategy is to incorporate as much of $\hat{H}$ into $\hat{H}_0$ as possible, so that the corresponding Born expansion converges quickly.

For example, for Hamiltonians of the standard $\hat{T} + \hat{V}$ form, the Born series proper[22] is generated by choosing $\hat{\Delta} \equiv \hat{V}$. The corresponding preconditioner, known

as the "kinetic energy preconditioner,"[83] is effective when $\hat{V}$ is much smaller than $\hat{T}$, as would be predicted on physical grounds. In contrast the "diagonal preconditioner,"[83] for which $\hat{H}_0$ consists of the diagonal matrix elements of $\hat{H}$ in the DVR representation, is effective when $\hat{V}$ is much *larger* than $\hat{T}$. The "optimized preconditioner" derived from the optimal separable $\hat{H}_0$ (to be introduced in the next section), is more efficient than either of these; although it can be shown to subsume the other two in the appropriate limits.

It should be mentioned that although the correspondence described herein is very close, it is not exact. For instance, the analytic expansion of Equation 2.26 may or may not converge; yet in DVR applications, the conjugate gradient methods are guaranteed to converge to numerical precision after a known number of iterations—usually the matrix size N. Usually, one expects convergence to acceptable limits with far fewer than N iterations however. Given that Equation 3.23 is a geometric series, the convergence properties of the Born series are fairly straighforward, albeit there are some complications that arise due to the operator nature of $\hat{A}$, as discussed in the appendix (page 85). In contrast the various Krylov algorithms can display somewhat erratic convergence behavior, depending on the specifics of how they are implemented.

Nevertheless, these methods share more similarities than differences—being all variations of the iterative conjugate gradient approach. Moreover, we anticipate that a good preconditioner will have a drastic effect on reducing the calculational effort, that will far outweigh the differences associated with which particular algorithm is being used. This has certainly been observed in our calculations to date (Section 3.6).

Note that since the convergence of Equation 2.26 is related to the norm of the kernel, we can use the latter as a heuristic indicator of preconditioner performance. The numerical value determined for $|\hat{A}|$ will depend on the various DVR parameters such as grid density. On physical grounds however, $|\hat{A}|$ should not change very much as these parameters are varied. This suggests that the convergence of the linear algebra calculation should not vary significantly with the size of the matrix, as has previously been thought to be the case. These assumptions are tested numerically in

Section 3.6.

3.5 Optimized Preconditioning via Jacobi Block Diagonalization

In this section, we are concerned with one particular choice of preconditioner: namely, the optimized preconditioner corresponding to the optimal separable $\hat{H}_0$ of Section 2.3. Simply put, this preconditioning scheme is generally expected to outperform all others of comparable separability, because the interaction $\hat{\Delta}$ has been reduced by as much as possible. To obtain $\hat{G}_0$ explicitly, it is not necessary to diagonalize $\hat{H}_0$; however, we do need to obtain the inverse of $(E+i\epsilon-\hat{H}_0)$. Once again, it is convenient to perform the inversion in the partially diagonal representation wherein $\hat{H}_0$ is block-diagonal. Consequently, the problem reduces to a k-dimensional one parametrized by the outer index m.

Obtaining $\hat{G}_0$ is thus considerably easier than solving for $\hat{G}$, as expected. However, it is first necessary to find the optimal outer basis. A reduced-dimensional algorithm for this procedure is presented in Section 3.5.2. Before getting into the details of the algorithm however, we first present a brief but necessary discussion of multi-dimensional DVR's.

3.5.1 Multi-dimensional Discrete Variable Representations

Consider a DVR representation of a multi-dimensional Hamiltonian of the $(\hat{T}+\hat{V})$ form of Section 2.5. For multi-dimensional systems, a different DVR must be constructed for each degree of freedom. The DVR basis functions are just products of the individual functions for each degree of freedom. Thus, instead of being labelled by a single index i, the multi-dimensional grid points are labelled by the collection $\{i_1,\ldots,i_n\}$.

Since $\hat{V}=V(\hat{q}_1,\ldots,\hat{q}_n)$, the DVR matrix representation of $\hat{V}$ is still diagonal. In contrast, the representation of $\hat{T}$ necessarily involves off-diagonal elements, as per Section 3.2. Although the one-dimensional kinetic energies such as the rectilin-

ear case of Equation 3.2 are usually represented by full matrices, higher-dimensional representations of the kinetic energy are usually sparse. This is particular true if the kinetic energy is orthogonal, in which case each component $\hat{T}_l$ includes delta function factors for all but the l'th degree of freedom.

Any explicit representation must depend, however, on a convention for representing rank-$2n$ tensors as *matrices*—i.e. tensors of rank 2. We imagine the simplest scenario for our DVR grid; i.e. an n-cubic lattice with d points per degree of freedom, where $N = d^n$. Each row index k of the $N \times N$ matrix representation must correspond to a complete *set* of n indices $(i_1, \ldots, i_n)$ where each i ranges from 0 to $(d-1)$ and labels a different degree of freedom. Similarly, each column index k' corresponds to the set $(i'_1, \ldots, i'_n)$.

A convenient way to explicitly associate the $(i_1, \ldots, i_n)$ with the composite index k is to define

$$k = i_1 + di_2 + d^2 i_3 + \cdots d^{n-1} i_n \tag{3.24}$$

which has the effect, as k is incremented, of traversing the lower-numbered indices most quickly. In light of our prior distinction between inner and outer coordinates, the matrix representation as defined by Equation 3.24 acquires a natural block structure. Variation of the inner coordinates corresponds to motion within a single block; whereas the outer coordinates are represented by the blocks themselves. Thus is the use of the terms "inner" and "outer" justified.

Using Equation 3.24, the explicit matrix representation of $\hat{T}_{\text{in}}$ takes on the following block-diagonal form:

$$\hat{T}_{\text{in}} = \begin{pmatrix} T_{11}^{\text{in}} & T_{12}^{\text{in}} & \cdots & & & & & & \\ T_{21}^{\text{in}} & T_{22}^{\text{in}} & \cdots & & & & & & \\ \vdots & \vdots & \ddots & & & & & & \\ & & & T_{11}^{\text{in}} & T_{12}^{\text{in}} & \cdots & & & \\ & & & T_{21}^{\text{in}} & T_{22}^{\text{in}} & \cdots & & & \\ & & & \vdots & \vdots & \ddots & & & \\ & & & & & & \bullet & & \\ & & & & & & & \bullet & \\ & & & & & & & & \bullet \end{pmatrix} \tag{3.25}$$

Thus, the off-diagonal blocks—corresponding to $m \neq m'$—are all zero. The diagonal blocks are all the same, since $\hat{T}_{\text{in}}$ by presumption is independent of the outer coordinates.

The explicit matrix form of $\hat{T}_{\text{in}}$ above is to be contrasted with that of $\hat{T}_{\text{out}}$

$$\hat{T}_{\text{out}} = \begin{pmatrix} T_1^{11} & & & T_1^{12} & & & \bullet & & \\ & T_2^{11} & & & T_2^{12} & & & \bullet & \\ & & \ddots & & & \ddots & & & \bullet \\ T_1^{21} & & & T_1^{22} & & & \bullet & & \\ & T_2^{21} & & & T_2^{22} & & & \bullet & \\ & & \ddots & & & \ddots & & & \bullet \\ \bullet & & & \bullet & & & \bullet & & \\ & \bullet & & & \bullet & & & \bullet & \\ & & \bullet & & & \bullet & & & \bullet \end{pmatrix} \tag{3.26}$$

which can aptly be termed a "diagonal-block" matrix. Note that in both cases the majority of the matrix elements are indeed zero; in fact the memory storage requirements are proportional to d^{2k} and d^{2n-k} respectively.

The representation of the full Hamiltonian is just the matrix sum of $\hat{T}_{\text{in}}$, $\hat{T}_{\text{out}}$, and $\hat{V}$. The inverse Green's function is obtained by subtracting the Hamiltonian from

the diagonal matrix $E\hat{I} + i\hat{\epsilon}$, where the absorbing potential $\hat{\epsilon}$ is a function of the $\hat{q}_i$.[69] Note that the explicit matrix representations of both the Hamiltonian itself and the inverse Green's function share the same sparse form. As discussed in Section 2.5, this form is preserved under a change of basis involving the outer coordinates only. Thus, when $\hat{H}$ is represented in the new basis, the off-diagonal blocks remain diagonal.

If the new basis is chosen so as to minimize the off-diagonal block elements, then the basis functions are the optimal φ_m, and the new representation of the inverse Green's function is the partially diagonal representation of Section 2.3.1. The transformed diagonal blocks meanwhile, constitute the inverse of the preconditioner $\hat{G}_0$. The inversion is readily accomplished by inverting each of the diagonal blocks separately. Since the CPU time required for numerical matrix inversion scales as the linear dimension cubed, we have a $d^{n-k} \times (d^k)^3 = d^{n+2k}$ dependence for obtaining the full preconditioner. Note however that these blocks are complex symmetric rather than Hermitian, as will be shown in the next subsection, wherein we also present a reduced-dimensional algorithm for obtaining the optimal outer basis.

3.5.2 Block Jacobi Algorithm for Minimizing the Residual

The heart of optimized preconditioning—indeed, the heart of the success of the optimal separable basis approach as a practical and widely-applicable numerical technique—lies in the fact that the optimal outer basis can be systematically obtained using a simple algorithm whose operation is far less costly than a direct numerical solution for $\hat{G}(E)$. As will be shown shortly, this "outer diagonalization" procedure is a kind of reduced-dimensional diagonalization that is similar to solving a parametrized collection of subsystem eigenproblems (Section 2.2.2), though not quite the same thing.

We now present the details of the procedure. In essence, the algorithm is a block version of the well-known iterative Jacobi method for diagonalizing a symmetric matrix.[95] Fundamental to the latter is the "Jacobi rotation"—a one-parameter orthogonal transformation involving just a single pair of indices (k, k'). The rotation angle is chosen so as to zero the off-diagonal matrix elements $H'_{kk'}$ and $H'_{k'k}$ in the

transformed representation. By applying $N(N-1)/2$ separate Jacobi rotations, one could zero all of the off-diagonal elements in succession.

The resulting matrix would still not be diagonal because a given Jacobi rotation may "unzero" elements that were previously zeroed. The off-diagonal elements would be collectively smaller, however; and in fact, the Jacobi rotation angle is optimal in *precisely* the Frobenius norm sense of Equation 2.11! Thus, by iteratively applying successive sweeps of $N(N-1)/2$ Jacobi rotations, one would obtain a matrix that is diagonal to arbitrary numerical precision. Furthermore, the product of all of the successive Jacobi rotation matrices that define the diagonalizing unitary transformation would also define the eigenvectors of the original matrix.

In our case however, the final transformation matrix is constrained in that it can only involve the outer coordinates. Consequently, every block must be a multiple of the inner coordinate identity matrix. This is required if the inner coordinates are to be unaffected by the transformation; and it is clear that the corresponding Jacobi rotations must operate at the block level. When the corresponding block Jacobi or "outer diagonalization" procedure is applied, however, the transformed Hamiltonian does not generally approach even block-diagonality—let alone diagonality—owing to the fact that H is not generally weakly separable. What *is* approached to arbitrary precision however, is the orthogonality condition of Equations 2.17 and 2.30, which can be considered the proper generalization of the standard diagonality condition.

We are interested in applying Jacobi rotations that involve the *outer coordinates only.* Let i and j represent the inner and outer coordinate indices respectively, so that a single k is now associated with a *pair* of indices (i,j). Thus, if k and k' specify a particular matrix element, then j and j' specify a particular *block* within the full matrix, whereas i and i' locate a specific element *within* a block. A "block rotation" can be defined as an orthogonal transformation involving a single pair of outer indices (j_1, j_2) which is independent of the inner indices. We can write, in explicit block form,

$$\hat{R}_{j_1 j_2} = \begin{pmatrix} \tilde{I} & & & & & & \\ & \ddots & & & & & \\ & & \tilde{I}\cos\theta & \dots & \tilde{I}\sin\theta & & \\ & & \vdots & \tilde{I} & \vdots & & \\ & & -\tilde{I}\sin\theta & \dots & \tilde{I}\cos\theta & & \\ & & & & & \ddots & \\ & & & & & & \tilde{I} \end{pmatrix} \tag{3.27}$$

where the use of the tilde signifies that each entry above is an entire inner-coordinate block; and the blocks that involve θ correspond to j_1 and j_2.

A block rotation thus transforms $\hat{H}$ on a block-by-block basis. Only those blocks in the same row or column as $\tilde{H}_{j_1 j_2}$ or $\tilde{H}_{j_2 j_1}$ are affected. Specifically,

$$\begin{aligned}
\tilde{H}'_{jj_1} &= \tilde{H}'_{j_1 j} = \tilde{H}_{jj_1}\cos\theta - \tilde{H}_{jj_2}\sin\theta \\
\tilde{H}'_{jj_2} &= \tilde{H}'_{j_2 j} = \tilde{H}_{jj_1}\sin\theta + \tilde{H}_{jj_2}\cos\theta \qquad\qquad j \neq j_1, \quad j \neq j_2 \\
\tilde{H}'_{j_1 j_1} &= \tilde{H}_{j_1 j_1}\cos^2\theta + \tilde{H}_{j_2 j_2}\sin^2\theta - 2\tilde{H}_{j_1 j_2}\sin\theta\cos\theta \\
\tilde{H}'_{j_2 j_2} &= \tilde{H}_{j_1 j_1}\sin^2\theta + \tilde{H}_{j_2 j_2}\cos^2\theta + 2\tilde{H}_{j_1 j_2}\sin\theta\cos\theta \\
\tilde{H}'_{j_1 j_2} &= \tilde{H}'_{j_2 j_1} = \tilde{H}_{j_1 j_2}(\cos^2\theta - \sin^2\theta) + (\tilde{H}_{j_1 j_1} - \tilde{H}_{j_2 j_2})\sin\theta\cos\theta
\end{aligned} \tag{3.28}$$

Note that the block rotation—like the conventional Jacobi rotation—depends on a single parameter θ. In the block case however, we cannot in general zero the entire $\tilde{H}_{j_1,j_2}$ block with some choice of θ. Instead, θ is chosen so as to *minimize* the components of $\tilde{H}_{j_1,j_2}$ in the least squares sense[84]—a choice which also turns out to minimize the Frobenius norm of the entire residual.

It can be shown from Equation 3.28 that the minimizing choice of θ satisfies

$$\tan 4\theta = \left(\frac{\vec{T}_{j_1 j_2} \cdot (\vec{V}_{j_2} - \vec{V}_{j_1})}{|\vec{T}_{j_1 j_2}|^2 - |\vec{V}_{j_2} - \vec{V}_{j_1}|^2/4} \right) \tag{3.29}$$

where the notation $\vec{V}_j \equiv \tilde{H}_{jj}$ and $\vec{T}_{jj'} \equiv \tilde{H}_{jj'}$ reflects the diagonal-block form of $(\hat{T}_{\text{out}} + \hat{V})$ which is preserved under $\hat{R}$. Note that the present formulation assumes a

symmetric—rather than Hermitian—DVR matrix $\hat{H}$ in Equation 3.28. If $\hat{H}$ refers to the Hamiltonian itself (as might be the case for bound state applications), then the distinction is usually unimportant because most DVR Hamiltonians are real symmetric. However, in scattering calculations the $\hat{H}$ of Equation 3.28 should be replaced with the inverse Green's function of Equation 2.24, which is actually *complex symmetric* because of the $i\hat{\epsilon}$ absorbing potential term.

The mathematically appropriate transformation is therefore a *complex orthogonal* transformation defined by analytically continuing θ. However, the transformation must be unitary on physical grounds; and by imposing both of these conditions we are left once again with real orthogonal rotations. The minimizing real angle θ turns out to be just the real component of the corresponding complex θ, as determined by Equation 3.29 (with non-complex-conjugated dot products). Equivalently, the real θ can also be obtained by simply using (symmetrized) complex-conjuguted dot products in Equation 3.29, which is the procedure that is actually adopted in practice. In any event, the ratio of imaginary to real components of the complex angle is generally small, because $i\hat{\epsilon}$ is generally small in comparison with the rest of $\hat{H}$.

Having thus defined the Jacobi block rotation $\hat{R}$, we proceed in a manner analogous to the conventional Jacobi method. Every off-diagonal block is minimized in a succession of $d^{n-k}(d^{n-k}-1)/2$ block rotations. The process is repeated until convergence is reached, signalled by $\theta \to 0$ for all j_1, j_2. (Note that setting $\theta = 0$ in Equation 3.29 above duplicates the orthogonality condition of Equation 2.30.) In practice, the convergence is quite fast—usually requiring no more than about three or four sweeps. Since the CPU time required per block rotation scales as $d^k \times d^{n-k} = d^n$, the full outer diagonalization scales as d^{3n-2k}. In contrast, the CPU time and memory required for a direct numerical linear algebra assault would scale as $N^3 = d^{3n}$ and $N^2 = d^{2n}$ respectively.[96] Thus for reasonable d values, both the outer diagonalization and the block inversion are numerically quite easily achieved, in comparision with a brute force linear algebra calculation.

Note that depending on the kinetic energy, one may be able to alter the

value of k, so as to minimize the total time required for obtaining the preconditioner and performing the subsequent Krylov expansion. Generally speaking, increasing k increases the CPU requirements of the inversion, but decreases those of the outer diagonalization. An intermediate value of k such as $k = n/2$ usually makes the fewest overall CPU demands with respect to obtaining the preconditioner; but the subsequent Krylov expansion is often less efficient than it would be for a more lopsided division of coordinates. The specific partitioning of coordinates into inner and outer categories will also make a difference (Section 2.5).

3.6 Results—Collinear $H + H_2 \rightarrow H_2 + H$

In chemical dynamics, the collinear $H + H_2 \rightarrow H_2 + H$ system is a standard two-dimensional benchmark problem that is commonly used for evaluating theoretical reactive scattering methods. Within the Born-Oppenheimer approximation, an accurate ground state potential energy surface describing the nuclear dynamics is known,[97,98] and has been used extensively. We have used all of the methods described thus far in this chapter to calculate scattering quantities for this system: namely the cumulative reaction probability $N(E)$ and the state-to-state probabilities $P_{vv'}$, where v and v' label respectively the reactant and product H_2 vibrational quantum numbers.

These reaction probabilities have previously been calculated for this system, and can be found in the literature.[69,71,99–101] Exact quantum results have thus far been limited to relatively low energies however—typically less than about one eV—for which only one or two of the fifteen vibrational channels are energetically open. A more comprehensive treatment involving the higher channels thus requires analysis at higher energy. Unfortunately, the numerical difficulty of the linear algebra problem increases very rapidly with increasing energy.

One reason is that a larger density of DVR points is required to obtain meaningful results; in the present two-dimensional case for instance, the minimum required grid density increases linearly with energy. Moreover, as the excited state channels become available, the effective interaction region itself is enlarged. Thus, whereas one or two hundred DVR points will suffice at low energies, fifteen thousand

or so are required as the dissociation threshold is approached (~4.74 eV). To make matters worse, the density of energetic states becomes significantly prominent near the threshold—a numerically "stiff" situation corresponding to ill-conditioned DVR matrices that can be devastating for Krylov convergence. Fortunately, all of the above complications have been mitigated by the use of the optimized preconditioner, which has enabled us to obtain results for energies near and above the dissociation threshold.

In mass-weighted Jacobi coordinates[2,102] (Chapter 4), the $H + H_2$ Hamiltonian has the simple form[34]

$$\hat{H} = \frac{\hat{p_x}^2}{2\mu} + \frac{\hat{p_y}^2}{2\mu} + V_{\text{LSTH}}(\hat{x}, \hat{y}) \tag{3.30}$$

where V_{LSTH} is the LSTH potential energy surface,[97,98] μ is the reduced mass, and x and y are the Jacobi coordinates. Note that the form of Equation 3.30 is preserved under a rotation of coordinates. One might therefore consider applying such a rotation before laying down the DVR grid, as is done for instance, when using the normal mode coordinates of the transition state.[34] As it happens however, the straightforward Jacobi coordinates above yield the more efficient preconditioner. Note also that Equation 3.30 satisfies Equation 2.28, thus allowing for a direct comparison of the present method with other, less generally applicable methods that *require* the kinetic energy to be strongly separable and translationally-invariant.[83]

The DVR grid is rectangular with approximately the same number of points in each direction. However, V varies somewhat less with the Jacobi translational coordinate than with the vibrational coordinate; consequently, the former (x) is chosen as the inner coordinate.[84] A potential cutoff energy V_{cut} is assigned to those regions of the rectangular grid which are either unphysical or energetically improbable. The grid is truncated in the asymptotic reactant (product) regions using quartic absorbing potentials in the translational Jacobi coordinate x (x').

The use of a rectangular grid is not ideal from a DVR perspective, but constitutes—in the two-dimensional case only—a necessary limitation in the present state of affairs. Unfortunately, the outer diagonalization procedure in its current implementation requires the use of identically-sized blocks, necessitating a rectangular DVR grid. Consequently, extraneous DVR points are introduced which detract some-

what from the overall computational efficiency. In the present case, these have been reduced by using unrotated Jacobi coordinates; and in any event the benefits of outer diagonalization far outweigh the computational burden resulting from the enlarged grid. Were this not the case, one could skip the outer diagonalization altogether and proceed directly to the $\hat{H}_0$ inversion; for the latter is completely independent of the former and can easily be performed on an arbitrarily-shaped grid.

3.6.1 Reaction Probabilities

Using the DVR as described in the preceding few paragraphs—in conjunction with Equation 3.14 and the optimized preconditioner—we have obtained state-to-state reaction probabilities for energies ranging from 0–6 eV, and vibrationally excited channels up to $v = 9$. Cumulative reaction probabilities have also been obtained, using Equations 3.19 and 3.14. The results—presented in Figures 3.1 to 3.10—are in qualitative agreement with other quantum-mechanical and quasi-classical calculations for $H + H_2 \rightarrow H_2 + H$.[99,103,104]

The data was obtained separately for each energy, in increments of .01 eV; however, as the primary emphasis is evaluation of the method, convergence with respect to the DVR parameters was only explicitly checked every .20 eV or so. Evidently, this led to satisfactory results for the most part. However, convergence is notoriously difficult in the region just above the energy at which a given channel becomes accessible. The reason is that the low translational kinetic energy associated with the asymptotic states requires a very broad absorbing boundary region, and hence a considerably larger DVR grid. Moreover, these energies are often associated with resonant features. It was therefore necessary to reconverge the calculations near the threshold energies.

Convergence is to within a few percent at all energies except near channel thresholds. Tables 3.1 and 3.2 relate typical convergence features with respect to various grid parameters. As has been observed previously,[69] the grid spacing for a given energy was found to be about 3.5–4.0 points per deBroglie wavelength. Generally speaking, V_{cut} was about 3.0 eV higher than the energy in question, and the

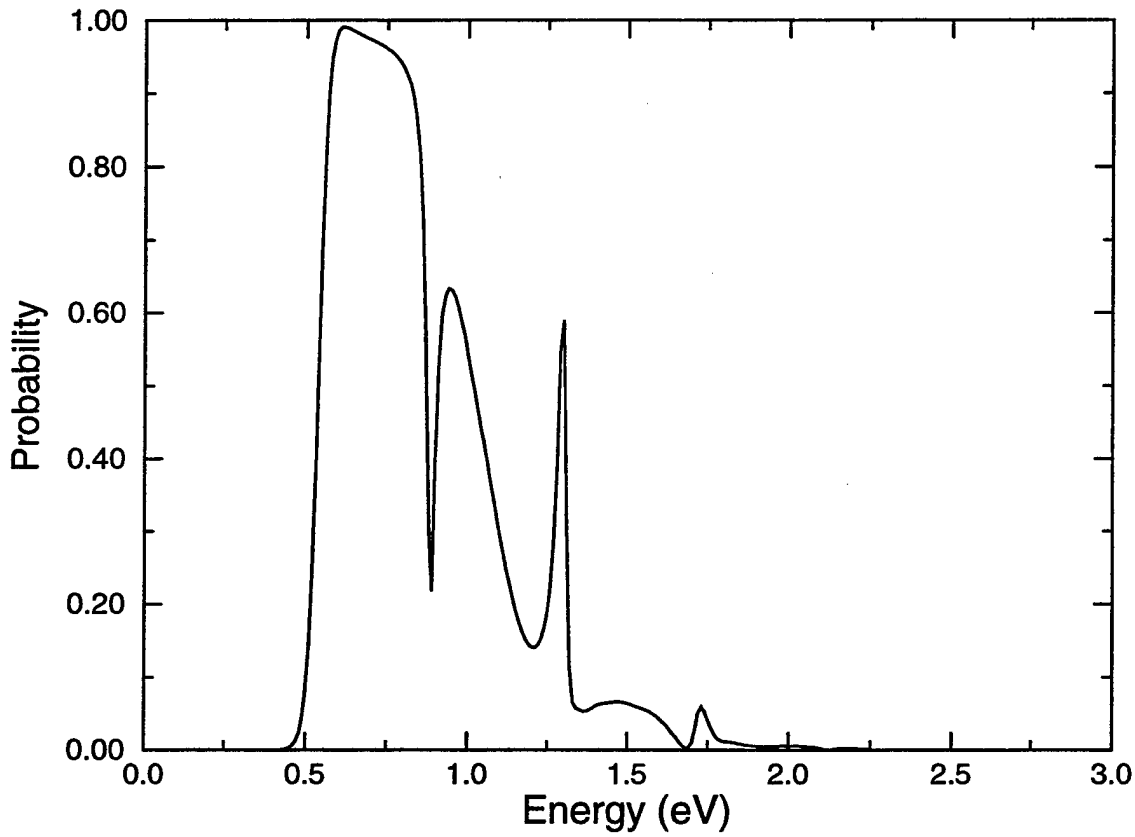

Figure 3.1: State-to-state reaction probabilities for the collinear H + H_2 → H_2 + H system: ——— (0–0)

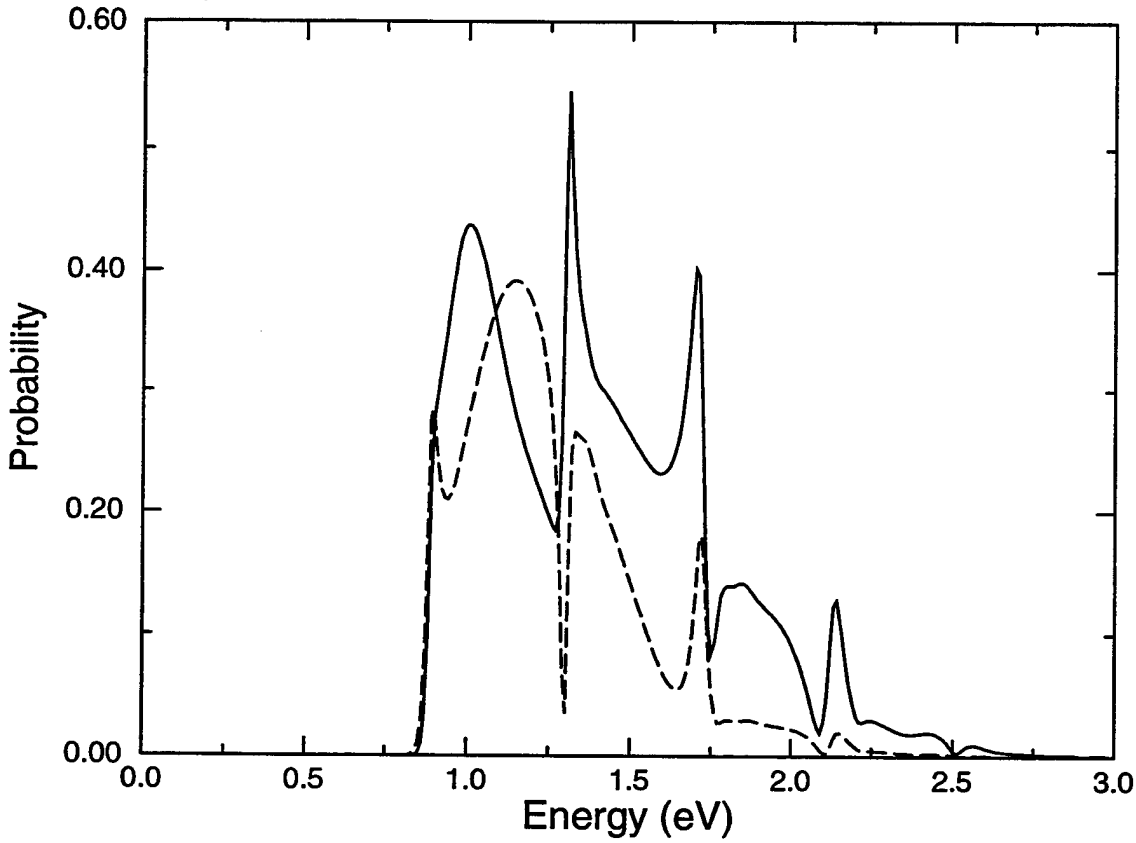

Figure 3.2: State-to-state reaction probabilities for the collinear $H + H_2 \rightarrow H_2 + H$ system: ——— (1–1); — — — (1–0).

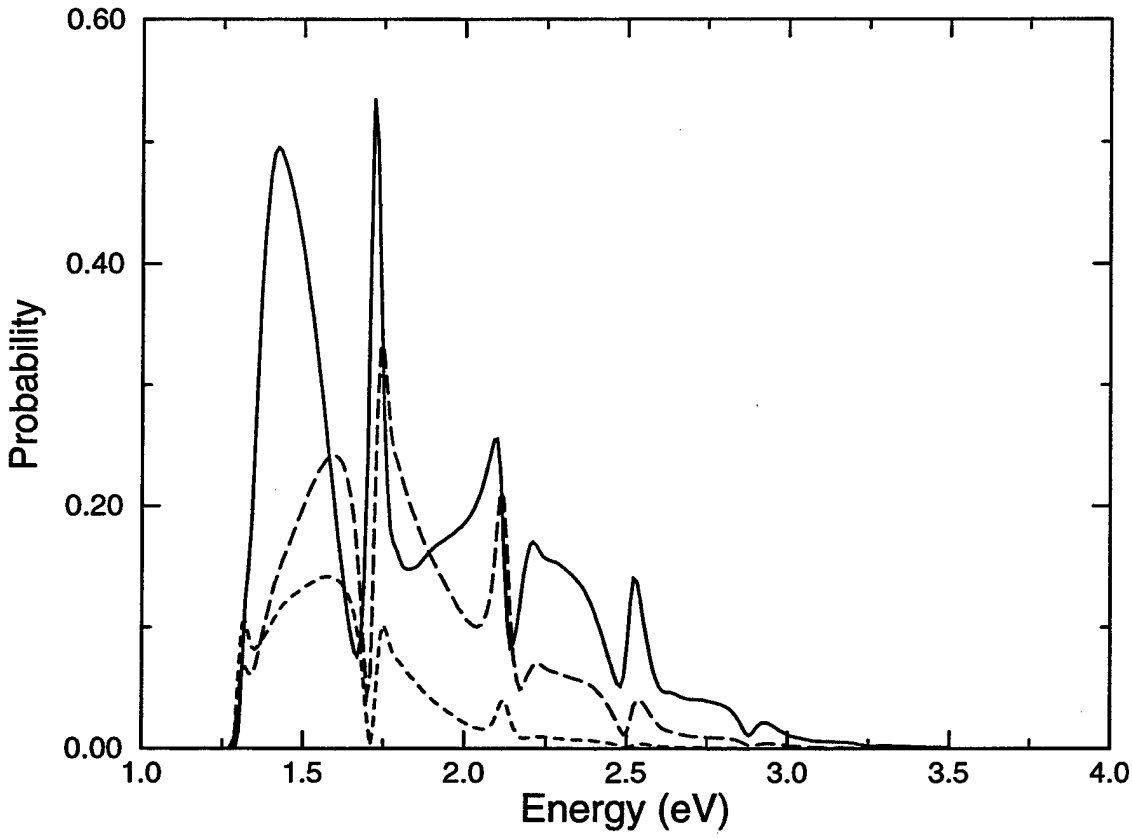

Figure 3.3: State-to-state reaction probabilities for the collinear $H + H_2 \rightarrow H_2 + H$ system: ——— (2–2); — — — (2–1); - - - - (2–0).

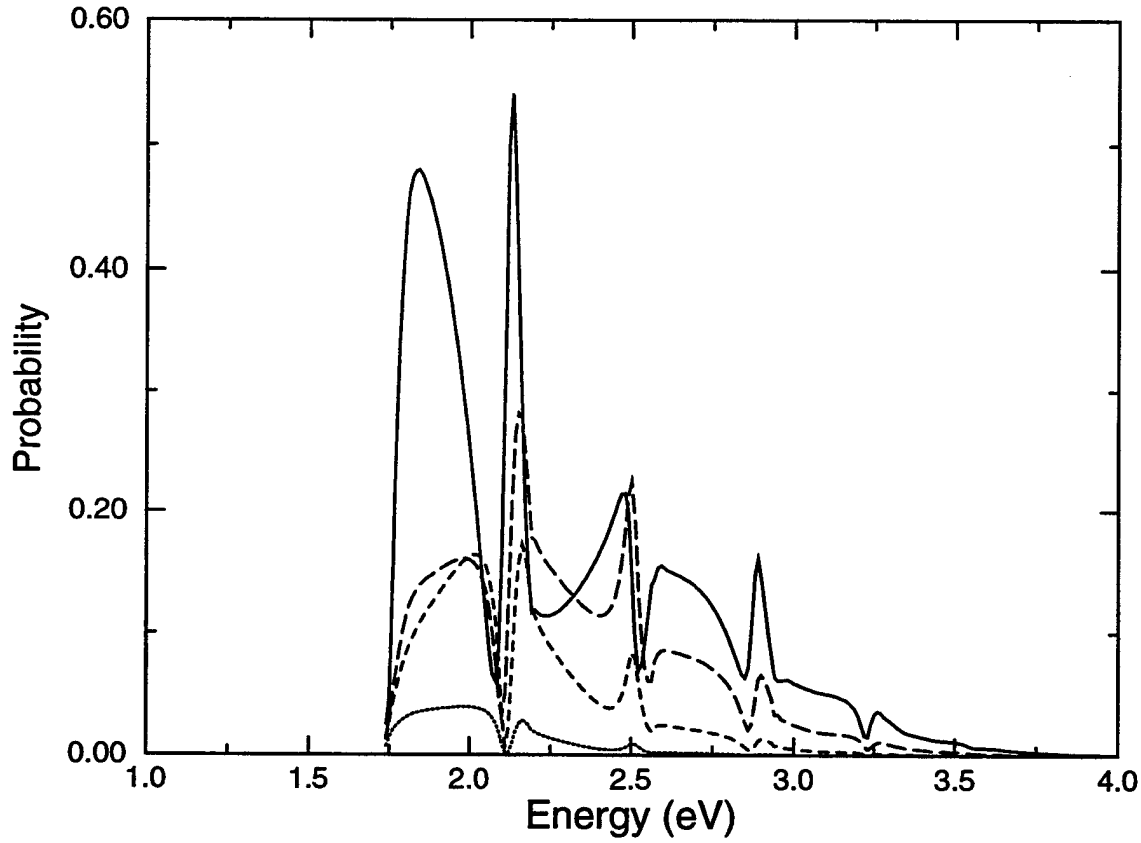

Figure 3.4: State-to-state reaction probabilities for the collinear $H + H_2 \rightarrow H_2 + H$ system: ——— (3–3); — — — (3–2); - - - - (3–1); - - - - - (3–0).

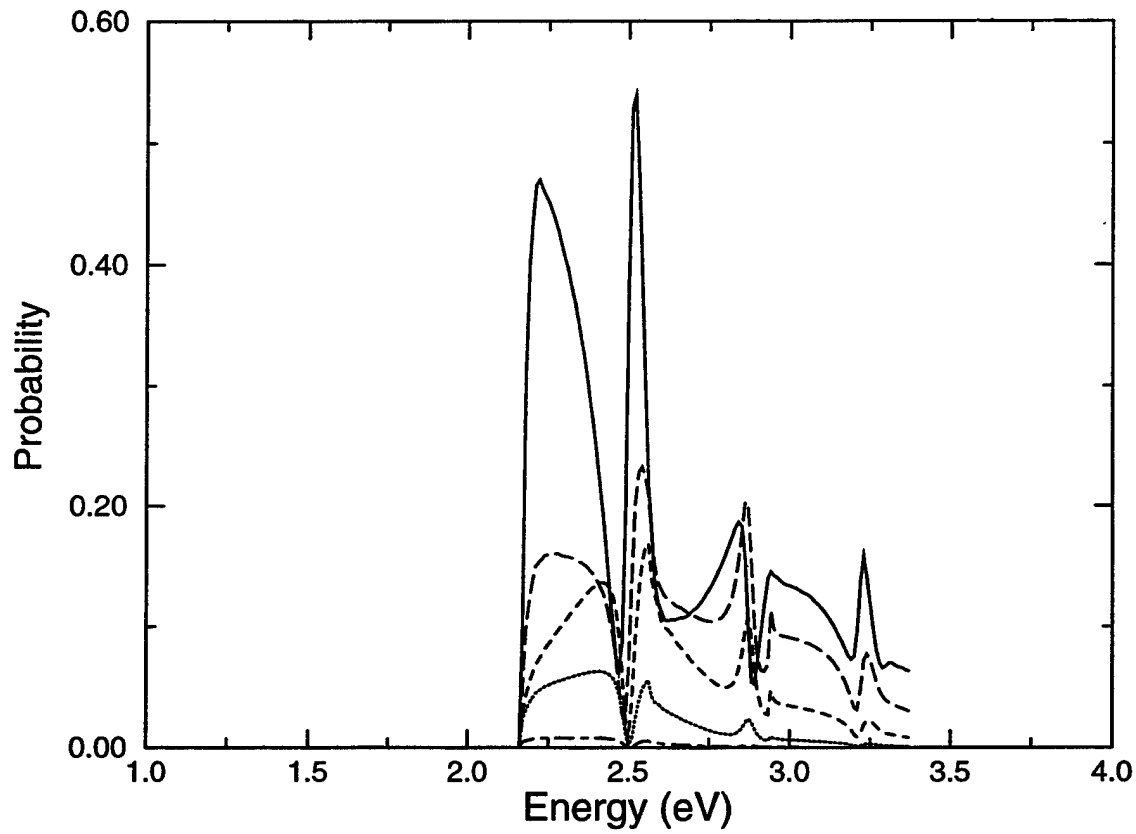

Figure 3.5: State-to-state reaction probabilities for the collinear H + H_2 → H_2 + H system: ——— (4–4); — — — (4–3); - - - - (4–2); - - - - - (4–1); - - - - - (4–0).

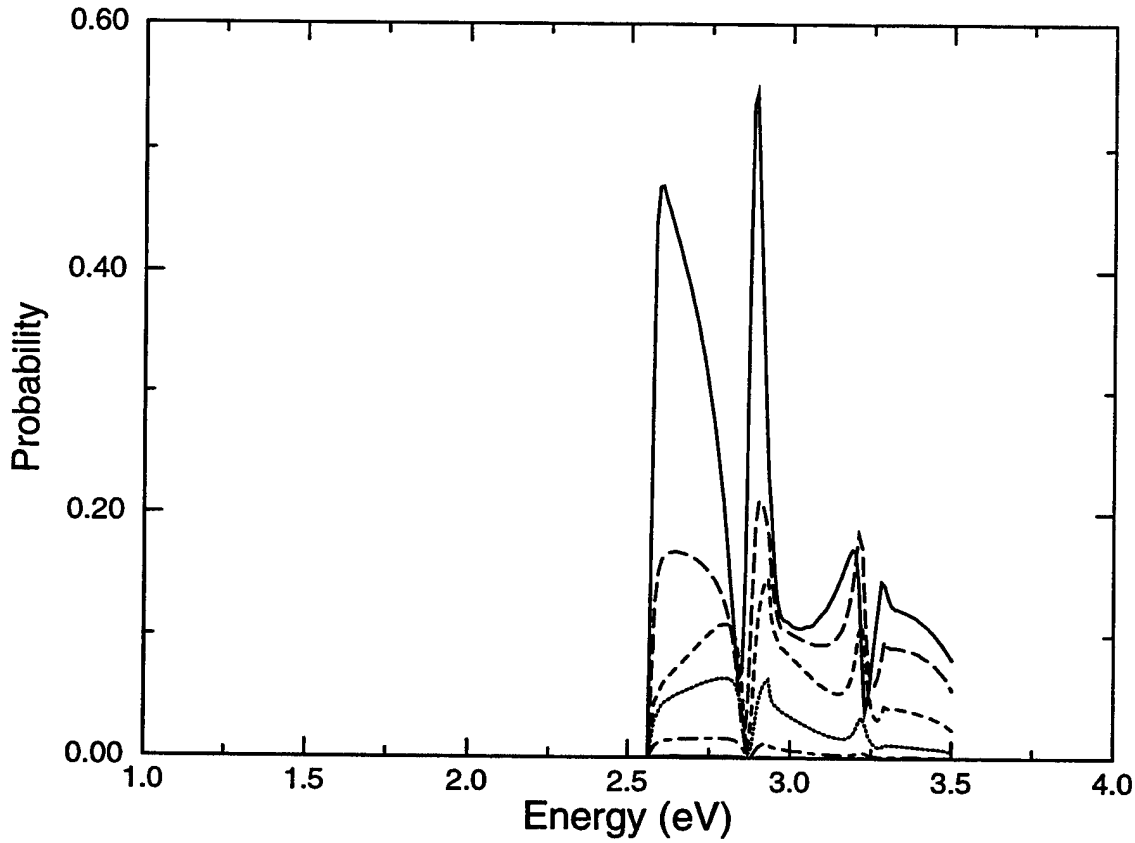

Figure 3.6: State-to-state reaction probabilities for the collinear $H + H_2 \rightarrow H_2 + H$ system: ——— (5–5); — — — (5–4); - - - - (5–3); - - - - - (5–2); - - - - - (5–1).

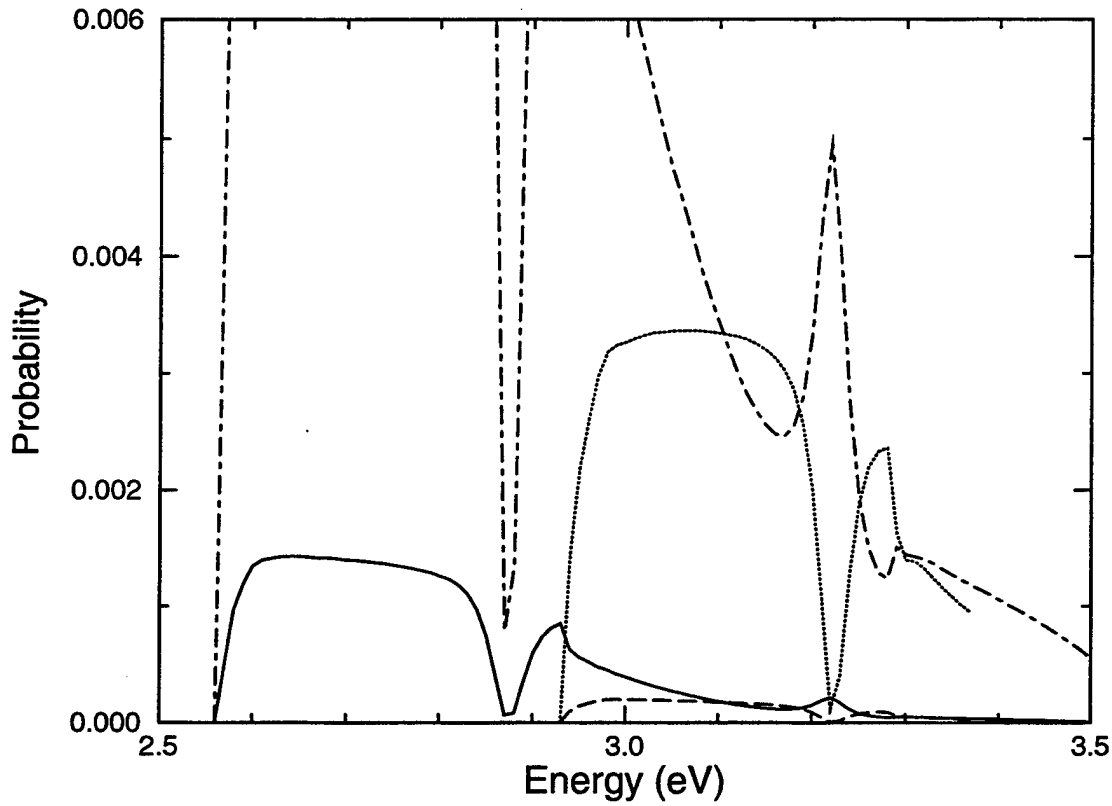

Figure 3.7: State-to-state reaction probabilities for the collinear $H + H_2 \rightarrow H_2 + H$ system (expanded graph): - - - - - (5–1); ——— (5–0); - - - - - (6–1); — — — (6–0).

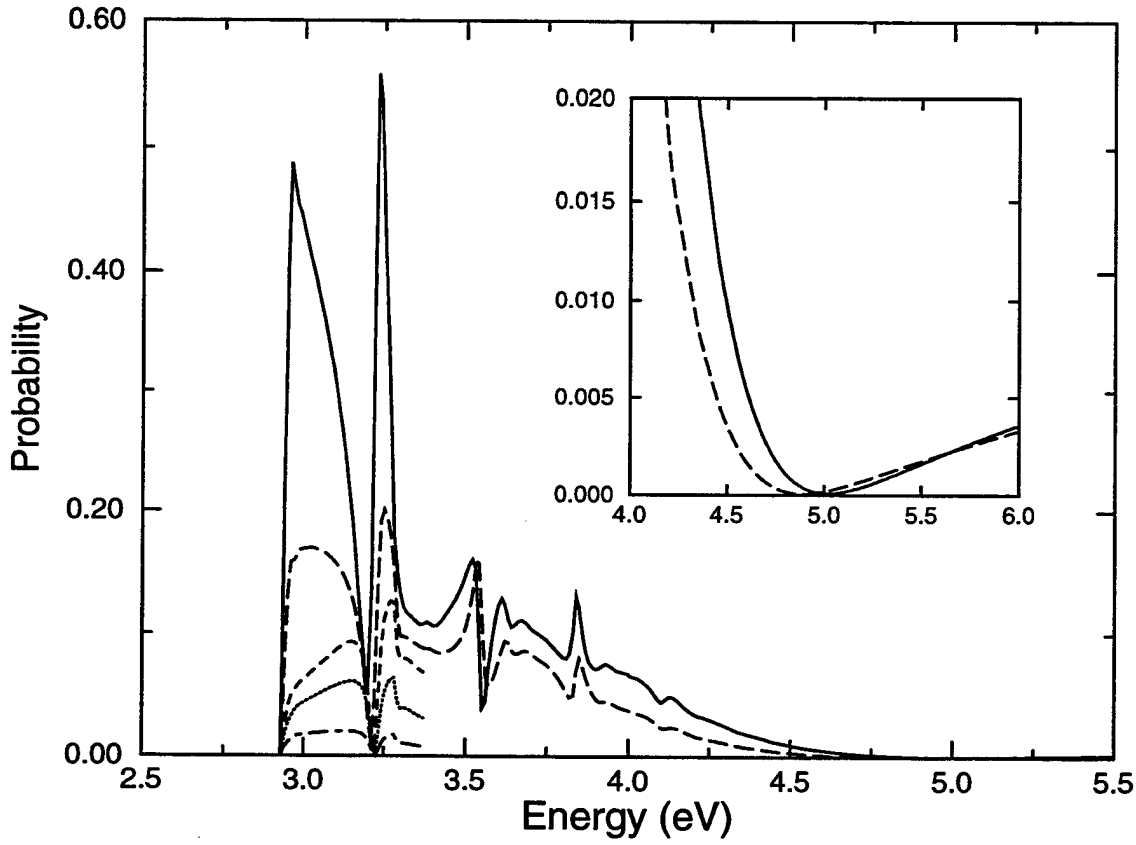

Figure 3.8: State-to-state reaction probabilities for the collinear $H + H_2 \rightarrow H_2 + H$ system: ——— (6–6); — — — (6–5); - - - - (6–4); - - - - - (6–3); - - - - - (6–2).

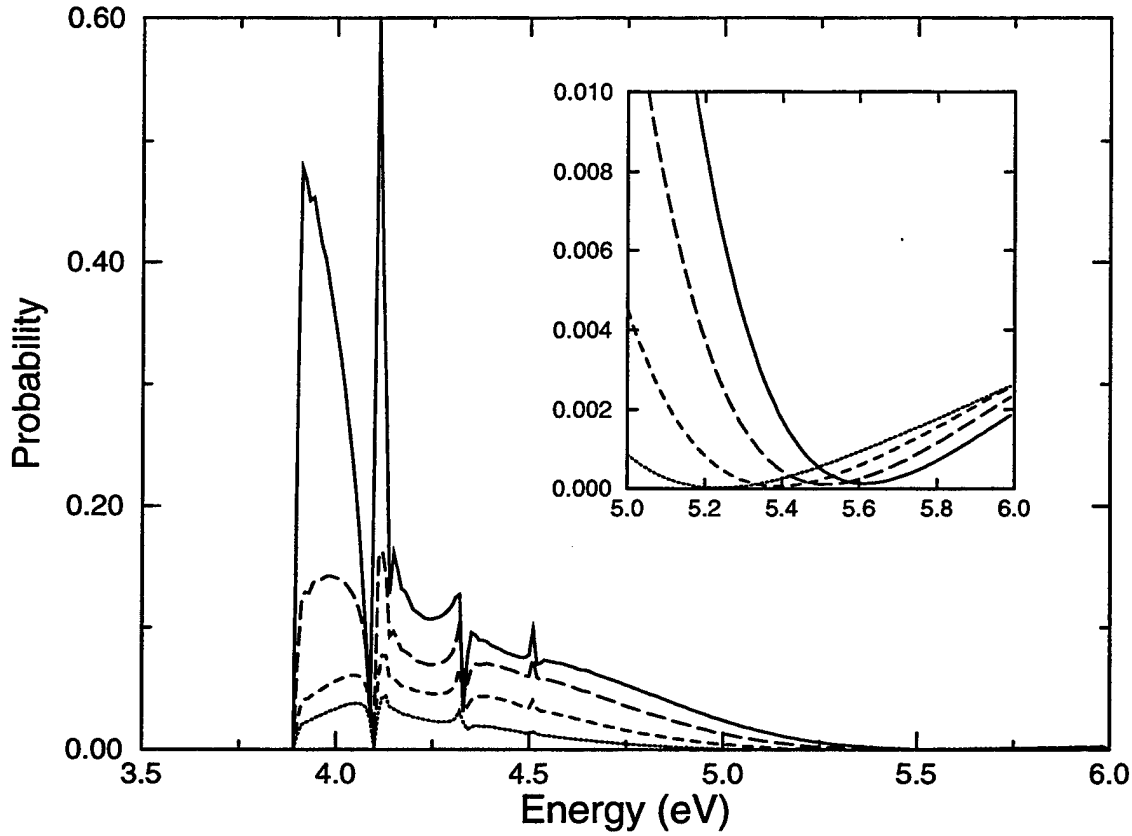

Figure 3.9: State-to-state reaction probabilities for the collinear $H + H_2 \rightarrow H_2 + H$ system: ——— (9–9); — — — (9–8); - - - - (9–7); - - - - - (9–6).

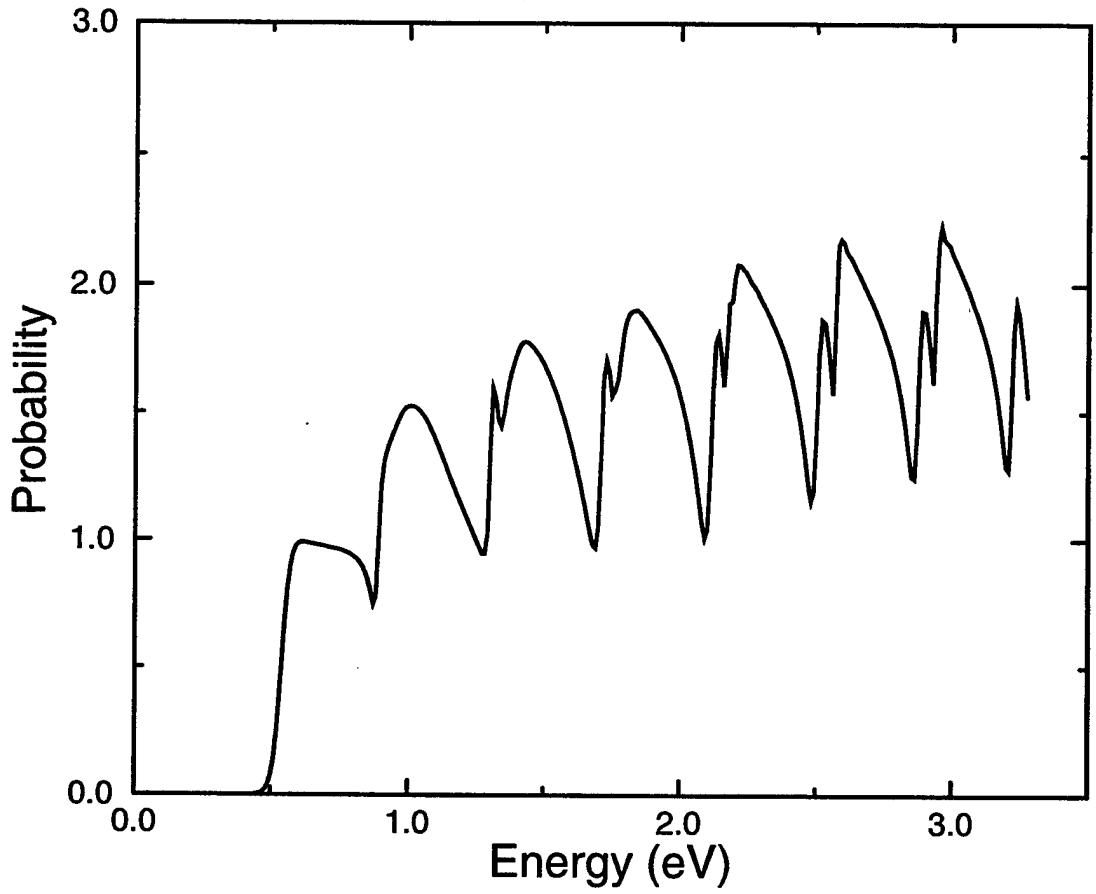

Figure 3.10: Cumulative reaction probabilities for the collinear $H + H_2 \rightarrow H_2 + H$ system.

Grid Spacing (a_o)	Transition Probabilities				
	4–0	4–1	4–2	4–3	4–4
.15	.0078	.0493	.0813	.1501	.4330
.13	.0077	.0492	.0807	.1489	.4311
.11	.0077	.0491	.0805	.1482	.4305

Table 3.1: DVR convergence data for collinear $H + H_2 \rightarrow H_2 + H$ calculations: convergence of state-to-state reaction probabilities with respect to grid spacing for the 4–v' transitions at 2.25 eV.

Grid Extent (a_o)	Transition Probabilities				
	4–0	4–1	4–2	4–3	4–4
9.5	.0080	.0510	.0830	.1508	.4330
10.0	.0078	.0499	.0827	.1541	.4479
10.5	.0078	.0503	.0843	.1593	.4596
11.0	.0080	.0512	.0859	.1627	.4627
11.5	.0080	.0519	.0867	.1633	.4597

Table 3.2: DVR convergence data for collinear $H + H_2 \rightarrow H_2 + H$ calculations: convergence of state-to-state reaction probabilities, with respect to the maximum grid extent into the asymptotic region, for the 4–v' transitions at 2.25 eV.

absorbing region extended out to 7–12 a_o, depending on the energy (for state-to-state calculations).

Near the threshold energies however, a much larger grid was used—in some cases extended out to 20 a_o. This was particularly true of the higher vibrational thresholds, for which the potential barrier is less significant, and the resultant step-function-like initial rise leads to non-negligible probabilities near the channel threshold energy. Despite the larger grid, convergence in these regions is somewhat less accurate; although this is mitigated somewhat by the use of Tukey nearest-neighbor smoothing.[91]

3.6.2 Numerical Issues

In obtaining these results, we have made use of certain numerical "tricks" to expedite the calculations. In Equation 3.14 for example, only a single action of the Green's function on $\vec{\phi}_v$ need be calculated for a variety of different $\vec{\phi}_{v'}$'s; though in practice simultaneous convergence may be difficult if the range of v' values is too great. Another technique is to use the same grid over a range of energies—in this case spanning about one eV. We choose DVR parameters which are simultaneously converged at both energy endpoints and in the middle. One can then go back and attack the "trouble spots" with a more accurate, but computatationally expensive DVR grid.

Using the same DVR grid for a range of energies also has positive ramifications for the preconditioner. Most notably, the outer diagonalization need be performed only *once* for the entire *set* of calculations; as the various inverse Green's functions differ only by a constant times the identity matrix. This represents a considerable computational reduction; for although both the outer diagonalization and the $\hat{H}_0$ inversion are N^2 processes, the prefactor of the former is considerably larger. It turns out however, that the $\hat{H}_0$ inversion can also be made much more efficient. This is accomplished by diagonalizing the block-diagonal $\hat{H}_0$ matrix for a single energy—a process that is also N^2. Then for any other energy, applying the inverse of $\hat{H}_0$ to a vector is easily effected via straightforward matrix-vector multiplications. Thus for a particular energy calculation, preconditioning reduces to an $N^{3/2}$ process.

These fine-tunings provide only marginal benefit, however if the processing time required by the subsequent, preconditioned Krylov routine is comparatively slow. In our case for example, where we perform the outer diagonalization only once but do not implement the $\hat{H}_0$ optimization, the Krylov step was consistently about three times slower than the preconditioning step over the full range of energies encountered. Nevertheless, Krylov convergence was still *much* faster than it would be *without* preconditioning, as is clear from Table 3.3. Although the precise dependence may vary somewhat with the particular algorithm, the CPU time required by most iterative Krylov methods scales *more* than linearly—typically quadratically—with the

Transition v–v'	Energy (eV)	DVR Points	Krylov Iterations		Residual Tolerance
			precond	none	
0–0	0.0–1.0	430	∼40	∼ 300	0.0001
1–0,1	1.0–2.0	1128	∼ 70	∼ 450	0.0001
2–0,1,2	1.3–2.1	1322	∼ 85	∼ 550	0.0001
3–0,1,2,3	1.8–2.8	2554	∼ 130	∼ 900	0.0001
6–5,6	4.0–6.0	5500	220–280	—	0.0001
9–6,7,8,9	3.8–4.8	14000	440–470	—	0.00005
9–6,7,8,9	4.8–6.0	12000	420–500	—	0.00005

Table 3.3: Krylov convergence data for state-to-state collinear $H + H_2 \rightarrow H_2 + H$ calculations: optimized preconditioner vs. no preconditioner.

number of iterations[73,92]. Thus for intermediate grid sizes, Table 3.3 implies a CPU time reduction factor of about fifty. The reduction would probably be even greater for larger grids. Note that the Krylov approach is only computationally advantageous when the number of iterations required for convergence is much smaller than N. We can thus infer from Table 3.3 that without preconditioning, Krylov approach is effectively useless as the energy approaches the dissociation threshold—in fact it does no better than a direct N^3 inversion.

The CPU memory requirements should also be addressed. Use of the present preconditioner requires storage of $\hat{H}_0$ and $\hat{\Delta}$, both of which scale as $N^{3/2}$. This should be compared with the Krylov memory, which depends greatly on the particular algorithm being employed. Those that admit preconditioners (GMRES) have historically scaled as KN, where K is the number of Krylov iterations. Recently, linear N algorithms such as CGS and QMR have been developed to work in conjunction with preconditioners; however the convergence properties do not yet seem as stable as for GMRES.[92–94]

From Table 3.3, we see that the preconditioned Krylov iterations increase—roughly linearly—with energy. We are led by earlier considerations to attribute this to an increase in the density of available states rather than grid size; although the latter certainly affects the processing time *per* iteration. In any event, in order to determine whether this and the other assumptions of Section 3.4 are in fact justified, we have performed several numerical tests.

The simplest test is to increase the density of grid points while keeping all other factors including the energy constant, and to determine the effect on the number of Krylov iterations required to converge to a specified tolerance. This was done for the 0–0 transition for densities ranging by a factor of about twenty-five (N = ~900–22000). For a tolerance of 10^{-4}, the number of iterations was almost constant—ranging from 42 to 44—suggesting that the convergence properties of the preconditioner are independent of grid size, provided the other DVR parameters are properly converged.

We also expect the eigenvalue structure of the kernel matrix $\hat{A}$ to be fairly independent of grid density. As Figure 3.11 demonstrates, the largest eigenvalue is indeed almost uniform for sufficiently converged grid densities. Figure 3.11 also presents results where the potential strength has been artificially increased or decreased. Note that in either limit the eigenvalues diminish. These are the limits in which the optimized preconditioner subsumes the diagonal and the kinetic energy preconditioners, respectively.[83] Finally, as the energy and Krylov iterations increase, we anticipate a correlated increase in the eigenvalues and associated norm of $\hat{A}$. Figure 3.12, which depicts $|\hat{A}|$ as a function of energy, shows that this is indeed the case. In order to obtain a fair comparison, the same DVR grid is used for all energies.

We have also tested the assumption that the translational coordinate should be the more efficient choice of inner coordinate, by repeating the calculations with the coordinates transposed. This did in fact lead to a 5% increase in the number of Krylov iterations. In addition, we have also performed calculations using a normal mode coordinate DVR grid. This grid has a larger number of extraneous points, representing an increase in N of about 25%—but it also increases the number of iterations by about 15%, presumably because the potential is less separable in these coordinates. The net result is that the normal mode version is about 1.7 times slower. As a final test, we compared the rectangular DVR grid plus full preconditioner, versus the smaller, irregular DVR grid with $\hat{H}_0$ inversion only. Despite the slightly smaller number of points, the latter required more than three times as many iterations, and an even greater increase in CPU time.

3.7 Conclusions

The primary purpose of this chapter has been to evaluate the effectiveness of the optimal separable basis approach as applied to a realistic reactive scattering calculation. In Section 3.4, a general quantitative method was suggested for evaluating preconditioners; and based on that criteria, a particular optimized preconditioner was developed. In Section 3.6, we have put these ideas into practice for a specific chemical system, and tried to determine whether the theoretical arguments presented herein are valid in the domain of computational linear algebra.

The results have been very reassuring. As indicated in Table 3.3, the optimized preconditioner has been shown to improve performance dramatically in the computational $H + H_2 \rightarrow H_2 + H$ system. Moreover, the benefits seem to be most pronounced in precisely those situations which are numerically most challenging. In addition to obtaining new scattering data for previously prohibitive energy regimes, several important connections with theory have been validated. It is significant that the principal assumptions[84] of Section 2.3 and of Chapter 2 are evidently borne out by our simple tests—even when sophisticated iterative algorithms are employed—for it strongly suggests that the general preconditioner optimization problem can in fact succumb to physical intuition.

Although the results were encouraging for the two-dimensional system discussed in this chapter, the preconditioning scheme presented here is expected to be even more useful for higher dimensionalities. In Chapter 4, we consider a more realistic reactive three-body system, for which the optimized preconditioner is applied to an explicit three-dimensional calculation.

3.8 Appendix: Convergence of a Geometric Operator Series

We are interested in evaluating the convergence of a geometric series expansion of an operator $\hat{A}$, such as the kernel in Equation 3.23. We are also interested

in establishing which definition of $|\hat{A}|$ is most closely correlated with the rate of convergence. Unfortunately, unlike the corresponding complex number series case, the result depends on the level of expansion k. Consider the residual of the k'th-level expansion of Equation 3.23—i.e., the vector

$$\vec{r} \equiv \vec{y} - \left(\hat{I} + \hat{A} + \cdots \hat{A}^k\right)\vec{b}. \tag{3.31}$$

Regardless of how the norm $|\hat{A}|$ is defined, we view $|\vec{r}|^2 \equiv \vec{r}^{\,*} \cdot \vec{r}$ as the quantity to be minimized.

The residual can be rewritten as follows:

$$\vec{r} = \hat{A}^{k+1}\left(\hat{I} - \hat{A}\right)^{-1}\vec{b} \tag{3.32}$$

Strictly speaking, the quantity $|\vec{r}|$—and hence the convergence properties of Equation 3.23—depend on the vector $\vec{b}$. We adopt the notion that nothing is known about $\vec{b}$ *a priori*, so that a given component is statistically equivalent to any other. In this sense, the residual magnitude depends on the matrix $\hat{A}$ only. Since $|\vec{r}|$ is a representation-independent quantity, by transforming to the basis in which $\hat{A}$ is diagonal it is easy to see that

$$\langle|\vec{r}|^2\rangle \propto \sum_i \left|\frac{\lambda_i^{k+1}}{1-\lambda_i}\right|^2 \tag{3.33}$$

where the $\{\lambda_i\}$ are the eigenvalues of $\hat{A}$.

At this point, we acknowledge a similarity with the Hölber "p-norm":[15]

$$\mathrm{norm}_p(\hat{A}) \equiv \left(\sum_i |\lambda_i|^p\right)^{\frac{1}{p}}, \tag{3.34}$$

although the form above is usually associated with vectors. In any event, for a k-level expansion, the definition $|\hat{A}| \equiv \mathrm{norm}_{2k+2}(\hat{A})$ is most closely correlated with the residual magnitude. The correspondence should be quite good particularly for larger k values, because $(1-\lambda_1)/(1-\lambda_2) \approx 1$ for two eigenvalues λ_1 and λ_2 which contribute significantly to the sum in Equation 3.33.

The various p-norm definitions depend on the eigenvalues only, and are therefore independent of representation as desired. Quantitatively however, they differ

significantly. In the limit $k \to \infty$ for example, $|\hat{A}| = \max(|\lambda_i|)$ is the so-called "Euclidean Norm."[16] The other limit ($k = 0$) would reproduce Equation 2.11—i.e. the Frobenius norm[14†] In any event, the most appropriate norm with which to minimize $\hat{A}$ would appear to depend on the level of expansion k, which is usually not known in advance.

Despite quantitative differences, we are interested not in the value of $|\hat{A}|$ itself, but in minimizing $|\hat{A}|$; and in this respect, the particular norm used may not matter very much. If the condition number is fairly small, for instance, then all p-norms will agree quite closely, apart from proportionality constants. Similarly, in the other extreme case of only one non-zero λ_i, all p-norms become equivalent to the Euclidean norm. Therefore, if $\hat{A}$ is optimized for the lowest level of expansion (i.e. by using the Frobenius norm), the result is usually expected to be near optimal at the higher expansion levels as well.

The quantity that is actually minimized however, is not $|\hat{A}|$ but $|\hat{\Delta}|$; so the relevant question is, how good a measure is $|\hat{\Delta}|$ of the convergence of Equation 2.26. Again, if the condition numbers are fairly small the matrix behavior is number-like; so the minimal norm representations for $\hat{\Delta}$ and $\hat{A} = \hat{G}_0\hat{\Delta}$ roughly coincide. But this is precisely the limit in which the optimal separable method is most effective. Even in the more general situation however, a strong correlation between $|\hat{A}|$ and $|\hat{\Delta}|$ certainly persists.

[†]Technically, this requires that the matrix $\hat{A}$ be Hermitian, which it is not. However, the appropriate modification via $|\hat{A}|^2 = \mathrm{tr}(\hat{A}^\dagger\hat{A})$ is straightforward.

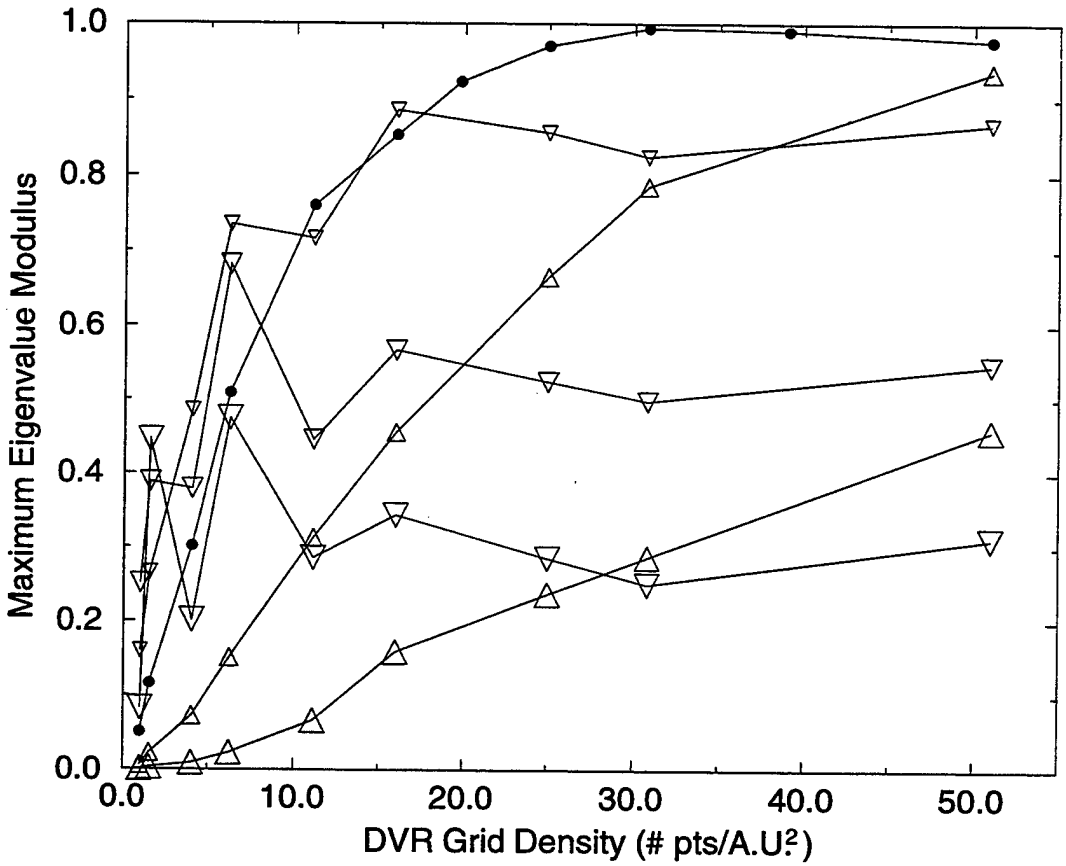

Figure 3.11: Largest $\hat{A}$ eigenvalue magnitude as a function of DVR grid density, for various potential energy strengths: •—•—• $V = V_{\mathrm{LSTH}}$; △—△—△ $V = 10V_{\mathrm{LSTH}}$; △—△—△ $V = 100V_{\mathrm{LSTH}}$; ▽—▽—▽ $V = V_{\mathrm{LSTH}}/5$; ▽—▽—▽ $V = V_{\mathrm{LSTH}}/25$; ▽—▽—▽ $V = V_{\mathrm{LSTH}}/100$.

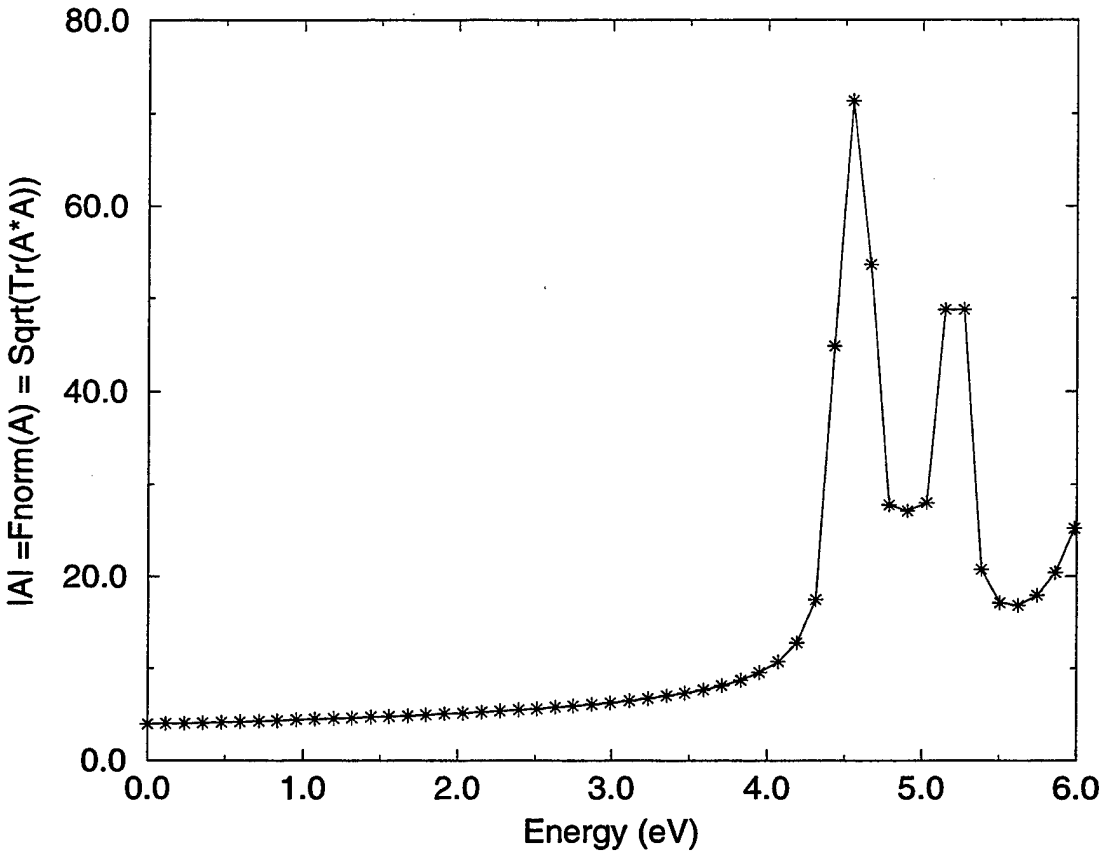

Figure 3.12: $|\hat{A}|$ as a function of energy. The norm of the matrix $\hat{A}$ is the Frobenius norm.

Chapter 4

Thermal Rate Constants and Coriolis Minimization

4.1 Introduction

In this chapter, we apply the optimal separable basis methods of the previous chapters to a realistic three-body system that is not artificially constrained to lie on a straight line.[105] All of our explicit numerical calculations are for the microcanonical quantities of Chapter 3. In practice, the thermal quantities such as the rate constant $k(T)$ are often more desirable; but these can be obtained via Boltzmann-averaging the microcanonical quantities. It should be mentioned that DVR methods have also been developed for obtaining the thermal quantities directly.[106–108] although we do not make use of such methods here.

Although recent years have seen great strides in the use of computers to obtain accurate quantum scattering quantities, calculations for arbitrary chemical reactions have not yet progressed to the point of becoming routine. Using current numerical techniques as described in Chapter 3, exact quantum calculations for the full $3N-3$ dimensional translationally-reduced Hamiltonian are still challenging for most chemical systems, even when $N = 3$. Consequently, explicit numerical calculations are usually only performed for certain dimensionally-reduced special cases, such as the restriction to zero total angular momentum.

Once the reduced calculations have been obtained, results for the full problem can be approximated using various adiabatic or "sudden" methods, such as the helicity-conserving[109,110] (HC), infinite order sudden[109] (IOS), and J-shifting[111] (JS) approximation schemes. Our interest lies in improving both the efficiency of the numerical calculations and the accuracy of the subsequent adiabatic approximations. We shall find that the optimal separable basis methods of Chapters 2 and 3 can be usefully applied in both cases.

To boost the efficiency of the numerical calculations, we apply the optimized preconditioning scheme of Chapter 3. In the two-dimensional collinear $H + H_2 \rightarrow H_2 + H$ system, the total computational effort was reduced by a factor of about fifty. In the three-body case however, the method is expected to be even more effective because the dimensionality is greater. In this chapter, we shall present an efficient and widely applicable version of the preconditioner designed specifically for the reduced three-body Hamiltonian.

Insofar as the adiabatic methods are concerned, we shall restrict attention to the HC and JS approximations only. Both of these are intimately related to the problem of disentangling rotational and vibrational degrees of freedom. Although this problem has been considered many times for particular coordinate systems such as the Eckart frame,[112] it has only recently enjoyed a proper mathematical treatment in the applied literature. In particular, a systematic and coordinate-independent analysis of the rotational gauge and associated "Berry's phase" was presented in a recent paper by Littlejohn.[12]

To the author's best knowledge, the rotational gauge *per se* has not been previously considered in the literature pertaining to quantum reactive scattering calculations. This issue has been explored in some detail by the author, who has developed some improvements over the conventional HC and JS approximations for three-body reactions.[13] Full derivations are not presented here due to space limitations; however, we shall make use of the suggested improvements, and evaluate their effectiveness with respect to the system at hand.

In particular, the coriolis coupling is minimized by applying both rotational gauge theory[12] and the optimal separable basis theory.[84] When the Hamiltonian is

represented in the new rotational and vibrational coordinates, an "effective" potential emerges which corresponds physically to the two-body central force analogue. As is true in the two-body case, the form of the three-body Hamiltonian strongly suggests that a different equilibrium or transition state geometry be associated with each distinct set of rotational quantum numbers.

All of the methods described in the preceding paragraphs are applied in this chapter to the $O + HCl \rightarrow OH + Cl$ reactive scattering system. This particular reaction, which is of interest to atmospheric and combustion chemists, is in many respects an ideal testing ground for the new methods. There is no symmetry in either the masses or the ground electronic potential energy surface. Moreover, the masses/actions are large in comparison with other systems for which exact quantum calculations have been performed,[69,76] even though tunneling contributions may be important. We use the $(^3A'')$ analytical potential surface developed by Koizumi *et al*,[113] for which there are multiple transition states, and whose reaction path has been described as "tortuous." These features all contribute to the formidable numerical difficulties associated with this system, although several other theoretical and experimental $O + HCl \rightarrow OH + Cl$ rate constant estimates are available from the literature for comparison with the present results.[107,108,113–119]

The remainder of this chapter is organized as follows. In Section 4.2, we present the requisite theoretical background. Section 4.2.1 summarizes some pertinent aspects of the rotation/vibration separation problem, and Section 4.2.2 describes the HC and JS approximations. The rest of Section 4.2 is concerned with the computational techniques used in the explicit calculations, i.e. a DVR grid with absorbing boundary conditions and optimized preconditioning. Section 4.3 discusses certain numerical details, such as the choice of coordinates and DVR, grid parameter values, etc. Finally, Section 4.4 contains the results for the $O + HCl \rightarrow OH + Cl$ system. Cumulative reaction probabilities and thermal rate constants are presented, as well as a comparison between the standard and improved JS approximation methods.

4.2 Theory

4.2.1 Separation of Rotation and Vibration

The full three-body Hamiltonian is initially characterized by nine degrees of freedom. Translational invariance reduces the effective dimensionality by three, but rotational invariance generally yields a reduction of only two degrees of freedom. This discrepancy exists despite the fact that translations and rotations are both three-parameter groups that can be used to define three translational and three rotational coordinates, respectively. In the aforementioned paper,[13] we discuss the reasons for this fundamental difference, which is related to the existence of a non-trivial rotational Berry's phase.[12]

Here, we simply reiterate some points that are pertinent to the present discussion. To begin with, there are many different ways to define three rotational coordinates, each of which is equivalent to specifying a set of body-fixed axes, or to selecting a particular gauge. Quantum-mechanically, each gauge gives rise to a different rotational basis set $|JKM\rangle$, defined (as for the symmetric top) as the simultaneous eigenstates of the angular momentum operators $\{\hat{J}^2, \hat{J}_z, \hat{J}_Z\}$, where $\hat{J}_z$ and $\hat{J}_Z$ are the body-fixed and space-fixed z-axis components of angular momentum, respectively.

In any gauge, J and M are conserved quantum numbers but K is not. Consequently, the block form of the Hamiltonian $\langle J'K'M'|\hat{H}|JKM\rangle$, although gauge-dependent, is always block-diagonal in J and M but not in K. Each block above operates on the three-dimensional configuration space of internal or "vibrational" coordinates. The diagonal blocks alone constitute the HC Hamiltonian

$$\tilde{H}_{JK} = \langle JKM|\hat{H}|JKM\rangle, \tag{4.1}$$

whereas the off-diagonal blocks comprise the coriolis coupling for the purposes of this chapter. The coriolis coupling can in principle be reduced via a gauge transformation, but can never be made to disappear altogether (excepting certain trivial special cases).

We shall make use of some set of Jacobi-like coordinates[13] on the six-dimensional translationally-reduced configuration space. These could be any of the

Jacobi or Radau arrangements, or possibly some interpolation.[12,13] In Jacobi-like coordinates, the translationally-reduced kinetic energy has the completely separable form of Equation 2.28. This comes about because these coordinates are in a certain sense "balanced" with respect to the mass distribution of the N bodies (Figure 4.1). For our purposes however, what is more useful is the fact that the fully-reduced kinetic energy is also completely orthogonal, albeit position-dependent.

In Jacobi-like coordinates, the translationally-reduced three-body quantum Hamiltonian is

$$\hat{H} = -\frac{\hbar^2\nabla_1^2}{2m_1} - \frac{\hbar^2\nabla_2^2}{2m_2} + V(\mathbf{r}_1, \mathbf{r}_2). \tag{4.2}$$

Equation 4.2 can be thought of as a pair of coupled two-body rotors with relative separations $\{\mathbf{r}_1, \mathbf{r}_2\}$ and reduced masses $\{m_1, m_2\}$.

Each set of Jacobi-like coordinates induces a rotational gauge and a set of internal coordinates $\{r_1, r_2, \varphi\}$, where φ is the angle between $\mathbf{r}_1$ and $\mathbf{r}_2$ (Figure 4.2).[13] In this representation, the Hamiltonian of Equation 4.2 becomes block-tridiagonal in K, and is given by

$$\begin{aligned}\tilde{H}_{JK} &= -\frac{\hbar^2}{2m_1r_1^2}\frac{\partial}{\partial r_1}r_1^2\frac{\partial}{\partial r_1} - \frac{\hbar^2}{2m_2r_2^2}\frac{\partial}{\partial r_2}r_2^2\frac{\partial}{\partial r_2} - \\ &\quad \left(\frac{\hbar^2}{2m_1r_1^2} + \frac{\hbar^2}{2m_2r_2^2}\right)\left(\frac{1}{\sin\varphi}\frac{\partial}{\partial\varphi}\sin\varphi\frac{\partial}{\partial\varphi}\right) + V_{\text{eff}}(r_1, r_2, \varphi)\end{aligned} \tag{4.3}$$

$$\begin{aligned}\tilde{H}_{JK\pm} &= \langle J(K\pm1)M|\hat{H}|JKM\rangle \\ &= \frac{\hbar^2}{2m_1r_1^2}\sqrt{J(J+1) - K(K\pm1)}\left(\mp\frac{\partial}{\partial\varphi} + K\cot\varphi\right),\end{aligned} \tag{4.4}$$

where

$$V_{\text{eff}} = V(r_1, r_2, \varphi) + \frac{\hbar^2J(J+1)}{2m_1r_1^2} + \left(\frac{1}{2m_2r_2^2\sin^2\varphi} + \frac{\cot^2\varphi - 1}{2m_1r_1^2}\right)\hbar^2K^2. \tag{4.5}$$

Equations 4.3 and 4.4 indicate that the coriolis coupling is small if the mass ratio m_1/m_2 is large. The problem of minimizing the coriolis coupling with respect to gauge transformations induced by all possible Jacobi-like coordinates has been

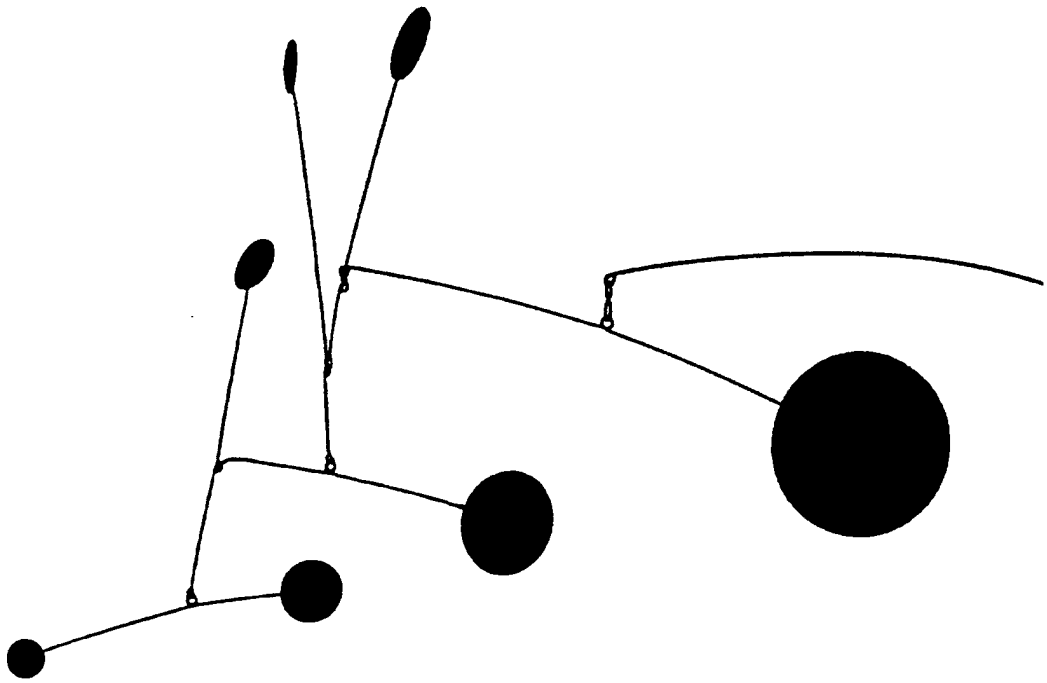

Figure 4.1: A particularly complicated arrangement of Jacobi coordinates, as exemplified by the Alexander Calder mobile entitled *Dots and Dashes*, 1959 (painted sheet metal, wire, 60") from the collection of Jean Lipman.[120] A hierarchy of masses is established, with a node located at the center of mass for each subhierarchy.

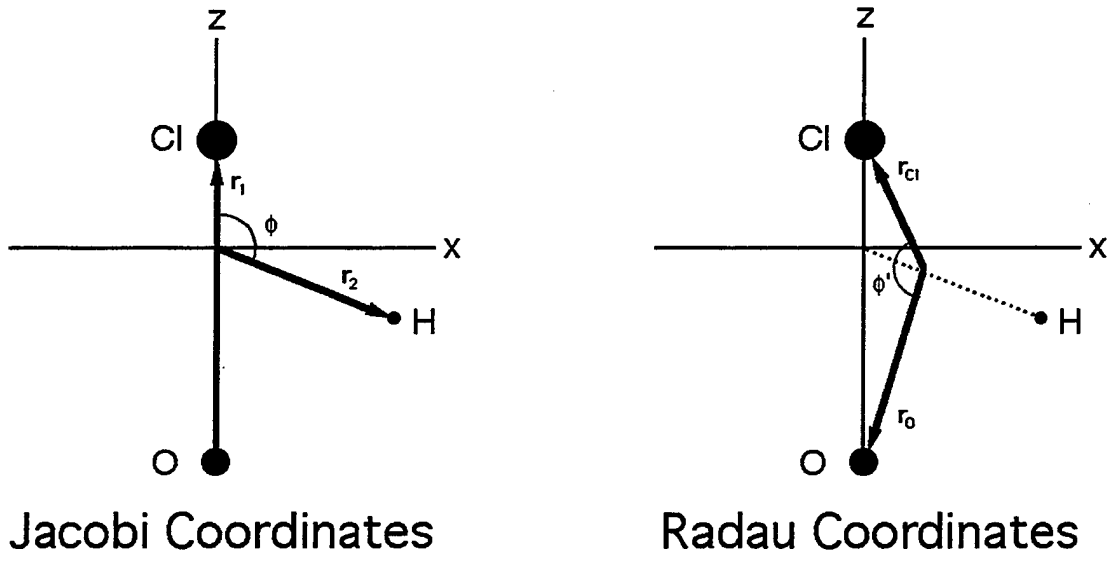

Figure 4.2: Two sets of Jacobi-like coordinates: on the left, the Jacobi coordinates for the OCl—H arrangement; on the right, Radau coordinates for O and Cl. The x and z axes refer to the body-fixed frame.

solved.[13] For heavy-light-heavy systems such as $O + HCl \rightarrow OH + Cl$, the most intuitive choice is to use the Jacobi coordinates associated with the OCl—H arrangement (Figure 4.2). Although not quite optimal,[13] this choice is very convenient, and is moreover required for comparison with other results. One might also apply the optimal separable basis methodology (Section 4.2.4) to reduce the coriolis coupling even further, by minimizing with respect to all unitary transformations of the rotational basis set. It has been shown however, that Equation 4.3 is already in optimal form.[13]

4.2.2 Helicity-conserving and J-shifting Approximations

The HC approximation (also known as the "centrifugal sudden" or "coupled states" approximation) results by simply ignoring the coriolis coupling, and solving each of the HC Hamiltonian blocks independently. Note that the $\tilde{H}_{JK}$ are equivalent to $\tilde{H}_{00}$, apart from the effective potential term of Equation 4.5. Since the diagonal blocks are treated independently in the HC picture, we should think of each $\tilde{H}_{JK}$ as having its own "effective" transition state, defined as the saddle point of the effective potential for that block.

For $J \neq 0$, the effective transition state never corresponds to a linear geometry, because the effective potential diverges as φ approaches 0 or π. This is simply a straightforward generalization of the analogous two-body central force situation (as $r \rightarrow 0$), and is by no means problematic for numerical applications; one simply uses V_{eff} to truncate the DVR grid in the usual fashion. Consequently, there is no need to resort to complicated, associated Legendre basis sets for the angular DVR that vary with the value of K.[59,61]

Using the numerical methods of Section 4.2.3, the cumulative reaction probabilities associated with each of the $\tilde{H}_{JK}$—i.e. the $N_{JK}(E)$'s—are independently calculated and then summed to obtain the HC estimate of the total cumulative reaction probability:

$$N(E) \approx \sum_{J,K} (2J+1) N_{JK}(E). \tag{4.6}$$

Since our ultimate goal is the thermal rate constant, however, it is more convenient

to define a block version of the rate constant

$$k_{JK}(T) = \frac{\int_{-\infty}^{\infty} e^{-\beta E} N_{JK}(E)\, dE}{2\pi\hbar Q_r(T)}, \tag{4.7}$$

from which the HC estimate for $k(T)$ is obtained as per Equation 4.6.

In the JS approximation, only the N_{00} block is calculated explicitly. The N_{JK} values are then estimated via

$$N_{JK}(E) \approx N_{00}\,(E - E_{\rm rot}(J,K)) \tag{4.8}$$

where the rotational shift energies $E_{\rm rot}(J,K)$ must be specified somehow. The standard JS method uses symmetric top kinetic energies; i.e.

$$E_{\rm rot}(J,K) = \hbar^2 AJ(J+1) + \hbar^2 BK^2 \tag{4.9}$$

where the rotor constants A and B usually correspond somehow to the transition state geometry. However, an improved JS method has also been developed,[13] for which $E_{\rm rot}(J,K)$ is defined as the value of $(V_{\rm eff} - V)$ at the effective transition state. The improved method exploits the fact that the effective transition state varies with J and K, and automatically incorporates centrifugal distortion effects and linear transition state geometries.

4.2.3 Determination of the $N_{JK}(E)$'s

The HC partial cumulative reaction probabilities $N_{JK}(E)$ are computed numerically using the DVR–ABC method of Section 3.2. Each $\tilde{H}_{JK}$ is represented as a matrix via a conventional sinc-function DVR in the radial coordinates (r_1, r_2), and a gauss-legendre DVR in the angular coordinate φ. The same general DVR scheme is used for all J and K, although the grid parameters may vary slightly. Note, however, that the kinetic energy is the same for each of the $\tilde{H}_{JK}$ blocks (Equation 4.3).

To determine $N_{JK}(E)$, we make use of the reaction probability operator[121]

$$\hat{P}(E) = 4\hat{\epsilon}_r^{1/2}\hat{G}(E)^{\dagger}\hat{\epsilon}_p\hat{G}(E)\hat{\epsilon}_r^{1/2}, \tag{4.10}$$

where $\hat{\epsilon}_r$ and $\hat{\epsilon}_p$ are the reactant and product absorbing potentials, respectively. The cumulative reaction probability is then given by

$$N_{JK}(E) = \mathrm{tr}\left[\hat{P}_{JK}(E)\right] = \sum_k p_k(E), \tag{4.11}$$

where the $p_k(E)$ are the eigenvalues of $\hat{P}$, which are obtained using a reorthogonalizing Lanczos iteration scheme.[7,121] The advantage of this approach is that only a small number of eigenvalues are usually required.

The Green's operator of Equation 2.24, or more accurately the action of $\hat{G}(E)$ on a vector, is obtained numerically using the GMRES algorithm (Section 3.4). This approach is efficient because the kinetic energy is completely orthogonal in the internal coordinates (r_1, r_2, φ), and therefore sparse in the DVR representation. We also make use of optimized preconditioning to reduce the number of Krylov iterations required for convergence.

4.2.4 Optimized Preconditioning

We are interested in obtaining an optimized preconditioner, as described in Chapter 3, for explicit DVR calculations of $N_{JK}(E)$ for three-body systems. Since the calculation involves three degrees of freedom, the algorithm developed in Section 3.5 is expected to be very effective. However, the efficiency of the optimized preconditioning algorithm requires that the kinetic energy be of the form expressed in Equation 2.29. To determine whether $\tilde{H}_{JK}$ satisfies this form, we must first decide whice of the (r_1, r_2, φ) are the inner coordinates and which are the outer coordinates.

A comparison between Equations 2.29 and 4.3 reveals that φ should definitely be an outer coordinate. However, Equation 2.29 will be satisfied if either one or neither of $\{r_1, r_2\}$ is also an outer coordinate. Symmetry considerations might persuade one to select $(r_1, r_2; \varphi)$ as the most natural division. A good case could also be made for $(r_1; r_2, \varphi)$ however, corresponding to $\mathbf{r}_1$ and $\mathbf{r}_2$ in the body-fixed frame. In practice, the decision should also be based on numerical convenience. In the O + HCl $\rightarrow$ OH + Cl case for example, we adopt the symmetric $(r_1, r_2; \varphi)$ choice because it results in the more efficient preconditioner.

4.3 Numerical Details and the O + HCl System

4.3.1 Coordinates

In Section 4.2.1, we argued in favor of the rotational gauge induced by the OCl—H Jacobi coordinates, and this is what we shall adopt from here on out. The corresponding masses $m_1 = m_O m_{Cl}/(m_O + m_{Cl})$ and $m_2 = (m_O + m_{Cl})m_H/(m_O + m_{Cl}+m_H)$ yield a mass ratio of about twelve. Thus, the HC approximation is expected to be quite accurate. To be consistent with previous theoretical results,[107,113] we use the following values for the atomic masses (in atomic units): $m_O = 32805$; $m_H = 1837$; $m_{Cl} = 64630$.

Note that all of our explicit calculations involve the internal coordinates only. Since these can be defined quite independently of the rotational gauge,[12,13] we can in principle use a different set of internal coordinates than those induced by the OCl—H Jacobi arrangement. Indeed, for the O + HCl → OH + Cl system, the Jacobi (r_1, r_2, φ) are less than ideal from a DVR perspective, because the singularity in the kinetic energy as $r_2 \to 0$ is unfortunately not precluded by large values of the potential.

As an alternate set of internal coordinates, it is natural to use the (r_1', r_2', φ') associated with a *different* set of Jacobi-like coordinates. Thus, we use one set of Jacobi-like coordinates to define the rotational gauge, and another to define the internal coordinates. This approach is very advantageous, because the $\tilde{H}_{JK}$ kinetic energy is gauge-independent, and therefore equivalent to that of the $\tilde{H}'_{JK}$ corresponding to the primed gauge. Thus, to obtain an expression for $\tilde{H}_{JK}$ in the primed coordinates, one simply adds the primed kinetic energy to the unprimed effective potential (rewriting the latter as a function of the primed coordinates).

The new internal coordinates can be defined using any desired set of Jacobi-like coordinates. A natural choice for a reactive scattering problem such as O+HCl → OH + Cl is the set that lies "halfway" between the reactant Jacobi arrangement O—HCl and the product arrangement OH—Cl; it has been shown[13] that these are just Radau coordinates in O and Cl (Figure 4.2). Indeed, we have found the Radau

coordinate DVR to be particularly effective. Not only is the kinetic energy singularity and other problems completely alleviated, but we also find the resultant $N_{JK}(E)$ calculations to be considerably more efficient.

Radau coordinates are often considered useful in light-heavy-light reactions, where they are approximately equal to valence bond coordinates.[122–124] In heavy-light-heavy applications, the light atom has to be fairly far away from the others to achieve a large bend in φ'. Thus, we find ourselves restricted by the O + HCl $\rightarrow$ OH + Cl potential to a fairly narrow angular range between $\varphi' \approx 140°$ and $\varphi' = 180°$. This greatly reduces the number of angular points required by the DVR; however these gains are offset somewhat by the need for a larger density of points. All in all though, fewer points are required by the Radau DVR than the Jacobi DVR; consequently, the former has been employed for most of our numerical calculations (Section 4.4.1).

4.3.2 DVR Grid Parameters

Another advantage of using Radau coordinates is that ascertaining reactant and product regions is a fairly straightforward matter; these correspond to large values of r_O and r_{Cl} respectively. As in other DVR applications, we find that roughly four points per de Broglie wavelength are required for the radial degrees of freedom. This amounts to roughly 60 DVR points for each radial degree of freedom, corresponding to about $5a_\circ$ (in r_O). The angular DVR points are truncated by the potential to about one-fourth of the total number $l_{\max}$. Convergence with respect to $l_{\max}$ is a subtle issue; however, $l_{\max} \approx 50$ is usually sufficient (Section 4.4.1). Roughly 9,000 to 20,000 DVR points are required in all, depending on the energy.

The reactant and product absorbing strips are laid out in r_O and r_{Cl} respectively, and are typically about $1a_\circ$ wide (in r_O). The dividing surface is defined via

$$r_{Cl}/r_O = 0.57 \tag{4.12}$$

which is appropriate throughout the allowed angular range. A quartic absorbing potential is employed,[69] with a maximum value of about 1.0 eV.

A potential cutoff energy V_{cut} is used to truncate the DVR grid. For the ener-

gies appropriate to the temperatures under consideration (200–700°K), a V_{cut} value of 1.40–1.85 eV is sufficient. Energies are taken with respect to the reactant asymptote minimum. Although the O + HCl → OH + Cl reaction is only slightly endothermic, the OCl—H arrangement energy is quite large (1.77 eV). This is considerably higher than our highest energy calculation, but lower than some of our cutoff energies. Consequently, DVR points are removed from the $V_{\text{cut}} \geq 1.77$ eV grids if either the oxygen or the chlorine is further away from the hydrogen than some specified distance ($4a_\circ$ is virtually always sufficient).

4.3.3 Preconditioner Details

Of the two internal partitionings considered in Section 4.2.4, $(r_1, r_2; \varphi)$ yields the more efficient preconditioner, because a much larger portion of the Hamiltonian is incorporated into $\hat{H}_0$. This is particularly true for the O + HCl → OH + Cl Radau DVR, for which there are far fewer angular points than radial points. On the other hand $\hat{G}_0$, although sparse by virtue of block-diagonality, is significantly less sparse than $\hat{H}$. CPU limitations may therefore be an issue for numerical calculations.

Obtaining the above preconditioner for O + HCl → OH + Cl is considerably faster than the resultant Krylov calculations, even with preconditioning; thus, speed is not a major concern. However, the memory limitations of our platform (IBM RS6000) definitely *are* a concern. This is largely because optimized preconditioning constrains the DVR grid such that all inner coordinate "sheets" (outer coordinates fixed) must contain the same points. Consequently, extraneous DVR points must be included that would not occur with a straightforward potential cutoff. The three-dimensional constraint is a lot less severe than the rectangular grid requirement of the two-dimensional case.[17] Nevertheless, we find that the number of DVR points for our application is increased by a factor of three or four—which unfortunately puts us over the memory limit of our CPU.

In the future, we hope to develop an algorithm that avoids the grid constraint limitation. For now we must find some other solution. One approach would be to transform the internal coordinates yet again; another would be to use the less efficient

$(r_1; r_2, \varphi)$ preconditioner. Instead, we adopt an earlier suggestion[17] to skip the outer diagonalization step altogether, and simply define $\hat{H}_0$ in the original representation. The resultant DVR grid is completely unconstrained. Moreover, the efficiency loss of the new preconditioner is fairly small in this case, as numerical tests reveal that outer diagonalization only reduces the residual norm by about 10%.

4.3.4 Estimating the Thermal Rate Constant

Although some of the $N_{(J>0)K}(E)$ are explicitly calculated, we are mainly interested in using a JS approximation to obtain the thermal rate constant. Consequently, our computational focus is primarily restricted to $N_{00}(E)$. We use the standard JS method with rotor constants (in atomic units)

$$A = 1.202 \times 10^{-6} \quad ; \quad B = 2.929 \times 10^{-4}, \tag{4.13}$$

rather than the improved JS version, so as to allow a direct comparison with other theoretical estimates of $k(T)$.[107,113]

The essence of deriving a thermal rate constant from an explicit calculation of $N_{00}(E)$ is described by Equation 4.13 and Section 4.2.2. However, there are a couple of additional modifications which must be implemented, once again to allow direct comparison with previous results. Following Koizumi *et al*,[113] we replace the sum over J in Equation 4.6 with an integral, which is approprate for O+HCl $\rightarrow$ OH+Cl because the effective potential varies only slightly with J. This results in the expression

$$k(T) \approx \frac{k_{00}(T)}{\beta\hbar^2 A}\left(1 + 2\sum_{K=1}^{\infty} e^{-\beta\hbar^2(A+B)K^2}\right) \tag{4.14}$$

which converges to reasonable accuracy with a small number of K values.

An additional modification was also introduced to account for a second electronic surface ($^3A'$) that correlates between reactant and product ground states, and lies fairly close to the ground electronic surface. In fact the two surfaces are coincident for linear geometries.[113] This surface clearly makes a significant contribution to the overall reaction rate and cannot be ignored. As per Koizumi *et al*, we multiply the above value for the rate constant by a statistical factor

$$f(T) = 3/(5 + 3e^{-228/T} + e^{-326/T}) \tag{4.15}$$

representing the fraction of collisions that wind up on the ground electronic surface ($^3A''$).

4.4 Results

We have used the methods described in the previous sections to calculate thermal rate constants and cumulative reaction probabilities for the O + HCl → OH + Cl reaction within the standard JS approximation. We have also compared the thermal rate constants with other theoretical and experimental results from the literature. In addition, we have used the HC approximation to calculate the $N_{JK}(E)$ explicitly for some relevant values of J and K. These latter results are used to evaluate the validity of the standard JS approximation, as well as the improved version discussed in Section 4.2.2.

4.4.1 Cumulative Reaction Probabilities for $J = 0$

Explicit $N_{00}(E)$ calculations have been obtained for energies in the range 0.30–0.60 eV, at 0.005 eV increments, and are depicted in Figure 4.3. The probability associated with $E = 0.30$ eV is around 10^{-5}, below which the DVR–ABC methods seem to be difficult to converge. By 0.60 eV, the cumulative reaction probability is on the order of unity; but the DVR grids become inordinately large. Despite the numerical difficulties associated with this particular reaction, we have been able to obtain fairly well-converged $N_{00}(E)$ values in the specified energy range. Indeed, these results are converged to within about 1–2% with respect to all grid parameters except $l_{\max}$.

The $l_{\max}$ convergence is quite unusual, and bears comment. For comparatively small values of $l_{\max}$ (35–45), one typically finds the usual monotonic convergence to within a few percent. However, there tends to be a critical value of $l_{\max}$ at which $N_{00}(E)$ suddenly leaps up or down by as much 40%. This is not very desirable from a convergence standpoint; although we have observed similar behaviour in Jacobi DVR calculations for this reaction and others. In any event, we have extended $l_{\max}$ as far

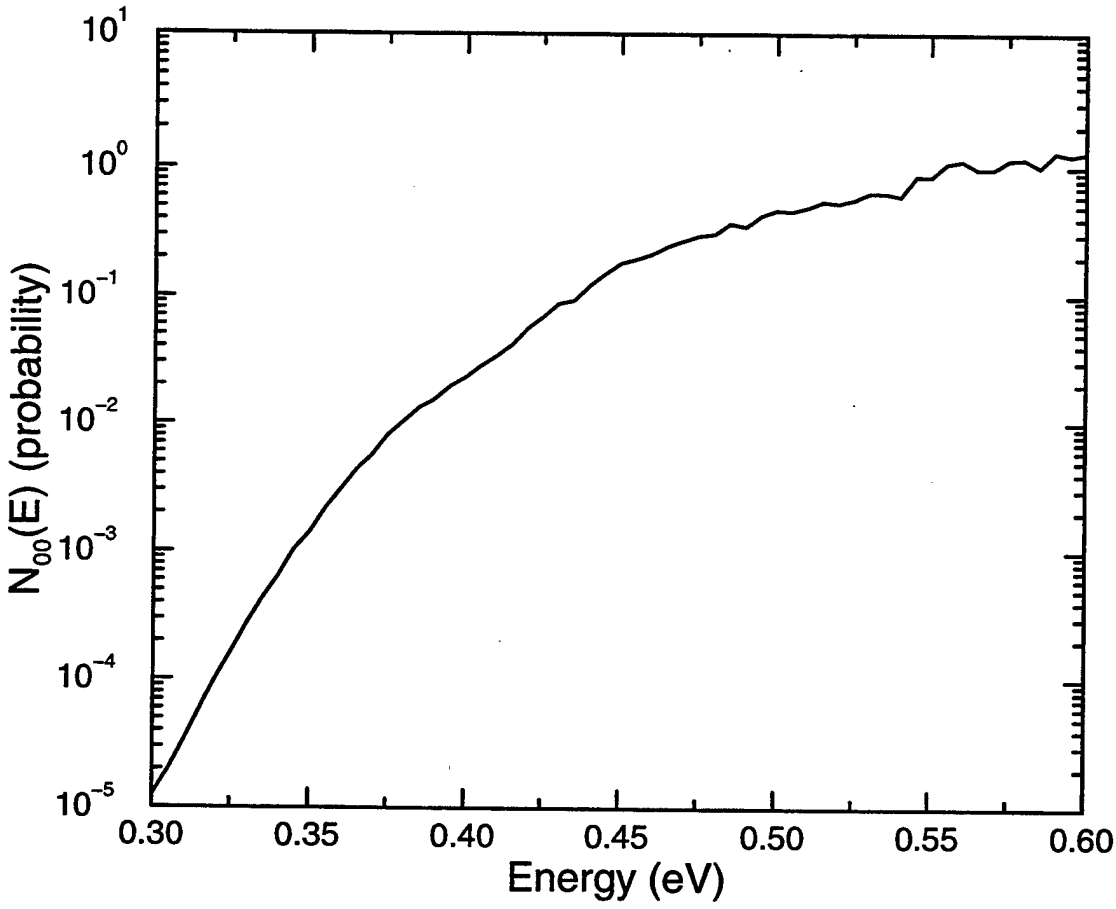

Figure 4.3: Logarithmic plot of $N_{00}(E)$, the $J = 0$ cumulative reaction probability as a function of energy, for the $O + HCl \rightarrow OH + Cl$ system.

as 120 to ensure the convergence of our results for O + HCl → OH + Cl. For lower energies, $N_{00}(E)$ tends to remain flat over the entire region except for a few isolated "spikes;" and we can probably safely claim convergence to within 10% or so. For large energies, $N_{00}(E)$ tends to alternate suddenly between two values whose mean variation increases from about 10% near E = 0.45 eV to about 25% near E = 0.60 eV. Despite this variation, there is very little "mean drift" as $l_{\max}$ ranges from 50–120 at fixed energy; and in this sense our results are converged. In any case, Figure 4.3 incorporates the average of the two $N_{00}(E)$ values for energies in the range E = 0.45–0.60 eV.

The above results were obtained with residual tolerances of about one part in 10^5 for both the Lanczos and GMRES components of the calculation. Around 5–10 Lanczos iterations and 50–200 GMRES iterations were required, depending on the values of E and $l_{\max}$. Given the number of grid points (∼15000) the preconditioner is evidently very efficient. A detailed comparison versus no preconditioning was performed, albeit for a somewhat smaller grid (4856 points) due to CPU constraints. Preconditioning on the reduced grid was found to reduce the number of GMRES iterations from 575 to 10. The preconditioner is so efficient that the GMRES bottleneck is the linear Hamiltonian multiplication step, rather than the quadratic linear algebra step.[92] The corresponding speed increase is a factor of ∼110.

For comparison's sake, we have also obtained numerical $N_{00}(E)$ results using DVR grids other than the one presented in Section 4.3.2. For instance, the Radau DVR with Jacobi absorbing strips and a valence bond dividing surface

$$r_{HCl} - r_{OH} = 0.29 \tag{4.16}$$

yielded results that were within a per-cent or so of Figure 4.3, although CPU requirements were somewhat higher. We also tried the OCl—H Jacobi DVR. This choice required almost double the number of grid points, primarily in the angular coordinate, resulting in increased CPU requirements and a comparatively less efficient preconditioner. Consequently, even the low energy results could only be converged to within ∼25% or so; although to this level of accuracy they seem to match the Radau values.

4.4.2 Thermal Rate Constants

The total cumulative reaction probabilities and thermal rate constants for $O + HCl \rightarrow OH + Cl$ have been determined as per Sections 4.2.2 and 4.3.4. The former were derived from Equation 4.6, and are presented in Figure 4.4. The thermal rate constants were obtained for several temperatures in the range 200–700°K, and are presented in Figure 4.5.

Within the JS approximation itself, we estimate an error of about 10% for our $k(T)$ results, except at the highest temperatures for which the error may be as high as 25%. The most fundamental source of error arises from the N_{00} results. This appears to be random rather than systematic, and is therefore mitigated somewhat by the Boltzmann averaging of Equation 4.7. The integration itself introduces error however, primarily due to the finite range of data available for the integrand. Figure 4.6 depicts the integrand for multiple temperatures. The gaussian-like pattern suggests a loss of about 5–25% of the integrand depending on the temperature. However, this error is significantly reduced by confining the integral of the reactant partition function $Q_r(T)$, in the denominator of Equation 4.7, to the same energy range as the numerator integral (0.30–0.60 eV).

Our thermal rate constants are compared with other theoretical[108,113] and experimental[116–118] results in Figure 4.5. The theoretical values should in principle match exactly. Reasonable agreement with the revised values of Thompson, *et al*[108] has been observed; however, the discrepancy with Koizumi *et al*[113] is not accounted for. Our results evidently match experiment fairly well. Given the accuracy of the JS and HC approximations for the present reaction (Section 4.4.3), this agreement is to be expected. On the other hand, it should be noted that the potential surface was empirically modified by Koizumi *et al* so as to force their results to agree with experiment at $T = 295°K$.[113]

4.4.3 HC and Improved JS Results

In addition to calculating $N_{00}(E)$, we have obtained explicit $N_{JK}(E)$ results for some of the $J \neq 0$ $\tilde{H}_{JK}(E)$'s (Figure 4.7). Specifically, we obtained fixed-K

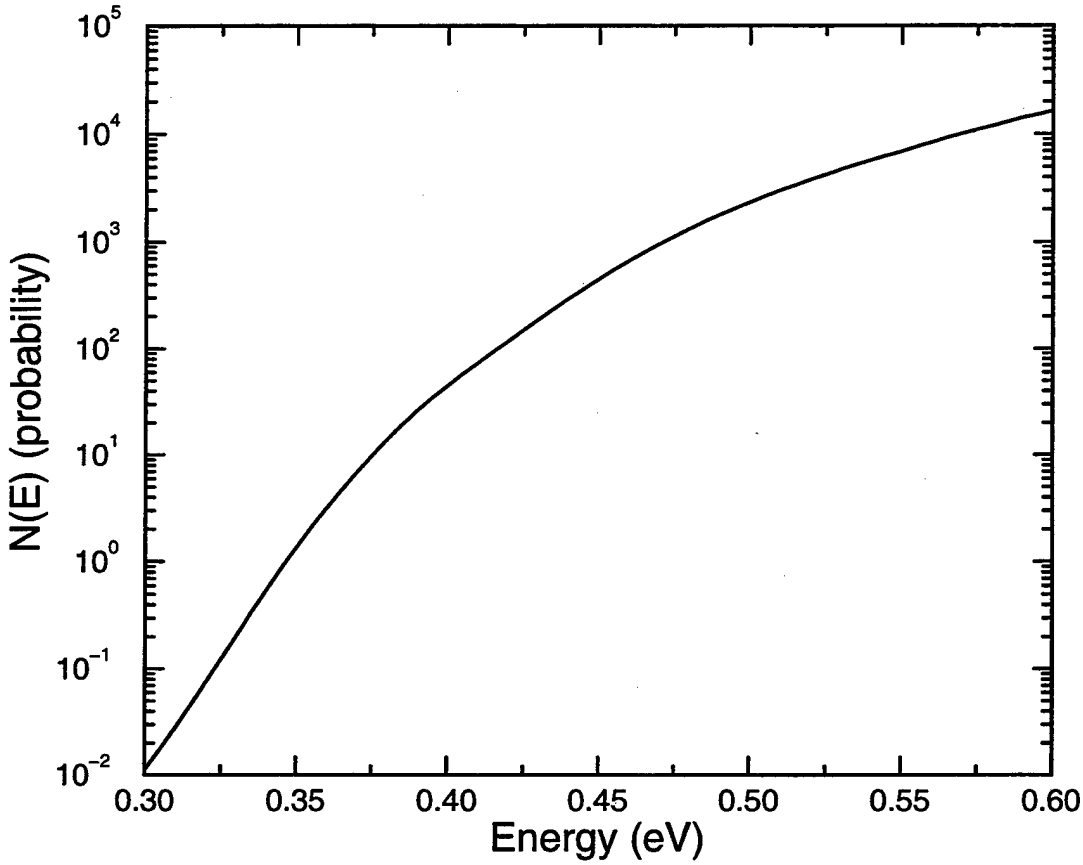

Figure 4.4: Logarithmic plot of the total cumulative reaction probability as a function of energy, in the standard JS approximation, for the $O + HCl \rightarrow OH + Cl$ system.

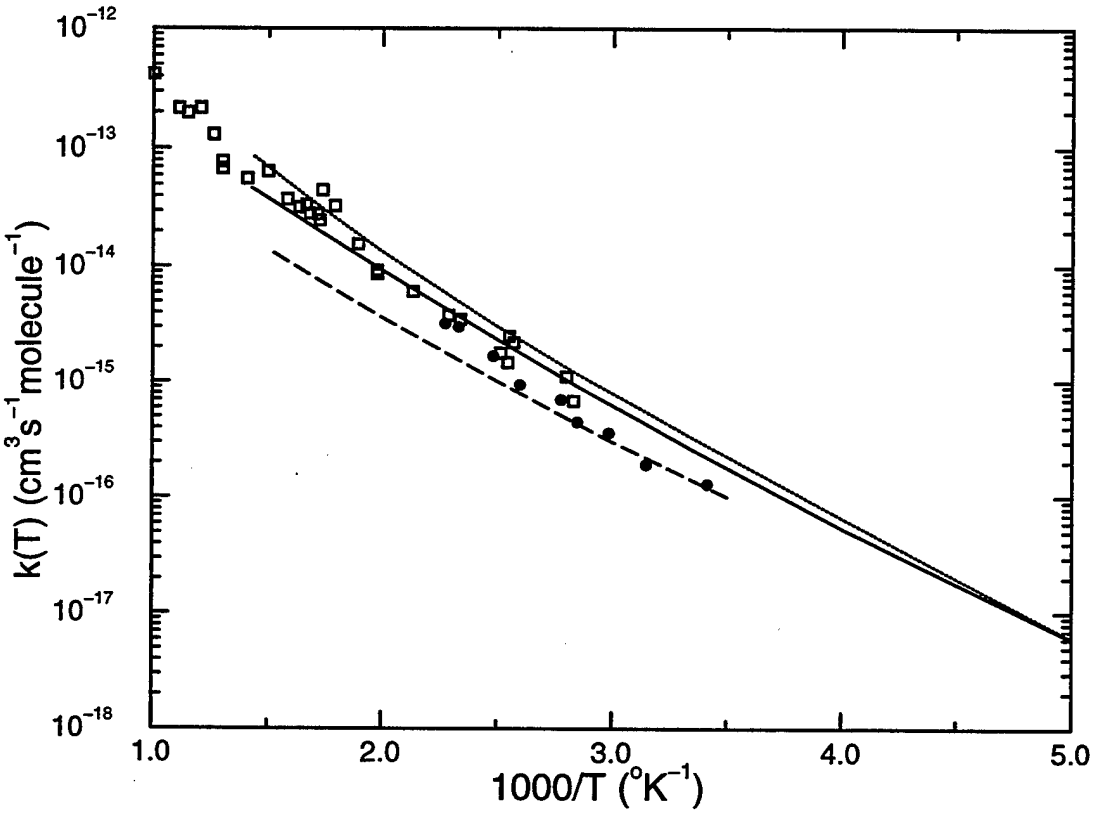

Figure 4.5: Arrhenius plot of theoretical and experimental thermal rate constants for the O + HCl → OH + Cl reaction. Theoretical results: ——— (present results); - - - - - - (Thompson *et al*[108]); — — — (Koizumi *et al*[113]). Experimental results: filled circles (Brown *et al*[116,117]); open squares (Mahmud *et al*[118]).

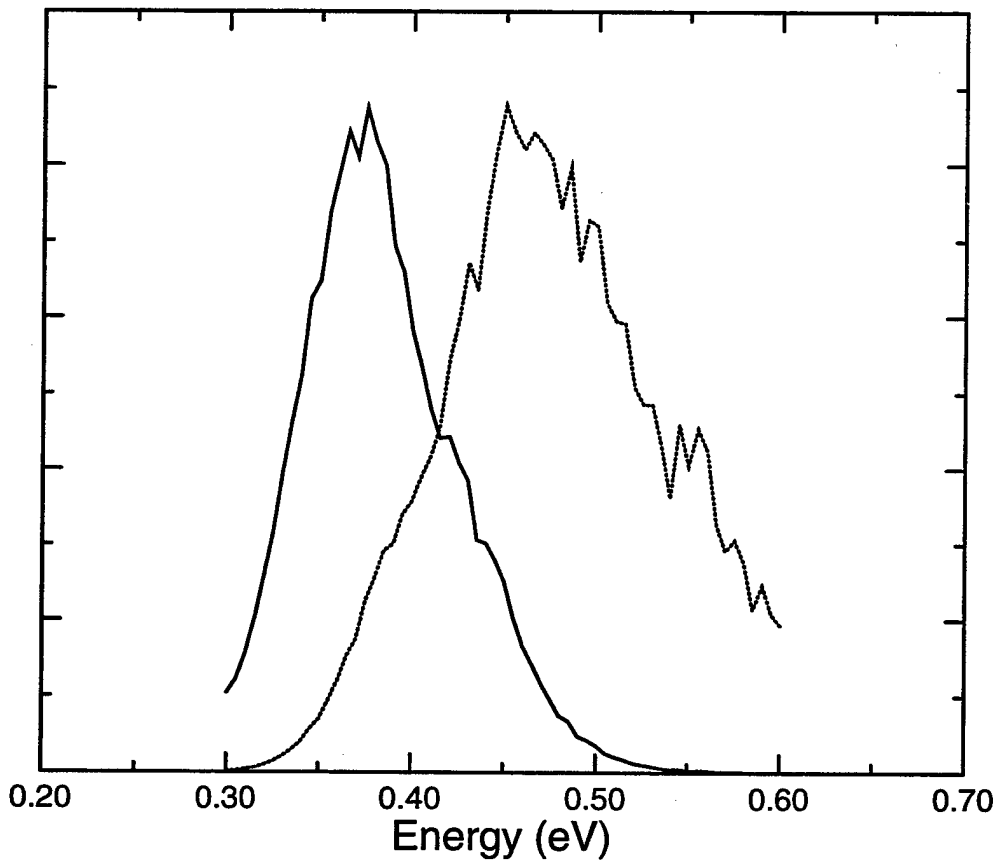

Figure 4.6: Renormalized Boltzmann integrands for $k_{00}(T)$ as a function of energy, for two different temperatures: ——— ($T = 200°\text{K}$); - - - - - - ($T = 500°\text{K}$).

($K = 0$) results for various values of J, and fixed-J ($J = 24$ and $J = 48$) results for various values of K. Due to time constraints, we have not evaluated convergence as thoroughly as in the $J = 0$ case; however, the results are certainly accurate enough to test the validity of the standard and improved JS approximations.

Note that qualitatively, the $N_{JK}(E)$ graphs really do resemble $N_{00}(E)$ graphs that have been shifted in energy. Quantitatively, this means that the variation in the energy difference between points of comparable probability in $N_{00}(E)$ and $N_{JK}(E)$ is small, over the probability (or energy) range of interest. Some kind of energy-shifting approach is therefore entirely justified; however, we must ensure that the shifting energies themselves are chosen appropriately.

It is reasonable to associate the shift with rotational kinetic energy.[13] In Figure 4.8, we compare the fixed-K rotational shift energies obtained from the $N_{JK}(E)$ graphs of Figure 4.7 with those predicted by the standard and improved JS methods. All three shift energies were found to agree fairly well. This indicates that there is not much centrifugal distortion when $K = 0$, and that the standard value of A in Equation 4.9 is comparable to that of the improved JS method. Both of these conclusions are consistent with what one would expect for the large mass ratio of the $O + HCl \rightarrow OH + Cl$ system.

The situation is somewhat different for the fixed-J rotational shift energies, presented in Figure 4.9. Note that the shifting energy varies much more quickly with K than with J. This is again due to the large mass ratio of the system, which causes the rotor constant B to be much larger than A. Consequently, an accurate $k(T)$ estimate requires about one hundred J's, but only six $|K|$'s. Another important difference is that the plot of shift energy versus K^2 is considerably non-linear, with most of the curvature occuring for small values of K. This feature cannot be accounted for in the standard JS theory, which necessarily predicts a straight line.

According to the improved JS theory however, the curvature is due to the centrifugal distortion of the effective transition state, which is large because the K^2 term of the effective potential is large. Figure 4.10 depicts the effective transition state geometries for several values of J and K, and clearly illustrates that K has the larger effect on the distortion. In any event, Figure 4.9 demonstrates that the

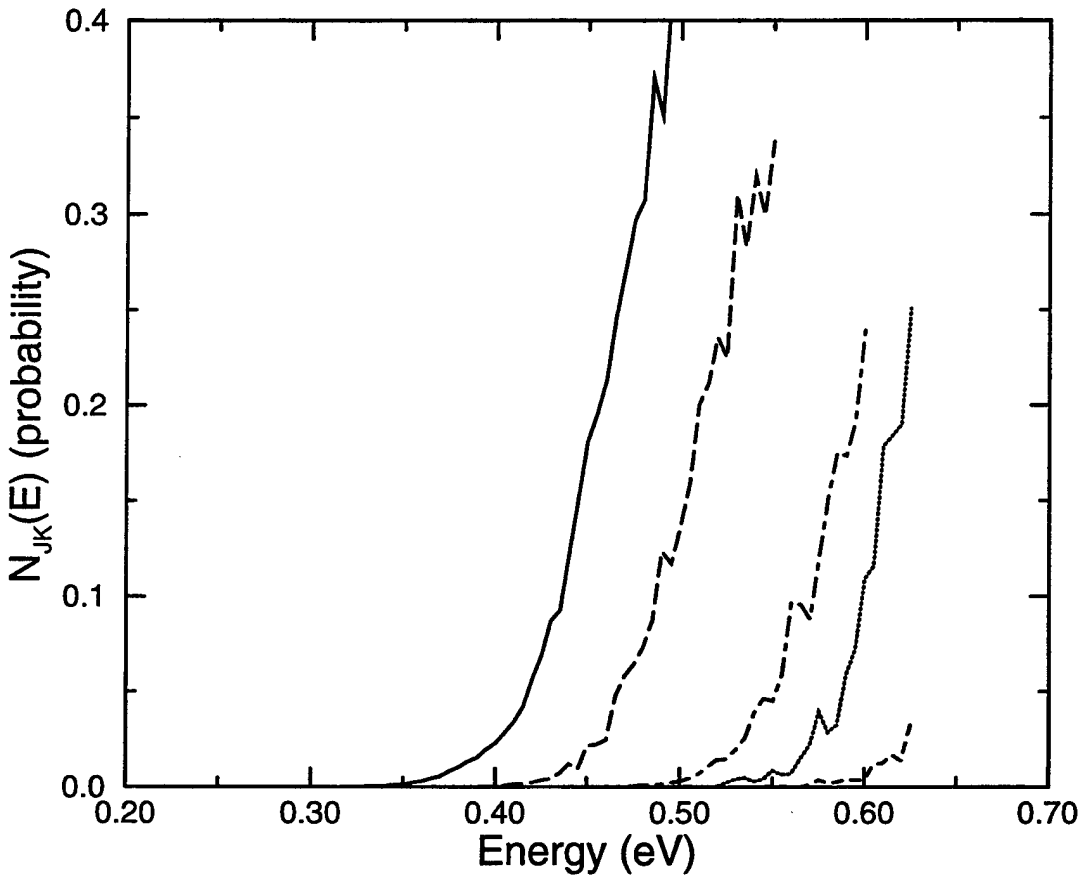

Figure 4.7: Helicity-conserving cumulative reaction probabilities as a function of energy, for several representative values of J and K: ——— ($J = 0$, $K = 0$); — — — ($J = 48$, $K = 0$); — - — - ($J = 72$, $K = 0$); - - - - - - ($J = 24$, $K = 5$); - - - - ($J = 48$, $K = 5$).

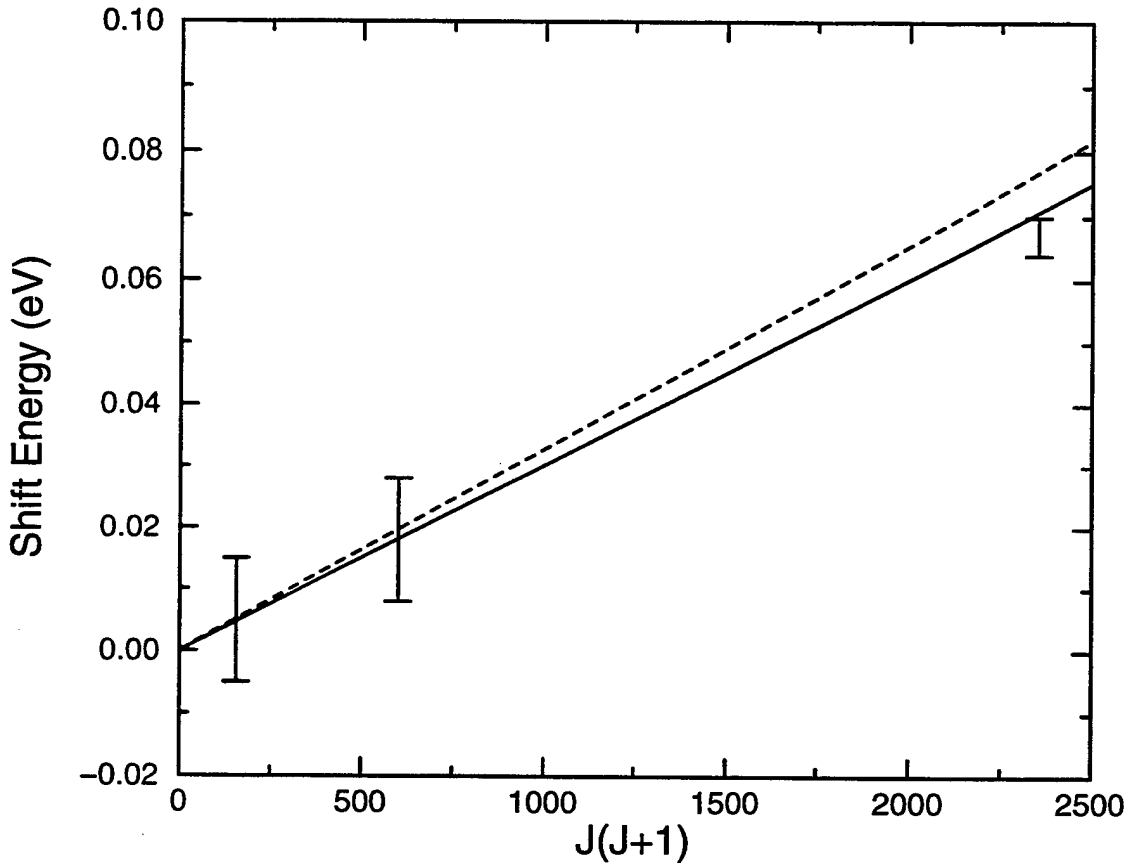

Figure 4.8: Rotational shift energies of the $N_{JK}(E)$'s as a function of J, for $K = 0$. The error bars reflect the variation in the HC results over the relevant energy range: ——— (improved JS); - - - - (standard JS).

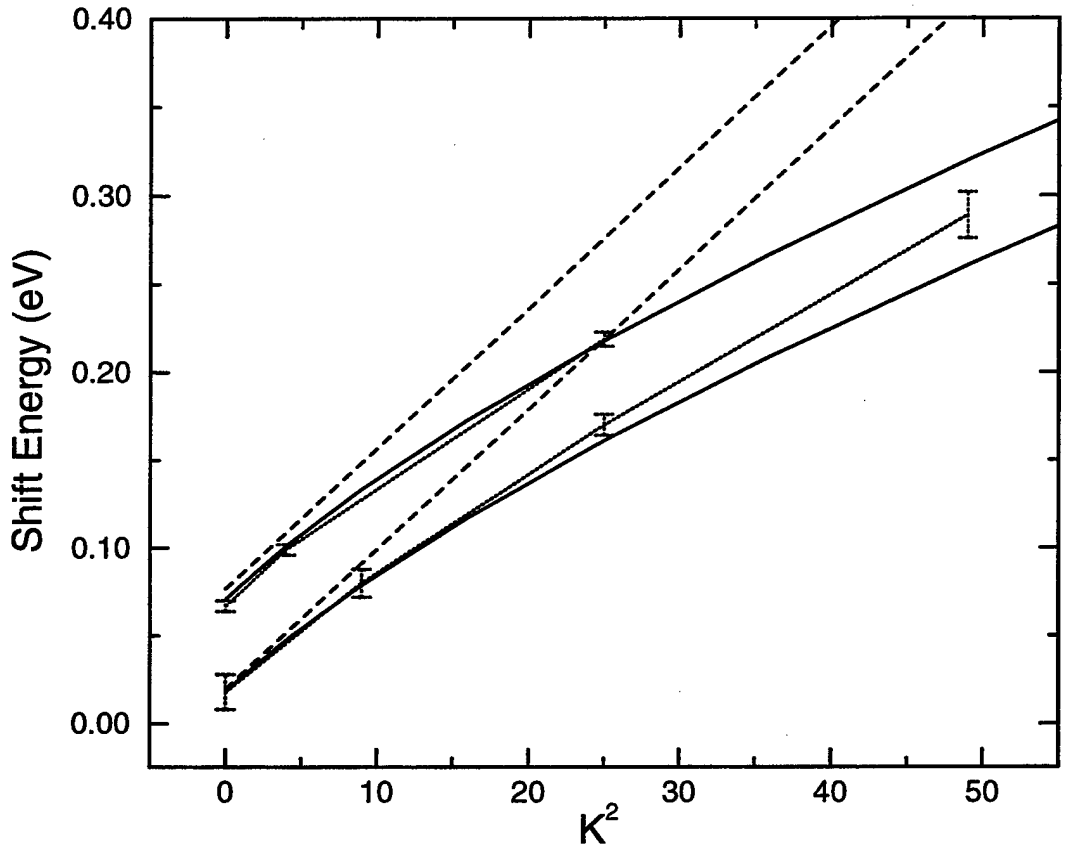

Figure 4.9: Rotational shift energies of the $N_{JK}(E)$'s as a function of K, for $J = 24$ (lower graphs) and $J = 48$ (upper graphs). The error bars reflect the variation in the HC results over the relevant energy range: ——— (improved JS); – – – – (standard JS); - - - - - - (HC).

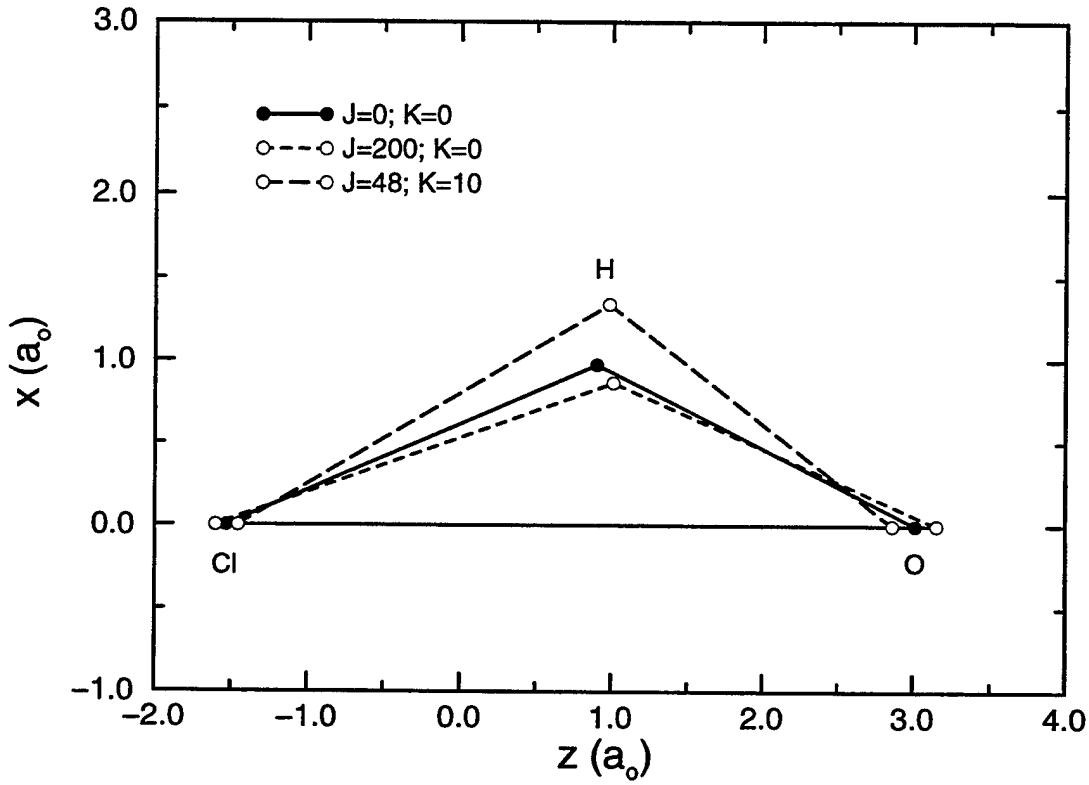

Figure 4.10: Effective transition state geometries of the O + HCl → OH + Cl system for several values of J and K: ——— ($J = 0$, $K = 0$); - - - - ($J = 200$, $K = 0$); — — — ($J = 48$, $K = 10$).

improved JS method does an excellent job of predicting the actual energy shifts—at least in the most crucial region where K is small. The standard JS results are still fairly good though; we estimate that the JS and HC values for $k(T)$ agree to within about 20%.

4.5 Conclusions

One of the principal goals of this chapter has been to evaluate the use of optimized preconditioning for generic three-body quantum calculations, with respect to both efficiency and practicality. By restricting consideration to Jacobi-like coordinates only, the Hamiltonian takes on the sparse, reduced-dimensional form of Equations 4.3 and 4.4 regardless of the particular coordinates used; yet the range of all possible Jacobi-like coordinates is quite broad.[13] Moreover, the uniformity of the $\tilde{H}_{JK}$ allows us to adopt the internal coordinate DVR of Sections 4.2.3 and 4.3.1 as a generic standard for the three-body case. From this standard, two candidate preconditioners naturally suggest themselves, corresponding to the two partitionings of Section 4.2.4.

We therefore have an optimized preconditioning scheme for three-body systems that is both practical and general. The next logical consideration is whether the method is also efficient. In general, one can always bolster efficiency by transforming from one set of Jacobi-like coordinates to another, as is done in Section 4.3.1. However, performance ultimately depends on the details of the particular system. Nevertheless, it is extremely encouraging to discover that even for a system such as $O + HCl \rightarrow OH + Cl$ which has no special properties, the optimized preconditioner reduces the computational effort by two orders of magnitude.

Another major objective of this chapter has been to exploit theoretical advances pertaining to rotational gauges and optimal separable bases in a practicable manner. In particular, one of our ongoing concerns is the minimization of the off-diagonal coriolis coupling blocks $\langle JK'M \mid \hat{H} \mid JKM \rangle$. Once again, the restriction to Jacobi-like coordinates has proven to be beneficial, in that the coriolis coupling vanishes except when $K - K' = \pm 1$. Moreover, minimization with respect to either

rotational gauge or outer diagonalization is a tractable, even solved problem.[13] The Jacobi-like restriction also gives rise to the effective potential picture of the HC approximation, which in turn leads to the improved JS method and the notion of the effective transition state.

The usefulness of the effective potential idea, apart from pedagogical value, is apparent in the predicted rotational shift energies of Figures 4.8 and 4.9. Although the improved JS predictions are accurate enough, it is perhaps even more relevant that one can actually assign a reasonably well-defined shifting energy to the $N_{JK}(E)$'s in the first place. According to the effective potential picture, this is simply due to the dominant role played by the transition state. We therefore anticipate a correlation between the reliability of the improved JS method and traditional transition state theory, and this may explain why the $N_{JK}(E)$ predictions of the former are less accurate for large K. In any event, the improved JS method is certainly much more feasible than a full HC calculation from a computational perspective. The bottleneck of the former lies in locating the saddle points of a three-dimensional potential surface, which is far less costly than the corresponding exact quantum calculation.

In the future, we would like to apply the improved JS method as well as optimized preconditioning to other three-body reactions, in order to better ascertain the generality of the current results. It would be interesting to see whether the curvature of the rotational shift energies for fixed-J actually does increase in the small coriolis coupling limit, as claimed. It would also be interesting to apply the new JS approximation to a system with a linear transition state, for which the Equation 4.9 dependences on J and K are no longer appropriate, and standard J-shifting is problematic. On the theoretical front, we would like to find the best Jacobi-like coordinates for more general mass distributions such as light-heavy-light, from the standpoint of minimizing the coriolis coupling. Finally, we would like to develop a version of the optimized preconditioning algorithm that does not constrain the DVR grid.

Chapter 5

Conclusions

As quantum mechanics is applied to ever increasingly complicated systems, one fact becomes very clear: that some form of separable approximation is required, if one is to make any headway. The reason is quite simply that the calculational effort required for an exact treatment scales exponentially with the number of particles, whereas a separable problem scales linearly, or in the worst case as a power law. Even taking the current exponential growth of computer technology into account, we will only be able to handle perhaps ten or twelve-body systems by the time that the current trend levels off, due to the fact that computer technology itself is approaching the quantum limit. Parallelization will certainly play an increasingly important role in bypassing this limitation. In parallel applications, however, separability is even more crucial, as it is imperative that the full problem can be divided into pieces that are as independent from one another as possible.

The use of separable approximations in physics is certainly nothing new. In quantum mechanics, we are all familiar with the separable approximations that arise from the Born-Oppenheimer approximation, Hartree-Fock theory, molecular orbital theory, density functional theory, and the various quasiparticles used in countless applications. These approximations have certainly enabled us to gain an understanding of a tremendous number of real physical systems. Yet, there are also many real systems for which the picture presented to us by these methods seems to break down. Thus, whereas the distinction between charged particles and photons that occurs in

quantum electrodynamics seems entirely appropriate (due to the smallness of the fine structure constant α), in elementary particle physics where the interaction is often much greater, the separation between particles and fields is far less compelling.

All of the separable approximation methods of the preceding paragraph rely upon one basic assumption for their success: that the interaction or coupling between separated pieces is small. If this is not the case, then the picture presented to us by these methods is inappropriate. But there are plenty of real systems for which the interaction is *not* small. However, there is a formal arbitrariness in the way one chooses to define the interaction. Therefore, if the the interaction is large for a particular system, one is naturally prompted to ask whether the definitions used by the methods above are really the most appropriate ones.

The novel aspect of the optimal separable basis approach presented in this dissertation is that it offers a systematic means of determining the most natural definition of the interaction on a Hamiltonian-by-Hamiltonian basis. In particular, no special assumptions about the form of the approximation are assumed *a priori*, other than that of separability. Indeed, we have found that the most natural separable approximation for a $\hat{T} + \hat{V}$ Hamiltonian need not even be of the $\hat{T} + \hat{V}$ form itself.

The optimal separable approximation thus obtained is useful in two distinct ways. First, the approximation itself has pedagogical value with respect to understanding the nature of the actual system. Since the interaction has been minimized, the description is expected to be more accurate than for any other separable approximation. For example, in Chapter 2, we found that the effective potential for the x coordinate of the shifted harmonic oscillator is best described by the well of Equation 2.37 rather than the barrier of Equation 2.39.

Second, if one is interested in calculating exact quantities, the use of the optimal separable basis renders such calculations more efficient. In this dissertation, we have only explored this aspect in one very specific manner, i.e. with respect to calculating microcanonical scattering quantities for the molecular systems of Chapter 3 ($H + H_2$) and Chapter 4 ($O + HCl$). However, In Chapter 2, we showed how the optimal separable approximation could improve the convergence of both the time-independent perturbation expansion and the Born series. More generally, we antici-

pate an improvement in computational efficiency regardless of the particular quantity being calculated or algorithm being used, due to the fact that the interaction has been minimized as much as possible.

For example, the direct $k(T)$ methods referenced in Chapter 4 are quite different from the microcanonical methods presented here, in that they make use of split operator propagations (to calculate the flux-flux autocorrelation function) rather than Green's function inversions. Nevertheless, the calculation could in principle be improved by splitting the Hamiltonian along $\hat{H}_0$ / $\hat{\Delta}$ lines, rather than $\hat{T}$ / $\hat{V}$ lines. The reason is that the commutator of the two pieces is reduced, as a result of which a larger time step can be used to obtain the same level of accuracy.

As another example, bound state calculations are often obtained using the Lanczos algorithm mentioned in Chapter 2. As suggested in that chapter, the optimal separable $\hat{H}_0$ could be used to obtain a starting vector which might reduce the number of iterations substantially. The idea would be to use a superposition of the first few states of $\hat{H}_0$ as the starting vector in a conventional Lanczos scheme, or to use the whole collection in an iterative* block application. Convergence is improved because the initial Krylov space overlap with the subspace spanned by the lowest few eigenvectors is expected to be fairly high.

Although both of these examples merit investigation, I have presented them here primarily to demonstrate the relative ease with which the optimal separable approach can be incorporated into current state-of-the-art numerical algorithms which were obviously not designed with our approach in mind. Clearly, the scope of the optimal separable basis methodology is much broader, however. In what follows, we present a more general but less detailed description of a few additional molecular applications which might benefit from an optimal separable treatment.

Based on the comments in Section 2.5.3, we expect the method to be particularly well-suited to inelastic scattering applications. This is because the potential is globally more separable than in reactive scattering, since there is only one asymptotic form to worry about. Even the translationally-averaged potential approximation of

*this time, in the sense of Cullum and Willoughby.[7]

Section 2.5 would result in a potential-like interaction that is small; although the optimal separable residual would be even smaller, of course. In light of Section 2.4.2, it would also be interesting to compare our performance for reactive and inelastic scattering applications versus that of the Kohn variational principle.

It might also be instructive to use the optimal separable theory to generate Hartree-Fock orbitals along the lines suggested in Section 2.3.4. By truncating the excitation numbers, one obtains a finite set of mutually orthogonal separable basis functions that is uniformly optimized over a range of energies. More accurate results can be obtained using a conventional perturbation approach, rather than the more complicated version required to handle non-orthogonal states. We have applied this idea to the six-dimensional helium atom, optimizing over all bound states (including doubly excited states). This work is still in progress; however, it is worth mentioning here that a strongly separable treatment results in a screened coulombic potential with $Z^* = 23/14$. This should be contrasted with the variational minimal result $Z^* = 27/16$ which in effect optimizes for the ground state only.

One could also apply the optimal separable method to the separation of nuclear and electronic motion in molecular systems—i.e. the Born-Oppenheimer problem. In the standard approach, one starts with a weakly separable approximation wherein the nuclear positions yield outer basis functions $\delta(Q - Q_0)$, and the inner coordinates are the electronic wavefunctions parametrized by Q. The "coupling" in this case is the nuclear kinetic energy, which is not small. However, a more refined approximation is obtained by solving the nuclear problem associated with each electronic surface. The results are more accurate, but the wavefunctions are no longer separable. The optimal separable approach, on the other hand, yields a separable approximation of intermediate accuracy, which might be useful in certain applications. Specifically, outer diagonalization of the nuclear coordinates yields compact Q eigenfunctions which are more accurate than Dirac delta functions. The corresponding electronic potentials are then improved, resulting in more accurate electronic states.

We conclude this chapter with a brief discussion of certain refinements of the optimal separable basis method itself, which might be considered in future work. It would certainly be useful to find a more general existence proof than the one

presented in Section 2.3.3; although a stationary point has been found to exist for all scattering potentials satisfying the appropriate asymptotic conditions. It would also be of interest to develop a version which takes a proper account of exchange and related symmetries.

On a more practical note, it would be very beneficial to improve the outer diagonalization routine so that an arbitrarily-shaped grid can be dealt with. The present limitation as discussed in chapters 3 and 4, while not too severe, is nevertheless probably unnecessary. Since the diagonalization *per se* is not necessarily computationally expensive (particularly if $k \approx n$), one practical approach would be to apply an energy cutoff criterion to truncate the size of the basis after the outer diagonalization has been performed. Such a procedure would be akin to the sequential diagonalization and truncation methods,[85] although the cutoff criterion would have to be more complicated. Most likely, the truncation would have to occur at the block level only.

Outer diagonalization is the one procedure which is common to all numerical applications that incorporate the optimal separable basis idea. Practical improvements for implementing this procedure are therefore desired. Although formally the off-diagonal blocks need not approach zero as a result of outer diagonalization, it is interesting to note how many of these elements actually *do* disappear in practice. It is hard to pin down precisely why this is the case, but it is clear that this must correspond to some sort of inherent symmetry, unknown ahead of time, which the outer diagonalization routine discovers automatically.

As a final improvement, we consider the recursive modification described in Chapter 2. Instead of defining just two categories of coordinates, one could in principle extend the number of categories, even to the point where each category includes just a single degree of freedom. Both Equations 2.5 and 2.8 can be easily generalized to incorporate this possibility. In the weakly separable case, the entire set of categories becomes ordered; one must start from the outermost category first, and work inwards.

Of course, the resultant approximation in and of itself is not as accurate as that of a two-tiered approach. Nevertheless this approach is computationally more

efficient if one also calculates the desired quantity itself recursively. In other words if X is the quantity, then one obtains X for each of the outermost diagonal blocks, after first minimizing the coupling via outer diagonalization. Since these outermost blocks include all degrees of freedom except those in the outermost category, this approximation is a very good one; and presumably convergence to the correct results is very fast. The method is recursive in that it is also applied to the X problem for each of the diagonal blocks.

It is to be hoped that some recursive procedure along these lines may eventually overcome the exponential scaling problem discussed at the beginning of this chapter, vis à vis exact quantum calculations. In any event, the optimal separable basis approach has already demonstrated its value in the theory and application pertaining to molecular collisions.

References

[1] G. A. Voth, in *Advances in Chemical Physics* (John Wiley & Sons, Inc., New York, NY, 1996), pp. 135–218.

[2] J. I. Steinfeld *et al*, *Chemical Kinetics and Dynamics* (Prentice Hall, Englewood Cliffs, NJ, 1989).

[3] Z. Bačić and J. C. Light, Annu. Rev. Phys. Chem. **40**, 469 (1989).

[4] J. M. Bowman, Comp. Phys. Commun., Special Issue on "Molecular Vibrations" **51**, (1988).

[5] J. Bowman and B. Gazdy, J. Chem. Phys. **94**, 454 (1991).

[6] J. R. Taylor, *Scattering Theory* (John Wiley & Sons, Inc., New York, NY, 1972).

[7] J. K. Cullum and R. A. Willoughby, *Lanczos Algorithms for Large Symmetric Eigenvalue Computations* (Burkhauser, Boston, MA, 1985).

[8] C. Lanczos, J. Res. Natl. Bur. Stand. **45**, 255 (1950).

[9] B. N. Parlett, Lin. Alg. Appl. **34**, 269 (1980).

[10] H. Goldstein, *Classical Mechanics* (Addison-Wesley, Reading, MA, 1980).

[11] E. B. Wilson *et al*, *Molecular Vibrations* (Dover Publications, New York, NY, 1980).

[12] R. G. Littlejohn and M. Reinsch, Rev. Mod. Phys. **69**, 213 (1997).

[13] B. Poirier, J. Chem. Phys. (1998), (submitted).

[14] R. Horn and C. Johnson, *Topics of Matrix Analysis* (Cambridge University Press, Cambridge, England, 1991).

[15] N. J. Higham, Numerische Mathematik **62**, S39 (1992).

[16] G. Strang, *Linear Algebra and Its Applications* (Academic Press, Orlando, FL, 1980).

[17] B. Poirier and W. H. Miller, Chem. Phys. Lett. **265**, 77 (1997).

[18] S. Weinberg, Phys. Rev. **131**, 440 (1963).

[19] S. Willard, *General Topology* (Addison-Wesley, Menlo Park, CA, 1970).

[20] E. H. Lieb and B. Simon, in *The Stability of Matter: From Atoms to Stars*, edited by W. Thirring (Springer, New York, 1997), Chap. 4, pp. 299–308.

[21] G. Barton, *Elements of Green's Functions and Propagation* (Oxford University Press, New York, 1989).

[22] J. J. Sakurai, *Modern Quantum Mechanics* (Addison-Wesley, Menlo Park, CA, 1985).

[23] S. M. Auerbach and W. H. Miller, J. Chem. Phys. **98**, 6917 (1993).

[24] K. S. H. Lehmann and W. Zimmermann, Nuovo Cimento **1**, 425 (1955).

[25] R. D. Mattuck, in *A Guide to Feynman Diagrams in the Many-Body Problem* (Dover Publications, New York, NY, 1976), p. 158.

[26] L. H. Ryder, in *Quantum Field Theory* (Cambridge University Press, London, 1985), pp. 221–228.

[27] R. G. Newton, *Scattering Theory of Waves and Particles* (McGraw-Hill, New York, 1996).

[28] J. Z. H. Zhang, S.-I. Chu, and W. H. Miller, J. Chem. Phys. **88**, 6233 (1988).

[29] J. Z. H. Zhang and W. H. Miller, J. Chem. Phys. **91**, 1528 (1989).

[30] L. M. Hubbard, S. Shi, and W. H. Miller, J. Chem. Phys. **78**, 2381 (1983).

[31] W. H. Miller and B. M. D. D. J. op de Haar, J. Chem. Phys. **86**, 6213 (1987).

[32] J. Z. H. Zhang, D. L. Yeager, and W. H. Miller, Chem. Phys. Lett. **173**, 489 (1990).

[33] W. Kohn, Phys. Rev. **74**, 1763 (1948).

[34] D. T. Colbert and W. H. Miller, J. Chem. Phys. **96**, 1982 (1992).

[35] G. C. Groenenboom and D. T. Colbert, J. Chem. Phys. **99**, 9681 (1993).

[36] R. Jost and A. Pais, Phys. Rev. **82**, 840 (1951).

[37] R. Marcus, J. Chem. Phys. **45**, 4493 (1966).

[38] R. Marcus, J. Chem. Phys. **49**, 2610 (1968).

[39] K. Yamashita and W. H. Miller, J. Chem. Phys. **82**, 5475 (1985).

[40] W. H. Miller, N. C. Handy, and J. E. Adams, J. Chem. Phys. **72**, 99 (1980).

[41] G. Pöschl and E. Teller, Z. Physik. **83**, 143 (1933).

[42] N. Rosen and P. Morse, Phys. Rev. **42**, 210 (1932).

[43] E. Brezin and J. C. LeGuillou, Phys. Rev. D **15**, 1544 (1977).

[44] S. Flugge, in *Practical Quantum Mechanics* (Springer-Verlag, New York, 1971), Vol. 1, p. 94.

[45] M. M. Nieto, Phys. Rev. A **17**, 1273 (1978).

[46] in *Handbook of Mathematical Functions*, edited by M. Abramowitz and I. Stegun (Dover Publications, New York, NY, 1972), pp. 332–341.

[47] in *Handbook of Mathematical Functions*, edited by M. Abramowitz and I. Stegun (Dover Publications, New York, NY, 1972), p. 332.

[48] in *Handbook of Mathematical Functions*, edited by M. Abramowitz and I. Stegun (Dover Publications, New York, NY, 1972), p. 556.

[49] in *Table of Integrals, Series, and Products*, edited by I. Gradshteyn and I. Ryzhik (Academic Press, New York, NY, 1980), p. 795.

[50] G. Arfken, *Mathematical Methods for Physicists* (Academic Press, New York, NY, 1985), pp. 666-683.

[51] in *Table of Integrals, Series, and Products*, edited by I. Gradshteyn and I. Ryzhik (Academic Press, New York, NY, 1980), p. 798.

[52] D. O. Harris, G. G. Engerholm, and W. D. Gwinn, J. Chem. Phys. **43**, 1515 (1965).

[53] A. S. Dickinson and P. R. Certain, J. Chem. Phys. **49**, 4209 (1968).

[54] J. V. Lill, G. A. Parker, and J. C. Light, Chem. Phys. Lett. **89**, 483 (1982).

[55] R. A. Friesner, Chem. Phys. Lett. **116**, 39 (1985).

[56] J. C. Light, I. P. Hamilton, and J. V. Lill, J. Chem. Phys. **82**, 1400 (1985).

[57] J. V. Lill, G. A. Parker, and J. C. Light, J. Chem. Phys. **85**, 900 (1986).

[58] Z. Bačić and J. C. Light, J. Chem. Phys. **85**, 4594 (1986).

[59] R. M. Whitnell and J. C. Light, J. Chem. Phys. **89**, 3674 (1988).

[60] S. E. Choi, J. Chem. Phys. **92**, 2129 (1990).

[61] C. Leforestier, J. Chem. Phys. **94**, 6388 (1991).

[62] G. C. Corey and D. Lemoine, J. Chem. Phys. **97**, 4115 (1992).

[63] J. D. Jackson, in *Classical Electrodynamics*, 2 ed. (John Wiley & Sons, New York, NY, 1975), Chap. 7.

[64] G. Arfken, *Mathematical Methods for Physicists* (Academic Press, New York, NY, 1985), pp. 421–426.

[65] A. Goldberg and B. W. Shore, J. Phys. B **11**, 3339 (1978).

[66] C. Leforestier and R. E. Wyatt, J. Chem. Phys. **78**, 2334 (1983).

[67] D. Neuhauser and M. Baer, J. Chem. Phys. **90**, 4351 (1989).

[68] D. Neuhauser, M. Baer, and D. J. Kouri, J. Chem. Phys. **93**, 2499 (1990).

[69] T. Seideman and W. H. Miller, J. Chem. Phys. **96**, 4412 (1992).

[70] T. Seideman and W. H. Miller, J. Chem. Phys. **97**, 2499 (1992).

[71] W. H. Thompson and W. H. Miller, Chem. Phys. Lett. **206**, 123 (1993).

[72] W. Hackbusch, *Iterative Solution of Large Sparse Systems of Equations* (Springer-Verlag, New York, NY, 1994).

[73] B. N. Parlett, in *The Symmetric Eigenvalue Problem* (Prentice-Hall, Englewood Cliffs, NJ, 1980), Chap. 12.

[74] T. J. Park and J. C. Light, J. Chem. Phys. **85**, 5870 (1986).

[75] T. Seideman and W. H. Miller, J. Chem. Phys. **95**, 1768 (1991).

[76] U. Manthe, T. Seideman, and W. H. Miller, J. Chem. Phys. **99**, 10078 (1993).

[77] U. Manthe, T. Seideman, and W. H. Miller, J. Chem. Phys. **101**, 4759 (1994).

[78] L. F. Gaucher, chemistry, University of California, Berkeley, California, 1994.

[79] W. H. Thompson and W. H. Miller, J. Chem. Phys. **101**, 8620 (1994).

[80] H. Hunt and T. Szymanski, Comm. ACM **20**, 171 (1977).

[81] G. C. Groenenboom, Technical report, NWO (unpublished).

[82] P. P. Korambath, X. T. Wu, and E. F. Hayes, J. Phys. Chem. **100**, 6116 (1996).

[83] U. Peskin, A. Edlund, and W. H. Miller, J. Chem. Phys. **103**, 10030 (1995).

[84] B. Poirier, Phys. Rev. A **56**, 120 (1997).

[85] J. C. Light *et al*, in *Supercomputer Algorithms for Reactivity, Dynamics and Kinetics of Small Molecules*, edited by A. Lagana (Kluwer Academic Publishers, New York, 1989), pp. 187–213.

[86] N. R. Wall and D. Neuhauser, J. Chem. Phys. **102**, 8011 (1995).

[87] V. A. Mandelshtam and H. S. Taylor, J. Chem. Phys. **102**, 7390 (1995).

[88] V. A. Mandelshtam and H. S. Taylor, Phys. Rev. Lett. **78**, 3274 (1997).

[89] B. Poirier, 1994, unpublished comment.

[90] C. W. McCurdy and B. C. Garrett, J. Chem. Phys. **84**, 2630 (1986).

[91] W. H. Press *et al*, in *Numerical Recipes*, 1st ed. (Cambridge University Press, Cambridge, England, 1989), pp. 539–546.

[92] Y. Saad and M. H. Schultz, SIAM J. Sci. Statist. Comput. **7**, 856 (1986).

[93] P. Sonneveld, SIAM J. Sci. Comput. **10**, 36 (1989).

[94] R. W. Freund and N. M. Nachtigal, Numer. Math. **60**, 315 (1991).

[95] W. H. Press *et al*, in *Numerical Recipes*, 1st ed. (Cambridge University Press, Cambridge, England, 1989), pp. 342–349.

[96] W. H. Press *et al*, in *Numerical Recipes*, 1st ed. (Cambridge University Press, Cambridge, England, 1989), Chap. 2.

[97] P. Siegbahn and B. Liu, J. Chem. Phys. **68**, 2457 (1978).

[98] D. G. Truhlar and C. J. Horowitz, J. Chem. Phys. **68**, 2566 (1978).

[99] D. K. Bondi and J. N. L. Connor, J. Chem. Phys. **82**, 4383 (1985).

[100] T. J. Park and J. C. Light, J. Chem. Phys. **88**, 4897 (1988).

[101] J. W. Tromp and W. H. Miller, Faraday Discuss. Chem. Soc. **84**, 441 (1987).

[102] R. D. Levine and R. B. Bernstein, *Molecular Reaction Dynamics and Chemical Reactivity* (Oxford University Press, New York, NY, 1987).

[103] J. E. Dove *et al*, J. Chem. Phys. **92**, 7373 (1990).

[104] K. Sakimoto and K. Onda, J. Chem. Phys. **100**, 1171 (1994).

[105] B. Poirier, J. Chem. Phys. (1997), (accepted).

[106] W. H. Thompson and W. H. Miller, J. Chem. Phys. **105**, 16 (1996).

[107] W. H. Thompson and W. H. Miller, J. Chem. Phys. **106**, 142 (1997).

[108] W. H. Thompson and W. H. Miller, J. Chem. Phys. **107**, 2164 (1997).

[109] R. T. Pack, J. Chem. Phys. **60**, 633 (1974).

[110] P. McGuire and D. J. Kouri, J. Chem. Phys. **60**, 2488 (1974).

[111] J. M. Bowman, J. Phys. Chem. **95**, 4960 (1991).

[112] C. Eckart, Phys. Rev. **47**, 552 (1935).

[113] H. Koizumi, G. C. Schatz, and M. S. Gordon, J. Chem. Phys. **95**, 6421 (1991).

[114] K. Moribayashi and H. Nakamura, J. Phys. Chem. **99**, 15410 (1995).

[115] B. Ramachandran, J. Senekowitsch, and R. E. Wyatt, Theochem **388**, 57 (1996).

[116] R. D. H. Brown and I. W. M. Smith, Intl. J. Chem. Kinet. **7**, 301 (1975).

[117] R. D. H. Brown and I. W. M. Smith, Intl. J. Chem. Kinet. **10**, 1 (1978).

[118] K. Mahmud, J.-S. Kim, and A. Fontijn, J. Phys. Chem. **94**, 2994 (1990).

[119] D. L. Singleton and R. J. Cvetanovic, Intl. J. Chem. Kinet. **13**, 945 (1981).

[120] J. Lipman, in *Calder's Universe* (Viking Press, New York, NY, 1976), p. 299.

[121] U. Manthe and W. H. Miller, J. Chem. Phys. **99**, 3411 (1993).

[122] R. Radau, Ann. Sci. École Normale Supérior **5**, 311 (1868).

[123] F. T. Smith, Phys. Rev. Lett. **45**, 1157 (1980).

[124] B. R. Johnson, J. Chem. Phys. **85**, 4538 (1986).

Report Number (14) LBNL--41182

Publ. Date (11) 199712

Sponsor Code (18) DOE/ER, XF

UC Category (19) UC-411, DOE/ER

DOE